TRABAJO ESPECIAL DE GRADO

ANÁLISIS DE UN SISTEMA ENERGÉTICO A CONCENTRACIÓN SOLAR INTEGRADO CON CALDERAS A BIOMASA

(ANALYSIS OF A CONCENTRATING SOLAR POWER GENERATION SYSTEM WITH BIOMASS BOILERS)

Presentado ante la Ilustre
Universidad Central de Venezuela
Por el Br. Flores B., Franilena M.
Para optar al Título
de Ingeniero Químico

Caracas, 2014

TRABAJO ESPECIAL DE GRADO

ANÁLISIS DE UN SISTEMA ENERGÉTICO A CONCENTRACIÓN SOLAR INTEGRADO CON CALDERAS A BIOMASA

(ANALYSIS OF A CONCENTRATING SOLAR POWER GENERATION SYSTEM WITH BIOMASS BOILERS)

TUTORES ACADEMICOS: Prof. Marco Masoero (Politecnico di Torino)
Profa. Anubis Pérez (UCV)

Presentado ante la Ilustre
Universidad Central de Venezuela
Por el Br. Flores B., Franilena M.
Para optar al Título
de Ingeniero Químico

Presentado ante el Ilustre
Politecnico di Torino
Por el Br. Flores B., Franilena M.
Para optar al Título
de Ingeniero Energético y Nuclear

Caracas, 2014

Caracas, noviembre de 2014

Los abajo firmantes, miembros del Jurado designado por el Consejo de Escuela de Ingeniería Química, para evaluar el Trabajo Especial de Grado presentado por la Bachiller Franilena Mónica Flores Brand, titulado:
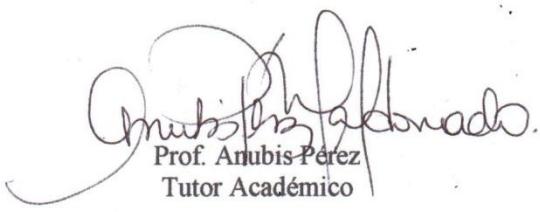
"ANÁLISIS DE UN SISTEMA ENERGÉTICO A CONCENTRACIÓN SOLAR INTEGRADO CON CALDERAS A BIOMASA"

Consideran que el mismo cumple con los requisitos exigidos por el plan de estudios conducente al Título de Ingeniero Químico, y sin que ello signifique que se hacen solidarios con las ideas expuestas por el autor, lo declaran APROBADO.

Prof. Andrés Rosales
Jurado

Prof. Omaira Camacaro
Jurado

Prof. Anubis Pérez
Tutor Académico

POLITECNICO DI TORINO

Area Gestione Didattica
DIPLOMA SUPPLEMENT

Il presente Supplemento al Diploma è stato sviluppato dalla Commissione Europea, dal Consiglio d'Europa e dall'UNESCO/CEPES. Lo scopo del supplemento è di fornire dati indipendenti atti a migliorare la trasparenza internazionale dei titoli (diplomi, lauree, certificati ecc.) e a consentirne un equo riconoscimento accademico e professionale. E' stato progettato in modo da fornire una descrizione della natura, del livello, del contesto, del contenuto e dello status degli studi effettuati e completati dallo studente identificato nel titolo originale al quale questo supplemento è allegato. Esso esclude ogni valutazione discrezionale, dichiarazione di equivalenza o suggerimenti relativi al riconoscimento. Le informazioni sono fornite in otto sezioni. Qualora non sia possibile fornire alcune informazioni, ne sarà data la spiegazione.

1 DATI ANAGRAFICI
1.1 Cognome
FLORES BRAND
1.2 Nome
FRANILENA MONICA
1.3 Data, città e paese di nascita
27/08/1991, CARACAS - VENEZUELA
1.4 Codice Fiscale
FLRFNL91M67Z614Z
Matricola
192336

2 INFORMAZIONI SUL TITOLO DI STUDIO
2.1 Titolo di studio rilasciato, qualifica accademica
Corso di Laurea Magistrale in INGEGNERIA ENERGETICA E NUCLEARE
Dottore Magistrale in INGEGNERIA ENERGETICA E NUCLEARE
2.2 Classe
Classe delle lauree magistrali in INGEGNERIA ENERGETICA E NUCLEARE
2.3 Nome dell'istituzione che rilascia il titolo di studio
Politecnico di Torino - Italia, università statale
2.4 Nome dell'istituzione che gestisce gli studi
Politecnico di Torino - Italia, università statale
2.5 Lingua/e ufficiali di insegnamento e di accertamento della preparazione

60% Inglese, 40% Italiano.

3 INFORMAZIONI SUL LIVELLO DEL TITOLO DI STUDIO
3.1 Livello del titolo di studio
Secondo ciclo
3.2 Durata normale del corso (in anni)
2 anni, a tempo pieno
3.3 Requisiti di ammissione
Laurea o titolo equivalente

4 INFORMAZIONI SUL CURRICULUM E SUI RISULTATI CONSEGUITI
4.1 Modalità di frequenza e di didattica utilizzata
Full-time. Didattica frontale.
4.2 Requisiti per il conseguimento del titolo
Il corso di laurea magistrale in ingegneria energetica e nucleare si propone l'approfondimento delle conoscenze scientifiche e tecnologiche avanzate che costituiscono le applicazioni dell'ingegneria energetica e nucleare. Oltre a completare le conoscenze nelle discipline ingegneristiche di base, il corso si pone l'obiettivo di formare competenze avanzate nell'energetica, nell'analisi degli impianti e dei sistemi di trasformazione e utilizzazione dell'energia nei vari settori di applicazione. Vengono anche affrontati i problemi di analisi di sicurezza e di localizzazione di impianti energetici.
La formazione ha come obiettivi specifici quello di rendere l'ingegnere magistrale in grado di svolgere le seguenti funzioni:
- Sviluppare modelli matematici e simulare numericamente sistemi energetici complessi che utilizzano fonti fossili, rinnovabili e l'energia nucleare;
- Impiegare le conoscenze metodologiche, tecnologiche e ingegneristiche alla identificazione, formulazione e risoluzione di problemi complessi dell'industria energetica utilizzando un approccio interdisciplinare;
- Pianificare e ottimizzare sistemi energetici complessi;
- Progettare componenti di sistemi energetici;
- Valutare la sicurezza e l'impatto ambientale dei sistemi energetici.
Il percorso formativo dedicato alle tecnologie energetiche si propone di fornire le competenze e gli strumenti conoscitivi per il calcolo, la progettazione e la gestione di componenti, impianti e sistemi per la generazione di energia elettrica, termica, meccanica ed elettrica con fonti sia fossili che rinnovabili. Si propone inoltre di fornire le competenze e gli strumenti conoscitivi per definire l'entità della domanda e individuare le misure necessarie per una utilizzazione razionale dell'energia nei vari settori produttivi, in ambito civile e nei trasporti. Sono affrontati anche i problemi connessi alla pianificazione energetico-ambientale, all'analisi del ciclo di vita, allo sviluppo e all'utilizzo di nu
4.3 Curriculum, crediti, valutazioni e voti conseguiti
Vedi Appendice A
4.4 Sistema di votazione, distribuzione dei voti ottenuti
I voti nelle singole attività formative vanno da 1 a 30. La sufficienza è 18, il massimo è 30 e lode. Per alcune attività formative non è previsto il voto ma la sola idoneità o approvazione.

iv

AGRADECIMIENTOS

Gracias a la ilustre Universidad Central de Venezuela por la oportunidad de crecer y estudiar en sus aulas, me siento honrada y orgullosa de ser parte de esta institución. Agradezco a los profesores de la Escuela de Ingeniería Química de la UCV, en especial a mis tutores, el Prof. Humberto Kum y la Prof. Anubis Pérez, por sus infinitos conocimientos y habilidades, tanto en el área de la ingeniería como en la capacidad de enseñar y captar el interés de sus estudiantes.

Expreso mis más sinceros y cálidos agradecimientos a mis tutores en el Politécnico de Torino, el Ing. Caldera y el Prof. Masoero, por su apoyo y vastos conocimientos.

Me gustaría agradecer a la ENEA, la empresa que me dió la oportunidad de realizar esta tesis, especialmente al Sr. Levizzari, la Ing. Roberto y todo el personal de la UTTS, quienes me proporcionaron las mejores condiciones de trabajo durante el desarrollo de la tesis.

Agradezco a mi familia en Venezuela, en particular a mi madre Rosa Maitte Brand, por su incondicional apoyo y amor.

Sin más que decir, a mi familia en Italia.

Flores B., Franilena M.

ANÁLISIS DE UN SISTEMA ENERGÉTICO A CONCENTRACIÓN SOLAR INTEGRADO CON CALDERAS A BIOMASA

Tutores Académicos: Profa. Anubis Pérez (UCV) y Prof. Marco Masoero (Politecnico di Torino). Tesis. Caracas, U.C.V. Facultad de Ingeniería. Escuela de Ingeniería Química. Torino, Politecnico di Torino. Departamento de Energía. Año 2014, 113 p.

Palabras Claves: calderas a biomasa, cogeneración híbrida, CSP solar, fluidos de trabajo a altas temperaturas, software TRNSYS®, MATLAB, simulador SAM.

Resumen. Actualmente la producción de electricidad y calor a partir de recursos renovables como la biomasa sólida y la radiación solar son procesos maduros y atractivos a nivel mundial. La integración de un sistema energético a concentración solar (CSP) con una caldera alimentada a biomasa, representa una solución interesante para mejorar la flexibilidad y competitividad del sistema energético, aumentando consecuentemente el número de horas operativas equivalentes y disminuyendo el tamaño del campo solar. Por otra parte, el sistema energético integrado resulta más sostenible, y si el sistema se diseña correctamente puede conducir a mayores eficiencias. El sistema de almacenamiento de la energía térmica o Thermal Energy Storage (TES) juega un rol fundamental en la reducción de la operación intermitente de plantas energéticas de tipo CSP e híbridas. A pesar de estas ventajas, se requiere aún de gran trabajo con el fin de apoyar la difusión en el mercado de las plantas energéticas híbridas de tipo solar-biomasa, como demuestran el muy limitado número de instalaciones actuales, como por ejemplo, la planta Borges Termosolar en España. El presente estudio se enfoca en el análisis del rendimiento anual de una planta híbrida CSP – biomasa de 1 MWe, compuesta por colectores de tipo cilindro parabólicos con 2 tanques de almacenamiento térmico directo. La correcta ubicación de la planta es un aspecto importante en términos de factibilidad y sostenibilidad del sistema híbrido. La localidad de Brindisi en el Sur de Italia ha sido seleccionada como área objetivo, con el fin de investigar la potencial aplicación del sistema energético, debido a la disponibilidad local de los residuos naturales proveniente de la poda de los olivos y las condiciones favorables de radiación solar. La planta energética híbrida ha sido simulada con el software TRNSYS®, y el rendimiento de la caldera a rejillas móviles, ha sido modelado a través de un conjunto personalizado de funciones implementadas en MATLAB®. Las funciones de MATLAB se integran en TRNSYS, con el fin de simular todo el sistema. Las simulaciones demuestran la viabilidad del sistema híbrido, lo que resulta en un incremento del 70 % de las horas equivalentes respecto a una planta CSP sencilla, y con una reducción del 30% en la demanda de biomasa en comparación con una planta a biomasa.

Flores B., Franilena M.

ANÁLISIS DE UN SISTEMA ENERGÉTICO A CONCENTRACIÓN SOLAR INTEGRADO CON CALDERAS A BIOMASA

Tutores Académicos: Profa. Anubis Pérez (UCV) y Prof. Marco Masoero (Politecnico di Torino). Tesis. Caracas, U.C.V. Facultad de Ingeniería. Escuela de Ingeniería Química. Torino, Politecnico di Torino. Departamento de Energía. Año 2014, 113 p.

INTRODUCCIÓN

Actualmente la radiación solar, así como, la biomasa son energías renovables muy explotadas y desarrolladas a nivel mundial. Los sistemas de concentración de la energía solar o Concentrated Solar Power (CSP) tienen el potencial de desempeñar un papel relevante en el desarrollo de las energías renovables, principalmente porque resuelven parcialmente la operación intermitente de las plantas solares comunes, por su capacidad de acumular la energía térmica.

Una planta CSP es un sistema que utiliza espejos o lentes para concentrar la radiación solar en un tubo absorbente. A través de este tubo fluye un fluido termo-vector o Heat Transfer Fluid (HTF) que conduce la energía térmica al bloque de potencia con el fin de producir energía eléctrica. El CSP produce energía a temperaturas más altas que las alcanzadas con los colectores de placa plana principalmente por la concentración de la radiación solar y por la disminución de las perdidas térmicas gracias a una menor superficie de contacto con el ambiente.

El principal atractivo de esta tecnología es la posibilidad de integrar el campo solar con un sistema de almacenamiento de la energía térmica o Thermal Energy Storage (TES). La combinación CSP-TES permite que la producción eléctrica coincida con la demanda, incluso en horas donde la radiación solar es escasa o nula. Comúnmente una planta CSP integrada con TES funciona de la siguiente manera: durante el día el calor producido por la radiación solar se utiliza para suministrar energía térmica al bloque de potencia y el exceso de energía se almacena. Esta energía térmica almacenada se utiliza para producir energía durante la noche, en días nublados y para cubrir la producción eléctrica durante las horas pico.

Generalmente el TES se compone de dos tanques, uno para el fluido a alta temperatura y la otra para el fluido a una temperatura menor. Por lo general, el calor es almacenado en sales fundidas, especialmente debido a su buena estabilidad a altas temperaturas (500 a 600 ° C), lo que mejora la eficiencia térmica del bloque de

potencia y reduce las dimensiones del almacenamiento térmico. En el caso de que el HTF sea una mezcla de sales fundidas, la conexión entre el campo solar y el sistema de almacenamiento de energía térmica es directa, mientras que si el HTF es aceite sintético, sería necesario añadir un intercambiador de calor para transferir la energía desde el campo solar al tanque de almacenamiento.

Actualmente, en Italia y Europa existe un creciente interés por las plantas de cogeneración basadas en fuentes renovables, especialmente por aquellas de pequeñas capacidades eléctricas. De acuerdo a este interés, el objetivo de la presente tesis es simular y analizar el rendimiento de una central de 1 MWe compuesta por colectores cilindro parabólicos, integrada a un sistema de almacenamiento térmico y una caldera de biomasa. La localidad seleccionada para el proyecto es la región de Puglia en Italia debido a sus excelentes condiciones solares y amplia disponibilidad de madera de olivo como residuo del proceso de poda natural.

METODOLOGÍA

Con la finalidad de predecir el comportamiento dinámico de la planta energética se han realizado diversas simulaciones del sistema. Las herramientas computacionales utilizadas con este fin han sido TRNSYS®, MATLAB® y SAM®, el último usado para validar los resultados obtenidos con TRNSYS.

SIMULADORES EMPLEADOS

TRNSYS

TRNSYS es un programa de simulación comercial y académico dedicado a sistemas dinámicos en el área de las energías renovables incluyendo la tecnología de concentración solar, de particular interés en el presente estudio.

El paquete de cálculo TRNSYS fue desarrollado en 1975 por el Laboratorio de Energía Solar de la Universidad de Wisconsin, en colaboración con el Laboratorio de Aplicaciones de la Energía Solar de la Universidad de Colorado, ambos en los Estados Unidos. Desde ese momento, TRNSYS ha ido desarrollándose continuamente gracias al trabajo de distintas instituciones. El software cuenta con usuarios y distribuidores a nivel mundial (Francia, Alemania, España, USA, Japón).

Actualmente el simulador cuenta con una interfaz gráfica. También ofrece una vasta librería de componentes estándar y otras librerías especiales con alrededor de 300 componentes adicionales. En la presente tesis el sistema energético ha sido modelado en su mayoría, por componentes provenientes de la librería estándar, sin embargo ha

sido adquirida una librería especial, conocida como TESS (Thermal Energy System Specialist) con el objetivo de modelar los colectores cilindro parabólicos.

Por otra parte, TRNSYS permite la integración de otros programas numéricos como por ejemplo Excel y MATLAB. Gracias a esta ventaja, ha sido posible modelar detalladamente el comportamiento de la caldera a biomasa con MATLAB y posteriormente integrarla al sistema energético.

La Figura 1 ilustra un esquema simplificado del sistema energético modelado con TRNSYS. Básicamente el sistema se compone de dos ciclos cerrados: El ciclo donde se calientan las sales fundidas, ya sea en el campo solar o en la caldera y el ciclo Rankine donde se transforma la energía térmica almacenada en las sales fundidas a energía eléctrica.

El sistema puede operar en 3 distintas modalidades. Cuando el tanque caliente (el tanque rojo en la Figura 1) está vacío o el nivel de las sales fundidas es menor al 50 % del nivel del tanque caliente, la potencia requerida por los usuarios es producida en un 100 % por la caldera a biomasa. Cuando el nivel de sales fundidas en el tanque caliente supera el 50 % del nivel del tanque, la potencia producida es una combinación en paralelo de la energía generada en la caldera y las sales fundidas calientes que se descargan del tanque caliente. Si el nivel de sales fundidas continúa creciendo y supera el 70 % del nivel del tanque caliente, la caldera entra en modo stand- by y el 100 % de la energía demandada es producida por la descarga del tanque caliente.
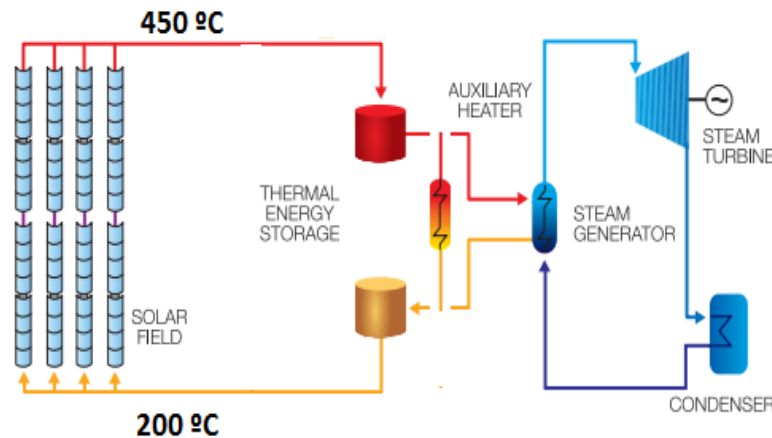

Figura 1. Esquema simplificado del sistema energético

La Figura 2 expone un esquema detallado del sistema simulado con TRNSYS, donde se modela una planta de generación eléctrica de 1 MWe integrada a un Ciclo Rankine Orgánico (ORC) por ser el ciclo de potencia más apto a pequeñas potencias de producción (< 2 MWe).

El sistema de regulación es representado por el control 1 y el control 2, controles de tipo feedback, empleados en la simulación debido a que son controles simples que se adaptan y cumplen con los requisitos del sistema. Las líneas negras discontinuas representan las señales que van desde el transmisor a los controles y de los controles al componente manipulado. El control 1 (type 22) se encarga de mantener la temperatura de las sales fundidas alrededor de la temperatura de set point al salir del campo solar, manipulando el flujo másico que ingresa en los colectores a través de la bomba 1. Por otra parte, el control 2 regula la temperatura del fluido del ciclo de potencia antes de entrar en la turbina, manipulando el flujo másico de sales fundidas que ingresan en el evaporador a través de la bomba 2. El sistema se encuentra continuamente en estado transitorio debido a las variaciones de las condiciones de la demanda, representado por el componente consumers profile (type14h).

El sistema antifreezing se compone de 3 calderas a gas natural, simbolizadas en la Figura 2 por el boiler 2, el boiler 3 y el boiler 4, los cuales se encienden solo en caso de que la temperatura de las sales fundidas descienda bajo una temperatura fijada. Generalmente se enciende durante días nublados o en la noche para evitar que la temperatura de las sales fundidas descienda hasta la temperatura de solidificación.

En esta imagen las líneas continuas azules y rojas representan el paso del fluido termo-vector por el sistema antes y después de absorber calor, respectivamente. Por ejemplo, la línea azul antes del componente solar collector (type 1257) representa las sales fundidas a 200 ºC ingresando al campo solar, mientras que la línea roja que procede al mismo componente simboliza las sales fundidas a 450ºC, saliendo del campo solar.
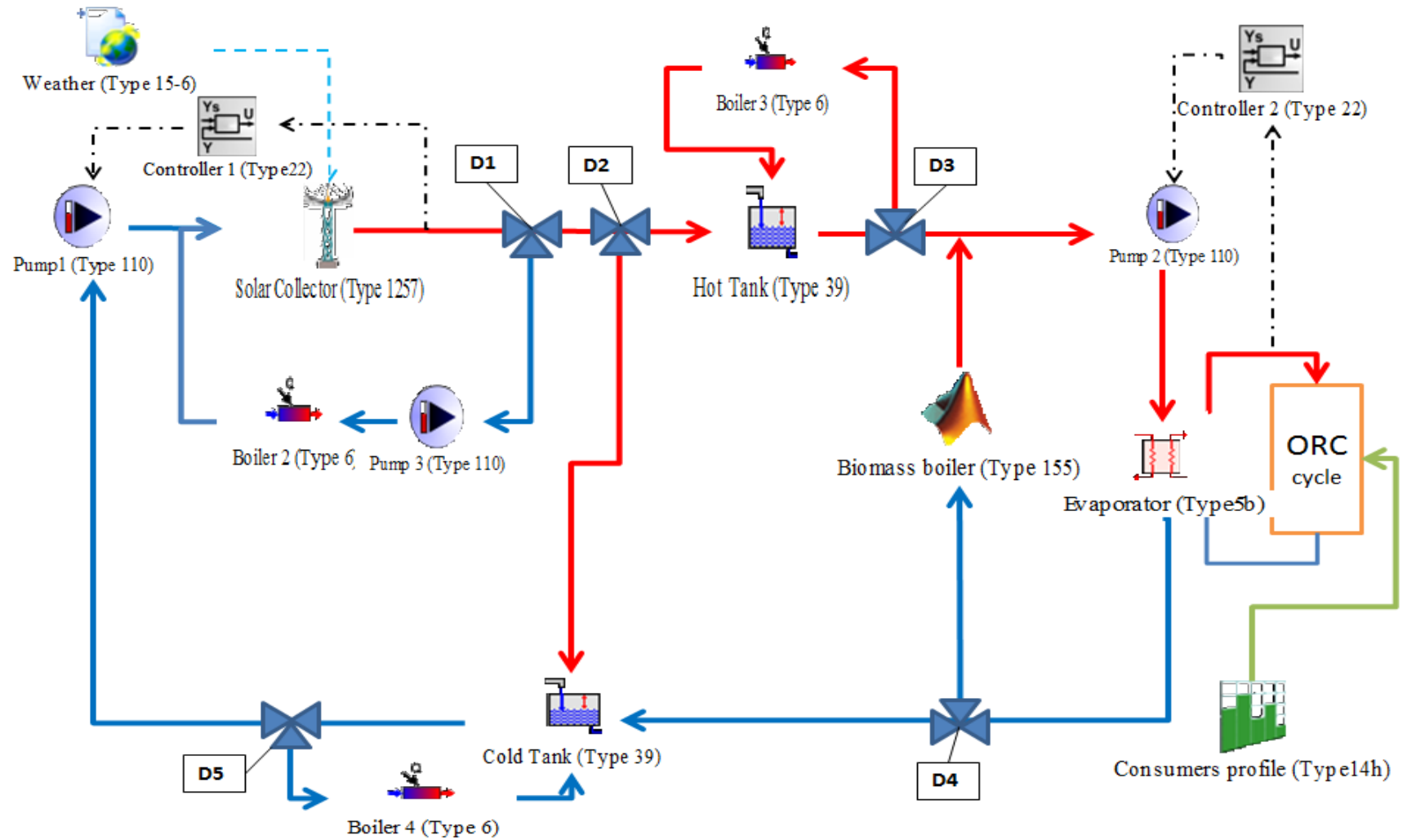
Figura 2. Esquema simplificado del sistema energético en TRNSYS.

Solar Advisor Model (SAM)

SAM fue desarrollado por el Laboratorio Nacional de Energías Renovables (NREL) en colaboración con el Departamento de Energía Solar de los Estados Unidos y los Laboratorios Sandia. Este software cuenta con sistemas energéticos a fuentes renovables preestablecidos, que permiten al usuario investigar y predecir el impacto energético y económico al variar los distintos parámetros del sistema (físicos y económicos).

SAM es un software gratuito, utilizado con fines didácticos y comerciales. Algunos de los resultados obtenibles con SAM relacionados al costo y comportamiento del sistema energético incluyen: la energía total producida en base horaria, mensual y anual, la eficiencia anual y pico del sistema, el costo de la electricidad en venta, el Valor Presente Neto, los costos de mantenimiento y operación (O&M), entre otros.

RESULTADOS Y DISCUSIÓN

El sistema energético se ha modelado con el objetivo de proveer una potencia de 1 MWe durante todo el año, a los usuarios de la ciudad de Brindisi al Sur de Italia. La caldera a biomasa ha sido diseñada para suministrar la capacidad máxima de la planta si es necesario, mientras que el sistema de almacenamiento instalado, podrá suministrar la potencia máxima de la planta durante 10 horas. El fluido que absorbe y acumula la energía térmica es una mezcla ternaria de sales fundidas conocida como HITEC XL.

El campo solar se compone por loops alineados en paralelo y a su vez un loop corresponde a 6 colectores cilindro-parabólicos localizados en serie. El primer objetivo del análisis es determinar la configuración óptima del campo solar, es decir, la cantidad de loops requeridos para alcanzar un alto factor de capacidad del campo solar y al mismo tiempo mantener un buen compromiso entre este valor y la cantidad de colectores.

El factor de capacidad se define como el porcentaje que representa la energía térmica proveniente del campo solar - TES respecto a la energía térmica total requerida para satisfacer la demanda. De acuerdo a la Figura 3, este porcentaje puede alcanzar hasta un 50 % cuando la cantidad de loops es igual a 15, sin embargo si se emplean solamente 5 loops, menos de la mitad de loops, el factor de capacidad es un poco superior a 30 %. Este fenómeno se debe a que la curva de la Figura 3 sigue una tendencia similar a dos líneas rectas, la primera recta que va de 0 a 5 loops tiene una inclinación mayor a la segunda recta, que va de 5 loops en adelante.
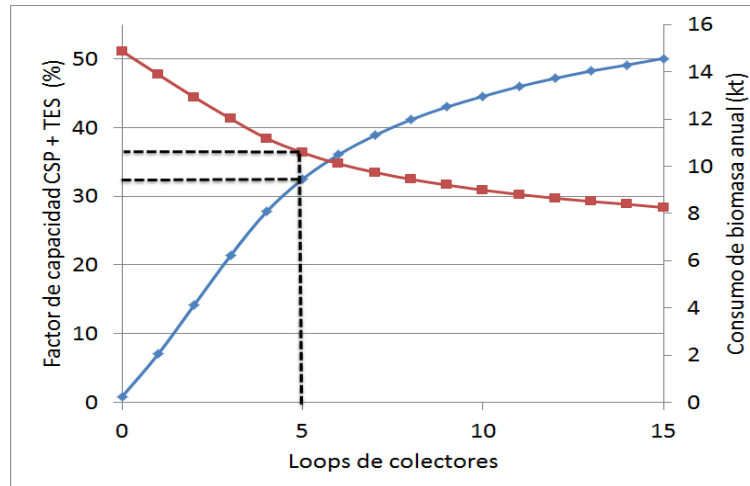
Figura 3. Factor de capacidad (línea azul) y consumo de biomasa (línea roja) al variar el número de loops de colectores.

Finalmente el campo solar ha sido diseñado con 5 loops de colectores resultando un factor de capacidad del CSP-TES cercano a un 32 % y un consumo de biomasa anual aproximado de 10 kt.

La Figura 4 ilustra un esquema simplificado de la planta energética, donde los 5 loops que representan el campo solar se ubican lo más simétricamente posible a los lados del resto de los componentes (tanques, ciclo de potencia, caldera a biomasa) con el objetivo de disminuir las perdidas térmicas y los costos de bombeo. El área total ocupada por la planta ha sido estimada y aproximada a 8 hectáreas.
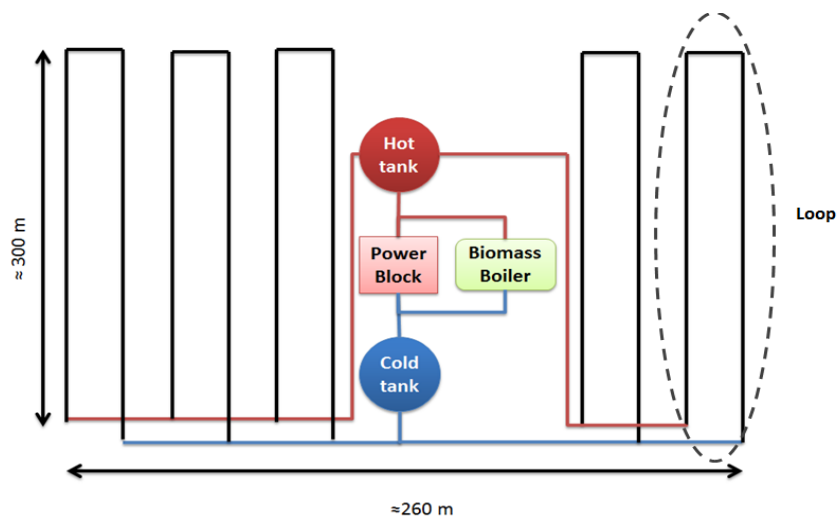
Figura 4. Esquema simplificado de la planta enérgetica.

La Figure 68 muestra el comportamiento de la temperatura del fluido termo-vector durante el mes de Julio, donde la línea azul y la línea roja representan la

temperatura de salida e ingreso del campo solar respectivamente. Se observa que la línea azul se mantiene durante la mayor parte de los días en la temperatura de set point, es decir el sistema de control funciona correctamente. Es fundamental que la temperatura no supere los 500 ℃ por razones de seguridad y estabilidad de la mezcla ternaria.
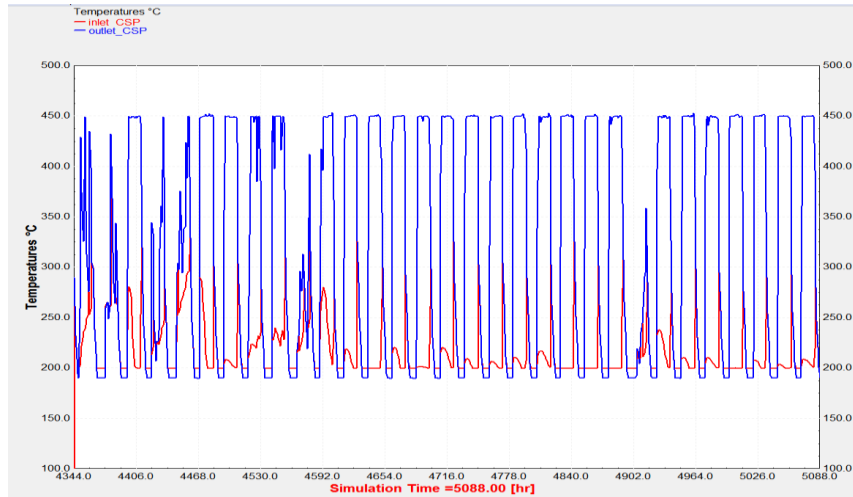

Figura 5. Temperatura de ingreso y de salida del fluido termo- vector del campo solar en el mes de Julio (creado con TRNSYS).

La eficiencia promedio del sistema energético es calculada a través de la ecuación (1)

$$\eta = \frac{Energía_{final}}{Energía_{inicial}} \qquad (1)$$

Donde Ŋ es la eficiencia promedio del sistema.

La Figura 6 ilustra el flujo de energía de la planta CSP - TES, donde la radiación solar que incide en los colectores representa la energía inicial que ingresa al sistema y es posteriormente transformada en energía eléctrica a través de un conjunto de procesos. Sustituyendo los valores expuestos en la Figura 6 en la ecuación (1) la eficiencia bruta promedio de la planta se aproxima a un 8%, similar a una planta existente con la misma capacidad eléctrica en Arizona, Estados Unidos.
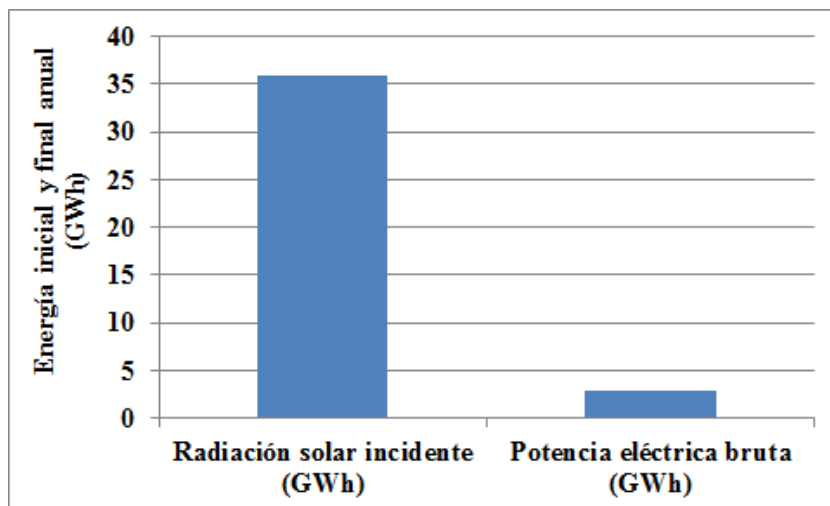
Figura 6. Energía inicial (Radiación solar incidente) y energía final (Potencia eléctrica bruta) en un año, en un sistema energético CSP- TES.

Por otra parte, cuando el sistema se convierte en CSP - TES – biomasa, la energía inicial que ingresa al sistema se convierte en la radiación solar incidente más la cantidad de biomasa consumida en la caldera, y la energía final es la energía eléctrica bruta producida. Sustituyendo los valores de las energías expuestas en la Figura 7 en la ecuación (1) la eficiencia bruta promedio del sistema alcanza casi un 14 %, es decir aumenta en alrededor un 75 % respecto al sistema sin la caldera a biomasa.
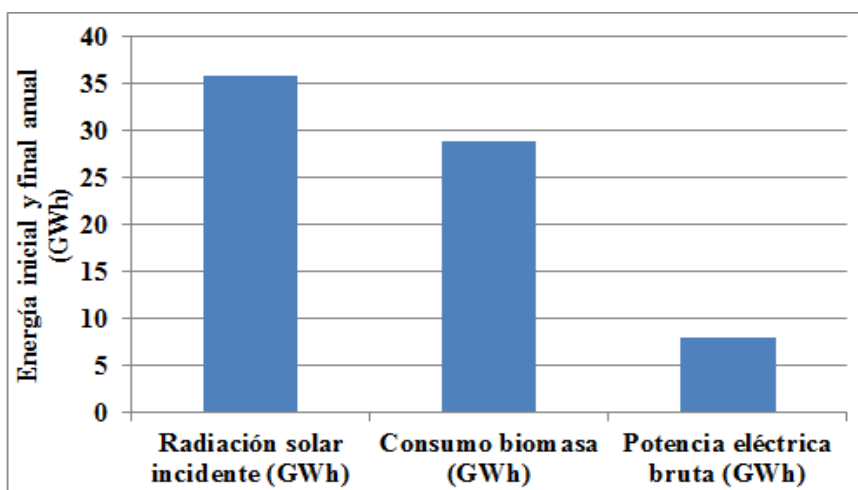

Figura 7. Energía inicial (Radiación solar incidente y biomasa) y energía final (Potencia eléctrica bruta) en un sistema energético CSP – TES – biomasa.

Comparación de los resultados obtenidos con TRNSYS y SAM

La energía solar puede ser muy intermitente en países con estaciones como es el caso de Italia, por esta razón, se considera necesario estudiar el comportamiento del sistema energético también en base mensual. La Figura 8 ilustra como el sistema CSP – TES alcanza un factor de capacidad máximo, cercano al 65 %, durante los meses de verano, mientras que en los meses de invierno, el factor de capacidad decrece hasta poco menos del 10 %, particularmente en el mes Diciembre.
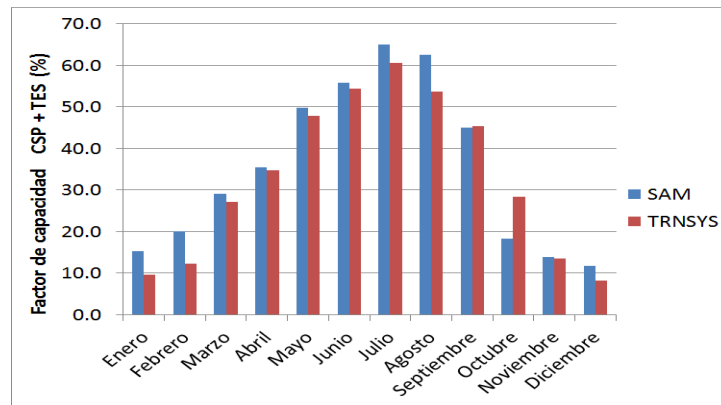

Figura 8. Factor de capacidad mensual del sistema energético CSP-TES.

Agregando la caldera a biomasa al sistema energético y calculando el factor de capacidad del sistema integrado se obtiene la Figura 9. Esta figura muestra como la caldera a biomasa permite el suministro del 100 % de los 8760 MWh requeridos al año, aumentando las horas equivalentes en un 70 % respecto a una planta solo CSP-TES.
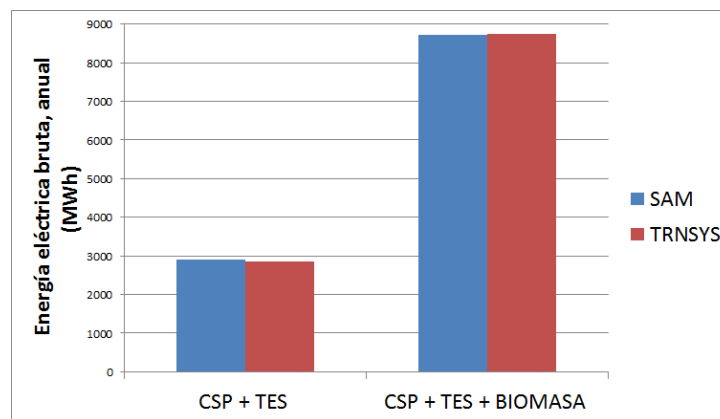

Figura 9. Energía eléctrica bruta anual de la planta CSP + TES y CSP+TES+Biomasa.

CONCLUSIONES

Las simulaciones demuestran la factibilidad del sistema energético híbrido CSP-TES-biomasa, resultando en un mayor número de horas equivalentes respecto a una planta energética solo CSP-TES y con la reducción en un 30 % de la demanda de biomasa respecto a una simple caldera a biomasa.

En el caso de que la caldera sea diseñada con el objetivo de proveer el 100 % de la potencia eléctrica cuando opera en modo individual, el aumento de las horas equivalentes respecto a un sistema CSP es de alrededor un 70 %.

El rendimiento medio de la planta es un factor que también mejora al integrar la caldera a biomasa al sistema CSP-TES, aumentando la eficiencia en aproximadamente un 70 % respecto a un sistema provisto solamente por el campo solar y el sistema de almacenamiento.

El aprovechamiento combinado de la energía solar y la energía de la biomasa permite una flexible adaptación a la demanda térmica y eléctrica de los usuarios, debido a que la producción de potencia es controlada y gestionada eficazmente.

El rendimiento medio de sistemas energéticos basados en la energía solar y biomasa tienden a mejorar con el incremento de la capacidad eléctrica, como se ha comprobado en plantas existentes.

INDEX

INTRODUCTION

Solar and biomass energy are currently very exploited and developed renewable energies around the world. The concentrated solar power technology, which partially solves the intermittent operation of actual solar thermal plants by its capacity of accumulate the thermal energy has the potential of play a relevant role in the renewable energy development.

A CSP plant is a system that uses mirrors or lenses to concentrate the solar radiation into an absorbing tube. Through this tube flows a heat transfer fluid (HTF) that leads the thermal energy to the power block in order to produce electrical energy. The CSP produces energy at temperatures higher than those possible with flat-plate collectors. This is because the small absorber will have smaller heat losses compared to a flat-plate collector at the same absorber temperature but especially by the concentrated solar radiation.

The main appealing of this technology is the possibility of integrating the solar field with a Thermal Energy Storage (TES) in order to match the electric production to the demand needs, even though no solar radiation is available. A CSP plant integrated with thermal energy storage operates in this way: during daytime the heat produced by absorbed solar radiation is used to supply thermal energy to the power block and the excess of energy is stored. Heat in the storage is then used to produce electricity nighttime, in cloudy days and to cover max electrical production during peak hours.

Generally TES is composed by two tanks, one for the fluid at high temperature and the other for the fluid at a lower temperature. Usually this fluid is a molten salt especially because of its good stability at high temperatures, up to 500 - 600 ° C, which improves the thermal efficiency in the power block and reduces the dimensions of the thermal storage. In the case that the HTF is a molten salt as well, the connection between the solar field and the thermal energy storage system is direct, while if the HTF is synthetic oil, it will be necessary to add a heat exchanger to transfer the energy from the solar field to the storage tank.

The object of this thesis is to simulate and analyzed the performance of a 1 MWe parabolic trough power plant integrated with 10h molten salt thermal storage system and a biomass boiler. The design capacity is equal to 1 MWe because it represents a good compromise between the more diffused sizes of boilers. The project is located in the region of Puglia in Italy due to its excellent solar conditions and the wide availability of olive wood from natural pruning.

For the present work has been carried out a dynamic simulation with an hourly basis in order to make a detailed prediction about the cogeneration plant annual performance. The employed models are TRNSYS and Sam Advisor Model (SAM), the latter used in order to validate the results obtained with TRNSYS. Unlike the rest of the components of the system the biomass boiler model was implemented with MATLAB, and then it was incorporated to the rest of the energy system in TRNSYS.

CHAPTER 1

Fundamentals of Concentrating Solar Power Systems

The increase of the prices of fossil fuels and the concern for global warming, due to CO_2 and greenhouse gases emissions, drives the world into the development of innovative technologies based on renewable energy sources.

One of these technologies is the Concentrated Solar Power (CSP) which is a system that uses mirrors or lenses to concentrate the solar radiation to heat an absorbing tube into which flows a HTF. The CSP produces energy at temperatures higher than those possible with flat-plate collectors. This is because the small absorber will have smaller heat losses compared to a flat-plate collector at the same absorber temperature but especially by the concentrated solar radiation. Thanks to the high temperatures reached by the fluid after the pass through the absorber, between 390º C and 550 ºC depending of the type of HTF, it is possible the conversion of solar to mechanical and electrical energy with an higher efficiency (Duffie & Beckman, 2013).

The conversion of solar to mechanical energy is carried out when the HTF acts like a heat source for a typically Steam Rankine Cycle or an Organic Rankine Cycle (ORC) (see Figure 1). The conversion from mechanical to electrical energy is then carried out when the turbine of the Rankine Cycle is connected to an electrical power generator.
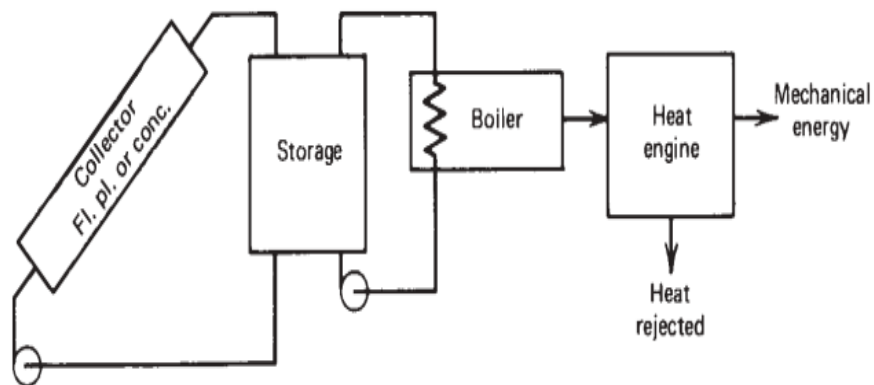
Figure 1. Scheme of conversion of solar energy into mechanical energy (source: Duffie & Beckman, 2013)

The first commercial CSP plant in the world was installed in New Mexico in 1979 by the Sandia National Laboratory (Ragheb, 2011). Since then the CSP technology has been developed exponentially around the world as illustrates Figure 2. The main development has been in Spain and the United States with around 50 and 17 operative plants, respectively, by 2014.
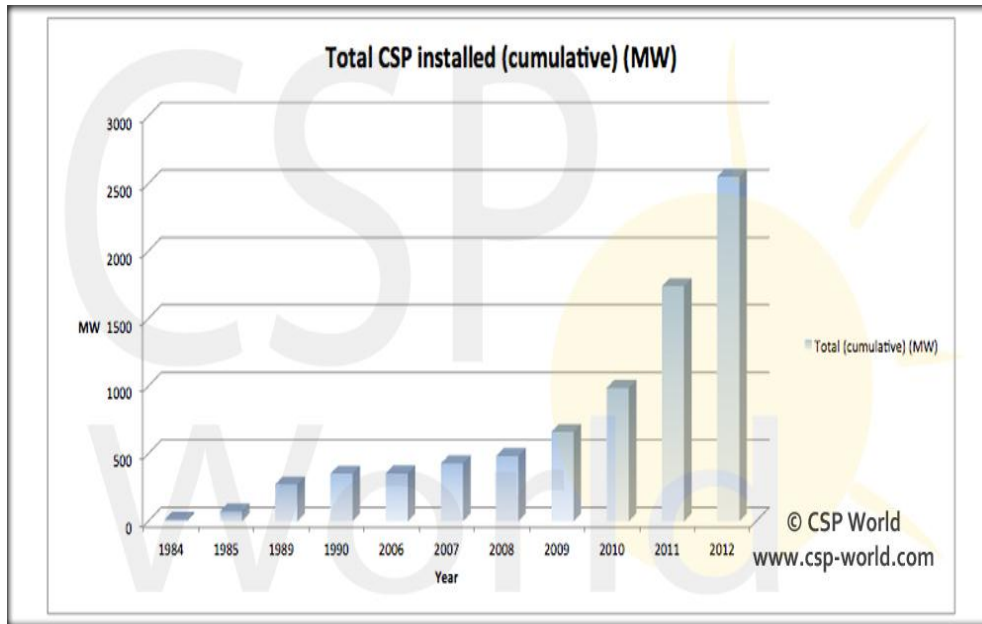
Figure 2. CSP installed capacity in the world between 1984 and 2012 (source: www.csp-world.com).

1.1 Actual technologies of solar concentrating collectors

1.1.1 Parabolic Trough Concentrators

Parabolic trough solar thermal power plants focus solar radiation onto a linear receiver which is located in the focal line of the parabola and through which a HTF flows, increasing its temperature. The selection of the HTF is mainly related to the operating temperatures of the solar field. Some examples of heat transfer fluids are demineralized water, synthetic oils and, more recently, molten salts. In order to maximize the absorption of solar radiation, the reflector follows the sun by tracking on a single axis (Ferrer, 2012).
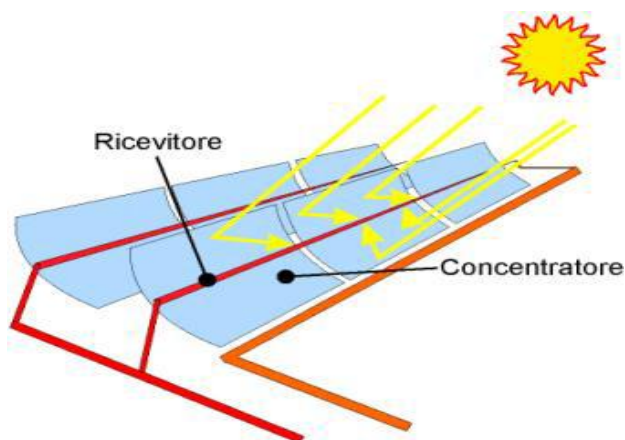
Figure 3. Schematization of the parabolic trough collectors (source: ENEA).

The parabolic trough technology was initially developed during the 80's, with a huge success and support especially in Spain and USA. Since then, the design and the implementation have made significantly progress compared to other solar concentration technologies. By now, this technology is mature and commercially available and the continuous technological improvement and economies of scale have allowed lower plant costs (Ferrer, 2012).

Currently there are approximately 84 parabolic trough power plants in operation, under construction and under development around the world (NREL, 2014). An interesting example is the "Solana Generating Station", a 250 MWe parabolic trough power plant located in USA and one of the largest CSP plants in actual operation. This power plant operates with synthetic oil as HTF, a molten salt thermal storage and a fossil boiler as backup system. The Borges Termosolar in Spain is another interesting example, with an installed capacity of 22 MWe and synthetic oil as HTF, is one of the few plants integrated with biomass boilers. The Saguaro power plant in USA represents one of the few with an Organic Rankine Cycle (ORC) instead of the conventional steam cycle.

Figure 4. Parabolic power plant in the Mojave desert in California (source: DESERTEC-UK).

1.1.2 Fresnel concentrators

The Fresnel concentrator is closely related to the parabolic trough collector, i.e. HTF flows in an absorbing tube that receives all the concentrated sunlight. The main difference between these two technologies is the configuration of the concentrator. The parabolic trough collectors use parabolic reflectors while the Fresnel collectors are composed by a series of large flat mirrors. This latter configuration is characterized by lower first costs, as the flat mirrors are easier and cheaper to manufacture than parabolic mirrors (Ferrer, 2012).
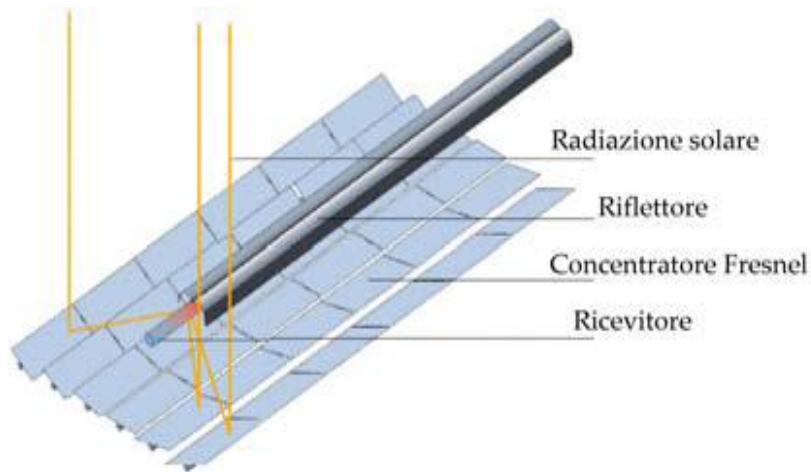
Figure 5. Schematization of the Fresnel collectors (source: ENEA).

Another advantage of the Fresnel configuration is that the collectors can be installed close to the ground and therefore they required simpler supporting structures, with a lower O&M costs, and are affected by less wind speed problems that could cause the shutdown of other CSP technologies.

Despite these advantages, the Fresnel technology is still under development, with very limited commercials examples currently available.

Some of the few operational plants with the Fresnel collectors are the Puerto Errado 1 and 2 (see Figure 6), located in Spain, with an installed capacity of 14 MWe and 30 MWe respectively and both plants use water as HTF. Currently there are some projects under construction and expected to be operative by 2014, e.g. the Alba Nova 1 in France with an installed capacity of 12 MWe, the Dhursar in India with a 100 MWe of installed capacity and the Kogan Creek in Australia, with a capacity of 44 MWe. All these plants use water as HTF (NREL, 2014).

Figure 6. Fresnel power plant in Southern Spain (Puerto Errado 2, source: www.csp-world.com)

1.1.3 Solar tower

Solar power tower plants are based on mobile reflectors which focus direct solar radiation on a receiver located on the top of a tower. The receiver is integrated by a heat exchanger where the HTF warms up and transfers thermal energy to the power block in order to produce electrical energy.
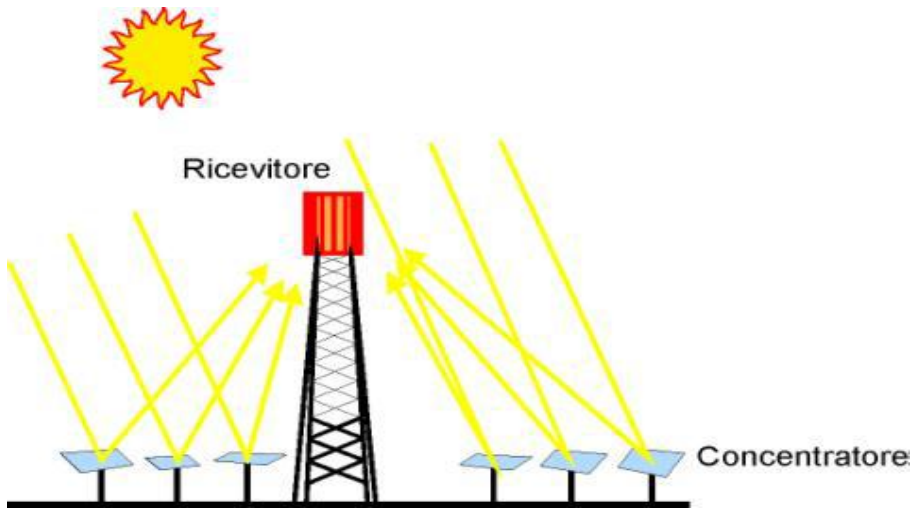
Figure 7. Schematization of a solar power tower (source: ENEA).

Initially, the most common HTF was water/steam, which was directly used in the power block in order to produce electricity in the turbine. Unfortunately, this solution was not very efficient, and molten salts were gradually preferred as HTF for the collection of solar energy, increasing the efficiency of the process and allowing the storage of the heat (Ferrer, 2012).

Despite this technology is characterized by higher efficiency than the parabolic trough technology due to its higher operative temperatures, the solar tower is still a technology under development, while the parabolic trough has a more commercial experience, and consequently lower costs.

Solar power towers are generally big size plants, and require larger availability of land than other CSP technologies, i.e. almost the double size of land than the Fresnel technology. Moreover, solar power tower is not a modular system like Fresnel and parabolic trough technologies.

Some actual existing plants based on the solar power tower technology are the Ivanpah complex (see Figure 8), located in USA. This complex consists of a total of three separate units, Ivanpah 1 with a total capacity of 126 MWe and Ivanpah 2 and 3, each one of 133 MWe. With a total installed capacity of 377 MWe, Ivanpah is the largest solar thermal power tower system in the world. Located in Spain, the Gemasolar Thermasolar plant is the first high-temperature solar receiver with molten salt as HTF, with 20 MWe of installed capacity and a natural gas boiler as backup system. Interest for

the solar tower technology is also notable in Germany, as well as in India and China ([NREL, 2014](#)).

Figure 8. Ivanpah solar tower complex in California, USA (source: Los Angeles Times).

1.1.4 Dish Stirling

The solar dish generates electricity by focusing the solar radiation onto a receiver, which transmits heat to a Stirling engine. The engine is a sealed system filled with hydrogen or other gases such as helium, air or nitrogen. As the gas heats and cools, its pressure rises and falls. The change in pressure drives the pistons inside the engine, producing mechanical power, which drives a generator and converts it into electricity ([Sandia Laboratory, 2008](#)). The reflector tracks the Sun along two axes ([Ferrer, 2012](#)).
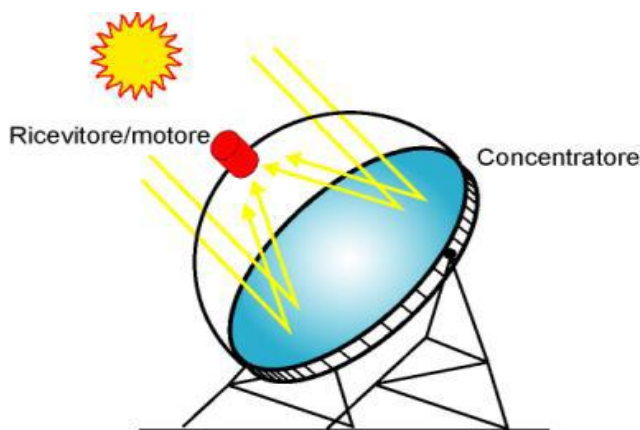
Figure 9. Schematization of a Parabolic Disc Concentrator (source: ENEA).

After the record of 31 % of solar to electricity efficiency reached by ([Sandia Laboratory, 2008](#)) this technology has demonstrated to be the most efficient of all CSP technologies.

The reason of this efficiency is its higher concentration rates that allow achieving very high temperatures.

However this technology is currently the less mature and therefore the few existing plants have been characterized by high first costs and are still not economically competitive with the other CSP technologies.

A 1.5 MWe plant is planned in the city of Tooele in the United States, with helium acting as working fluid. Another project was the Maricopa Solar Project (Figure 10).
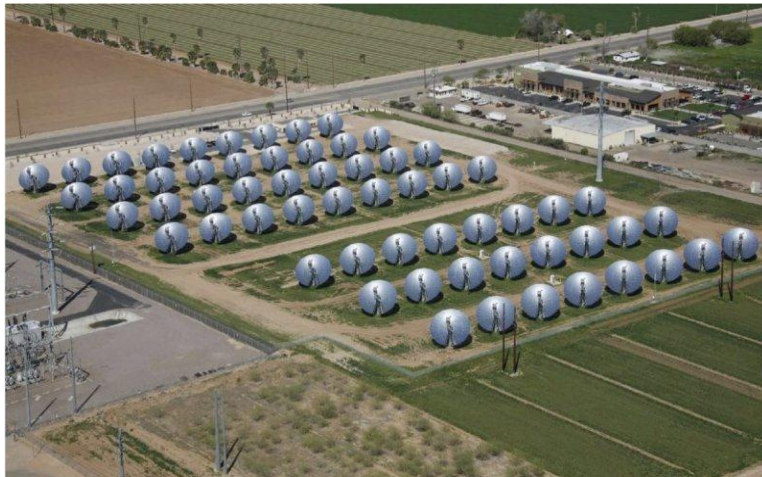
Figure 10. Maricopa Solar Project, USA (source: www.csp-world.com).

1.2 CSP plants in the world

Currently CSP plants in the world are mainly concentrated in Spain and the United States (see Figure 11). Since January 2014, Spain has become the world leader in CSP with a total capacity of 2,204 MW. On the other hand the world's largest solar thermal power plant project currently in operation is located in California's Mojave Desert in the United States; this project has an installed capacity of 377 MW and is based on the solar tower technology.

Interest for the CSP technology is also notable in North Africa and the Middle East, as well as in India and China.

In general the global market has been dominated by parabolic-trough plants, which account for 93 % of CSP plants under operation by 2011 (see Figure 12).

Figure 11 illustrates the location of the currently operational CSP plants worldwide, according to its technology:

- 🔴 Parabolic trough power plants
- 🟣 Solar tower power plants
- 🟢 Fresnel power plants
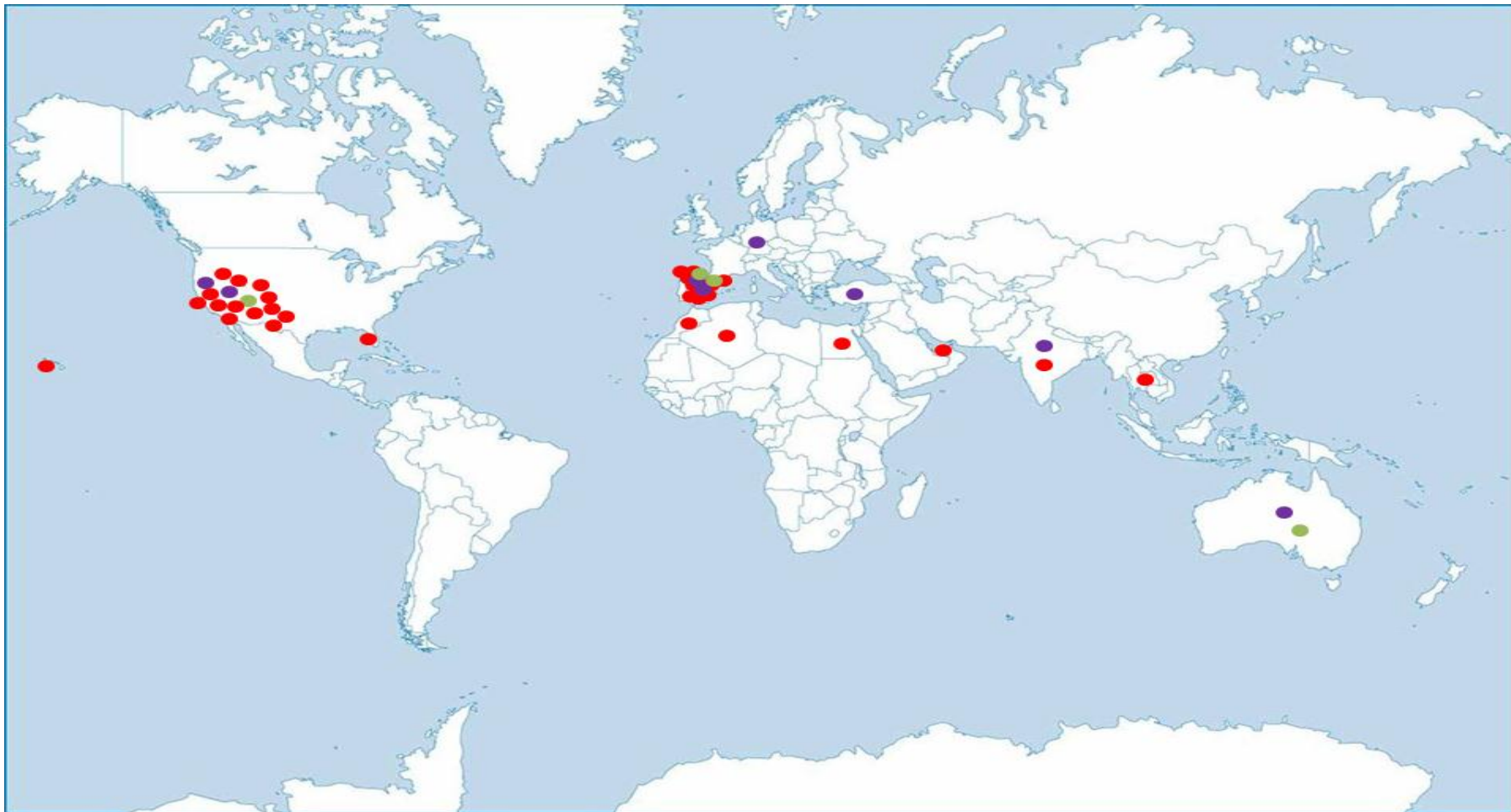
Figure 11. CSP plants location around the world (source: NREL, 2014).
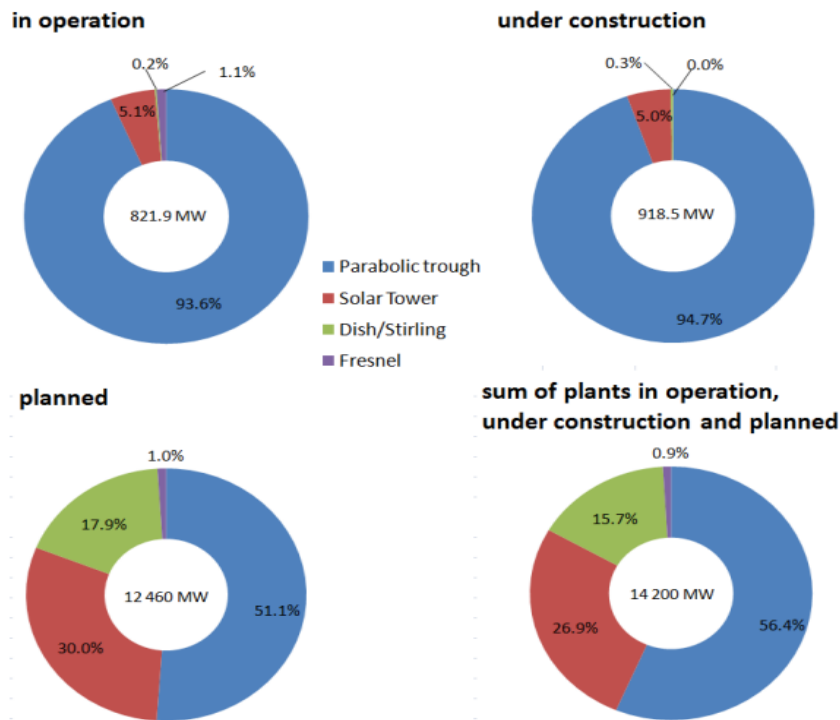
Figure 12. Sum of the CSP plants in operation, under construction and planned for each technology by 2011 (source: Gunther et al., 2011).

1.3 Biomass energy systems

Currently there is a growing interest around the world in the use of biomass as an energy source. This interest has led to various technological developments in the bioenergy field, especially in the biomass combustion, responsible for over 90 % of global contribution to bioenergy.

The type of biomass, the local environmental legislation, the costs and performance of the equipment necessary as well as the energy and capacity required (e.g. heat, electricity) affect the selection and design of the biomass boiler.

Generally large-scale systems use low-quality fuels (with inhomogeneous fuel characteristics concerning, e.g., moisture content, particle size, and ash-melting behavior), and high quality fuels are necessary for small-scale systems (Van Loo et al., 2008).

1.4 Parabolic trough power plants integrated with biomass boilers

In the energy field "Hybridization" is defined as the combination of several energy conversion technologies in one system. In the case of parabolic trough power plants, hybridization is the combination of the thermal energy provided by the solar field with the thermal energy supply by the combustion of fuels (Gunther et al., 2011).

Thanks to hybridization the first solar thermal power plants were able to enter into the renewable energy market, because of a more feasible and attractive system. Today hybridization still appears as a key point in the CSP systems development, a proof of this are the several plants around the world working with fuel boilers as backup system, some examples are the SEGS plants in California equipped with gas-fired boilers.

The backup boiler technology can be fuelled with gas, coal, biofuels, waste, etc. However, liquid and gaseous fuels are more suitable than solid fuels since the earliest allow a faster control and, therefore, they are more appropriate for quick changes in the radiation conditions.

In the case of parabolic trough power plants not equipped with a thermal storage the power is generated just when direct solar radiation is available, thus, the plant capacity factor is quite low. Some of the CSP plants integrate a backup system in order to increase its capacity factor generating electricity during night hours, peak hours, and cloudy days. Moreover, backup heaters can improve the power block efficiency if they are used to run the power plant more frequently at its rated power.

There are different options how to integrate a backup system into a parabolic trough plant. One option is that the backup heater heats directly the water/steam of the steam cycle. Another option is the integration of the backup heater into the solar field cycle. In the first option, the backup is quite independent from the solar field. The second option has the advantage that the backup heater can be used additionally to protect the heat transfer medium against freezing.

Figure 13 shows both integration options.
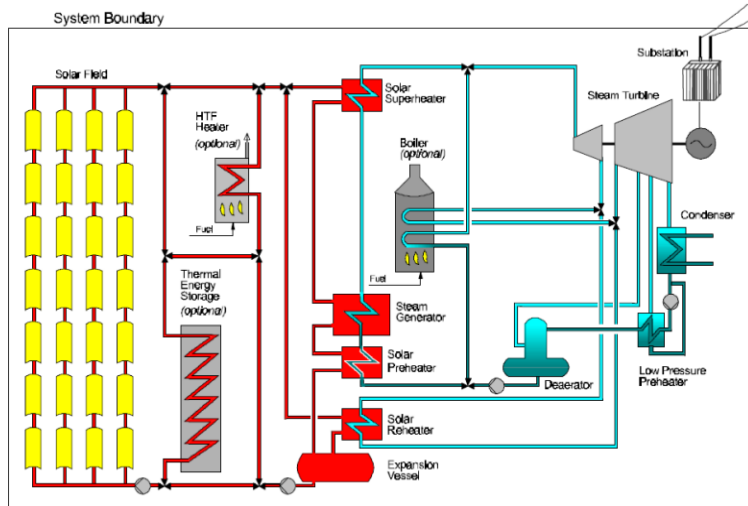
Figure 13. Parabolic trough power plant integrated with fossil fuel boilers as backup system (source: Gunther et al., 2011)

The implementation of a backup system and a thermal storage into a parabolic trough power plant makes possible to supply the entire power requested reducing the quantity of burned fuel. The daily power generation of the described system can be established according to Figure 14.
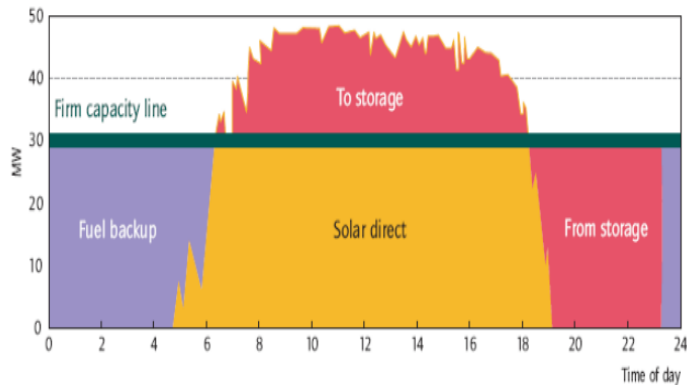
Figure 14. Daily power generation of a parabolic trough power plant integrated with thermal storage and a fuel heater as backup system (source: Gunther et al., 2011).

Although the majority of the actual CSP plants are hybridized with fossil fuels boilers there is a growing interest for the hybridization with renewables technologies, in order to reduce the environmental impact.

The Borges Termosolar project is a 22.5 MW hybrid parabolic trough – biomass plant being built in the North-East of Spain and it is the first commercial plant of its kind. The biomass boiler is integrated in the solar field cycle where it heats the HTF and it is fuelled by a combination of waste forest biomass (NREL, 2014). The entire plant layout is shown in Figure 15.
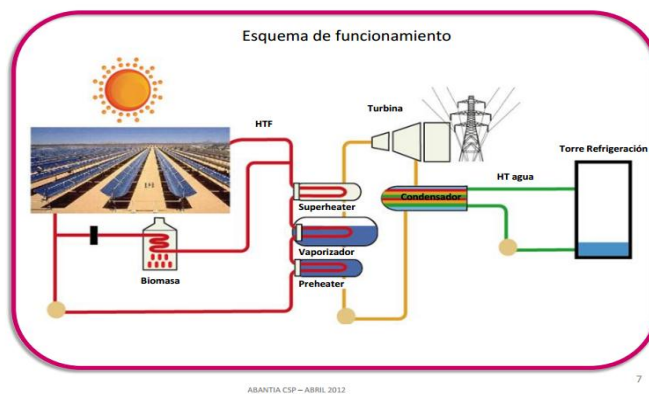
Figure 15. Scheme of the Borges Termosolar project (source: Abantia, 2012).

During normal operation with adequate availability of solar energy, Borges Termosolar plant converts solar radiation into electricity without other energy sources. If sunlight decreases for short periods (e.g. because of clouds) the gap in the thermal energy required to guarantee the nominal power is supplied by a natural gas backup boiler, while during

long periods of absence of solar radiation (e.g. during nighttime), thermal energy is provided by the biomass boiler.

Abantia, the principal developer of the Borges Termosolar project, affirms that "The CSP has great potential as the possibility of being hybridized. Moreover, the overall efficiency needs to be increased to increase the competitiveness of these plants in the renewable energy market" (Abantia, 2012).

Hybridization is very important also for a better management and O&M of the plant, since it allows a continuous electric energy production, also without or with poor solar irradiation, getting a plant operation exceeding 6,500 hours/year. Moreover, the solar field can be smaller, involving lower land use in comparison with solar only mode CSP plants with the same electric capacity (Abantia, 2012).

Some studies have been made in order to confirm the feasibility of hybridized CSP plants with biomass, e.g. Narvaez et al. (2013) have studied the viability of a solar thermal plant hybridized with biomass derived from the olive oil waste in Southern Spain, and have concluded that a minimum power plant capacity of 10 MWe is required in this location, in order to achieve an optimal utilization of biomass for hybrid electricity generation.

Nixon et al. (2012) have assessed the feasibility of hybrid solar-biomass power plants in India and for various applications including tri-generation, electricity generation and process heat.

Peterseim et al. (2014) have studied the possibility of improving the solar parabolic efficiency in hybrid plants integrated with biomass boilers. Hybrid plants can potentially reduce the cost of CSP but also have the potential to move CSP out of remote/arid into agricultural regions where biomass material is available.

Angrisani et al. (2013) have studied a new configuration for the CSP-biomass plants. This new configuration is based in a normal biomass combustion conducted using a fluidized bed combustor. This fluidized bed acts also as solar receiver when the solar direct irradiation is directed by a Scheffler type mirror. Then a Stirling engine integrated into the fluidized bed converts heat into electricity.

A model has been developed by Dominguez et al. (2014) which consider a fully renewable system, based on CSP plant with storage, and with wind and biomass power plants.

1.5 Environmental impact

Unlike traditional thermoelectric plants, parabolic trough power plants operating in the solar only mode does not produce any type of pollutant emission to the atmosphere. In the case of a CSP plant integrated with a biomass boiler the emissions are far less in comparison with the emissions produced by a coal backup system.

Table 1 lists the CO_2 production according to the burned fuel. The larger quantity of CO_2 is generated by the coal power plant with 1028 gr/kWh while the biomass power plant generates only 85 gr/kWh. These emissions are mainly related to the process of the collection and preprocessing of the biomass since the CO_2 emissions generated during the combustion are equivalent to the absorbed atmospheric carbon during the biomass life cycle.

Table 1. CO$_2$ emissions in a thermoelectric plant according to the fuel (source: Moreno, 2010)

Fuel	Thermoelectric plant emissions (gr CO$_2$/kWh)
Coal	1028
Fuel Oil	778
Biomass	85

1.5.1 Impacts during the power plant construction

The impacts associated with the construction process are equivalent to those that would occur in any civil project. They imply among atmospheric emissions, transport workers and materials.

1.5.2 Visual Impact

This impact is due, primarily, to the large area occupying by the parabolic trough collectors. This impact can be reduced by placing the plant away from residential areas and avoid to construct in areas considered as esthetic landscapes.

1.5.3 Water Resources

In a parabolic trough power plant the requirement of water is mainly for two purposes. The first is the cleanliness of the solar collectors and the second the refrigeration of the power block. In desert locations where the water availability is limited the impact in the water resources is more remarkable but also where the water is available there is the eventual impact of thermal contamination of rivers and seas, altering the balance of the living ecosystems.

1.6 Social Impact

The construction of a solar plant requires a lot of labors, which can be supplied by local people. It should be remarked that the number of staff required for the installation of this type of plant is higher than that needed for the case of a thermoelectric plant (Moreno, 2010).

It is estimated that professionals for the manufacturing stage of the CSP plant and building is about 1000 men a year. Furthermore, depending on the power plant size, other jobs are generated for the operation.

The construction of a solar thermal plant can help the development of the economy of the chosen location. The main contribution is related to the direct local employment due to the construction of the plant and the maintenance tasks to be performed throughout its lifetime, i.e. the cleaning of the solar collectors. Additionally, there is an activation of the local industry, which indirectly promotes the local employment.

CHAPTER 2

Analysis of the components of the power plant

2.1 Parabolic trough collector

2.1.1 Structure of a parabolic trough collector

- **Geometrical parameters of a parabolic trough**

Commonly the form and size of a parabolic trough collector is characterized according to the following four parameters: trough length, focal length, aperture width, i.e. the distance between one rim and the other, and rim angle, i.e. the angle between the optical axis and the line between the focal point and the mirror rim.
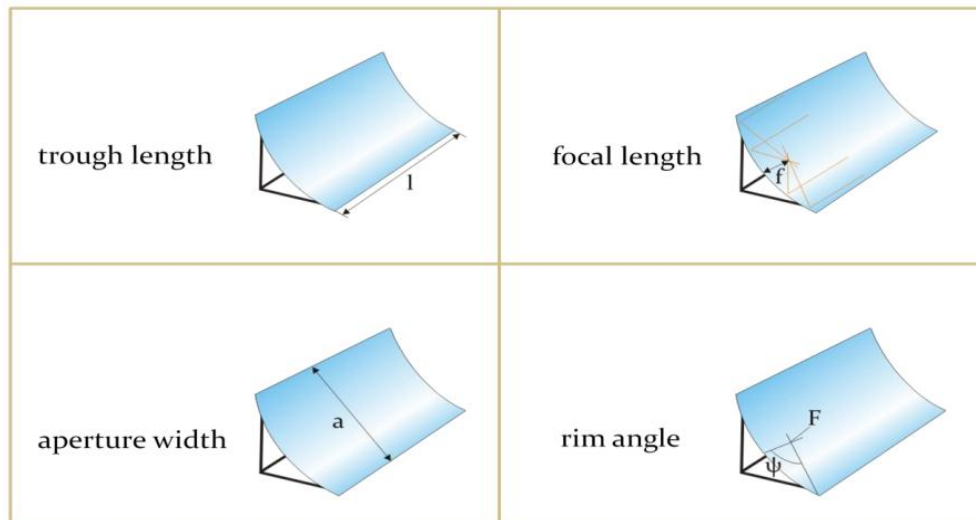
Figure 16. Geometrical parameters of a parabolic trough collector (source: Gunther et al., 2011).

The focal length is defined as the distance between the focal point and the vertex of a parabola. This parameter describes the parabola completely since is the only present in the mathematical expression of a parabola:

$$y = \frac{1}{4f} x^2 \qquad\qquad \textbf{Eq. 1}$$

Where f is the focal length.

The rim angle is a very significant geometrical parameter of parabolic trough collectors. For instance, it has an effect on the concentration ratio and on the total irradiance per meter absorber tube [W/m]. Qualitatively, the rim angle should neither be too small nor too large; actually there must be some ideal rim angle range. This

parameter is correlated to the distance between the different parts of the parabola and its focal point, as clarified by the following figure:
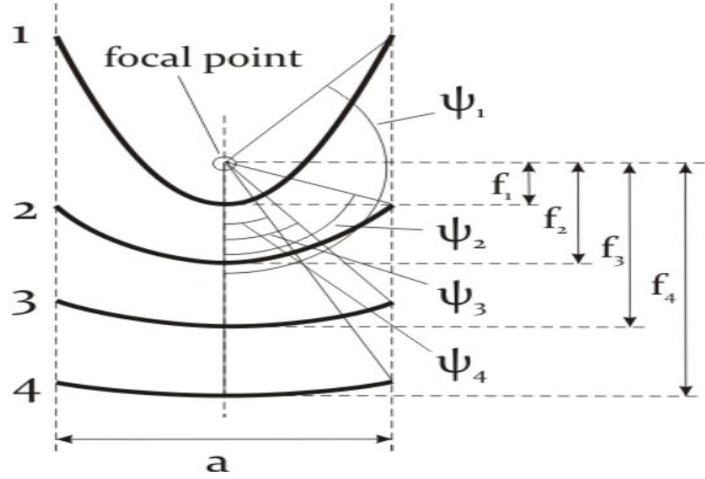
Figure 17. Relation between the focal length and the rim angle (source: <u>Gunther et al., 2011</u>).

- **Mirror area and aperture area**

There are also other important constructive measures that define the size of the parabolic trough. One of these is the aperture area of the collector, which determines at a given DNI and a given Sun position the radiation capture. The aperture area of a parabolic trough is defined by the following equation:

$$A_{ap} = a * l \qquad \text{Eq. 2}$$

Where a is the aperture width and l is the trough length.

The surface area of a parabolic trough may be important to determine the material need for the collector. The area is calculated as follows:

$$A = \left(\frac{a}{2} \sqrt{1 + \frac{a^2}{16f^2}} + 2f * \ln\left(\frac{a}{4f} + \sqrt{1 + \frac{a^2}{16f^2}} \right) \right) * l \qquad \text{Eq. 3}$$

- **Concentration ratio**

The punctual concentration ratio C describes the relation between the radiant flux density at one point of the receiver G_{im} to the direct irradiance at the aperture of the collector $G_{b,ap}$. The concentration ratio is a fundamental characteristic of a parabolic trough collector since it indicates how much of the solar energy is been utilized for heating the HTF.

$$C = \frac{G_{im}}{G_{b,ap}} \qquad \text{Eq. 4}$$

Since the punctual concentration ratio only describes one point of the receiver, in the practice it is substituted by the geometrical concentration ratio C_G. This new parameter is a useful approximation that allows specifying the concentration ratio of the collector through a more easy calculation. It is defined as the ratio of the collector aperture area to the receiver aperture area.

$$C_G = \frac{A_{ap,c}}{A_{ap,r}} \qquad \text{Eq. 5}$$

Where $A_{ap,c}$ is the collector aperture area and $A_{ap,r}$ is the receiver aperture area.
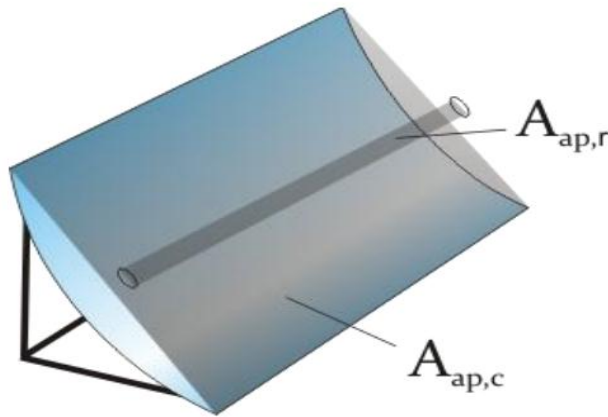
Figure 18. Collector and receiver aperture area (Source: <u>Gunther et al., 2011</u>).

Some references estimate the receiver aperture area as $d * l$ where d is the absorber tube diameter. In this case the concentration ratio will be:

$$C_G = \frac{a*l}{d*l} = \frac{a}{d} \qquad \text{Eq. 6}$$

Another possibility is to take the receiver aperture area as the receiver tube surface. In real parabolic troughs this would mean that the whole absorber tube area $pi * d * l$ is the receiver aperture area. The concentration ratio is, then:

$$C_G = \frac{a*l}{d*l*pi} = \frac{a}{d*pi} \qquad \text{Eq. 7}$$

This definition would lead to a lower geometrical concentration ratio. However, the concentration ratio according to the projected areas is more commonly used.

2.1.2 Mirror material in parabolic trough collectors

The principal characteristic of a material for been considered as a suitable mirror material is a high reflectivity. This property is defined as the fraction of the incident radiation that is reflected by the surface and depends on the wavelength. In this case the solar spectrum is of interest. Furthermore, the reflectivity can be distinguished in specular reflection and diffuse reflection. In CSP applications, only specular reflectivity is of interest, because the reflected radiation must have a defined direction. The decisive quality criterion for efficient mirrors is, hence, the "solar weighted specular reflectivity".

Currently the most used mirrors for the parabolic trough collectors consist of silver coated glass mirrors. There are experiences with these mirrors since the first parabolic trough power plants were built in the 1980s. The mirrors have proven to be durable: even after more than ten years of operation they hardly showed any decrease in specular reflectivity.

The silver coated glass mirror is formed by a multilayered structure. The first layer is constituted by a glass, especially low-iron glass in order to increase the light transmission in the solar spectrum. The next layer after the glass is the silver coating or the reflective material (see Figure 20) and below this are the protective layers composed by copper and three varnishes. At the end the thickness of the complete mirror amounts to 4 to 5 mm. Figure 19 illustrates the multilayered structure.
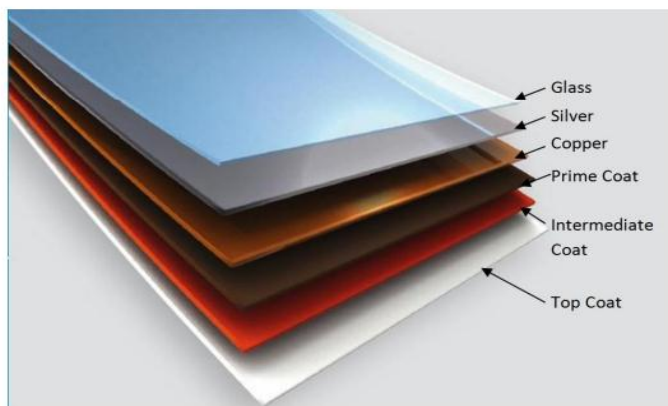
Figure 19. The multilayered structure of the parabolic trough mirror (source: Gunther et al., 2011).

18
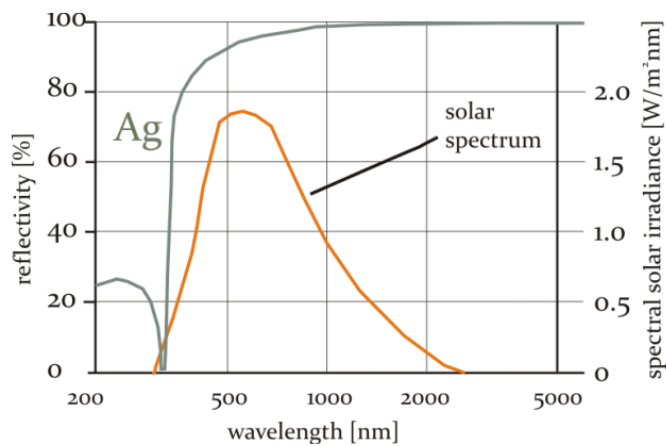
Figure 20. Silver reflectivity in the solar spectrum (Source: Gunther et al., 2011).

2.1.3 Bearing structure

A suitable bearing structure for a parabolic trough collector has to comply with the following requirements: stiffness and lightweight at the same time. The first will provide stability to the collector allowing an exact sun tracking and will also protect the collector from any deviation due to the wind loads. The second is required to avoid the deformation of the collector by its own weigh as well as to allow the usage of weaker foundations and tracking mechanisms.

Obviously while less material and manufacturing costs involve the bearing structure better. It has to be taken into consideration that the solar field is the most expensive part of a parabolic trough power plant and in some cases as the Andasol power plants in Spain the solar field covers 30% of the total costs. Therefore a cost reduction of the solar field has an important effect on the total power plant costs.

Usually the bearing structure is design as a space frame or a tube structure made out of steel or aluminum. Some of the elements of the total structure are:

- Mirror support points on the space frame structure or on special cantilever arms;
- Receiver support, also called heat collection element (HCE) support;
- Structure for the mounting to the pylon;
- Pylons and foundations.

19

Figure 21. Space frame structure of a Eurotrough collector module (source: <u>Gunther et al., 2011</u>).

2.1.4 Sun tracking system

The parabolic trough collectors as any of the CSP technologies need to follow the sun in order to reach a continuous concentration of the direct solar radiation.   Since the parabolic trough is a linear concentrating collector, the tracking system is implemented in just one axis, which depends on the collector orientation.

Figure 22 gives a general idea of the tracking system of a parabolic trough.
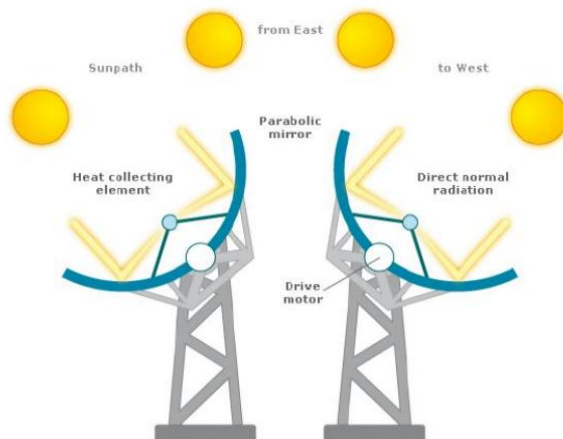
Figure 22. Single axis tracking of parabolic troughs from East to West (source: <u>Gunther et al., 2011</u>).

There are two possible collector orientations, the North-South alignment with the respective East-West tracking or the East-West alignment with the respective North-South tracking. According to the collector orientation will be specified the equation of the tracking angle:

- For a North-South alignment the tracking equation is defined as follows:

$$\tan s = \tan \theta_z * \ abs \ (\cos(\gamma - \gamma_s))$$ Eq. 8

Where s is the zenith angle of the collector, θ_z is the solar zenith angle, γ_s is the solar azimuth angle and γ is the azimuth angle of the collector. γ can have only two values: γ = -90° if γ_s < 0° and γ = 90° if γ_s >0°. This means that the mirror aperture is oriented to the East in the morning and to the West in the afternoon.
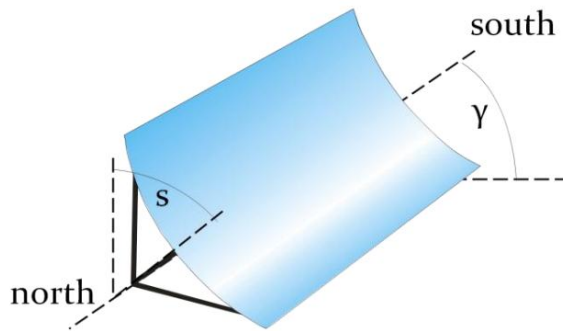
Figure 23. North-South collector orientation and solar tracking from East to West (source: <u>Gunther et al., 2011</u>).

- In the case of the East-West alignment, the tracking angle is determined as follows:

$$\tan s = \tan \theta_z * abs \ (\cos \gamma_s)$$ Eq. 9

For γ, the following determination holds: γ = 0° if $abs(\gamma_s)$ < 90° and γ = 180° if $abs(\gamma_s)$ > 90°, which means that the mirror aperture is oriented to the South if the Sun is South of the East-West line and to the North if the Sun is North of the East-West line (what happens on the Northern hemisphere between spring equinox and autumn equinox in the early morning, before 6:00 solar time, and in the late evening, after 18:00 solar time).
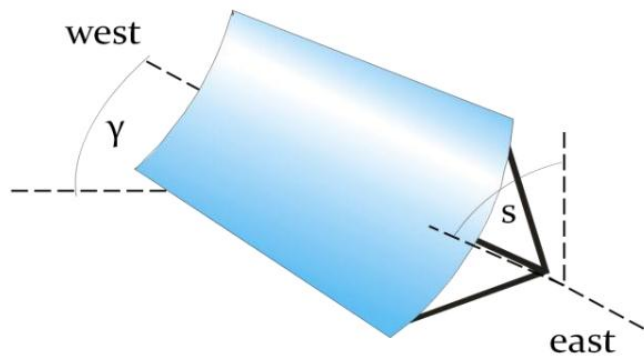
Figure 24. East-West collector orientation and solar tracking from North to South (source: <u>Gunther et al., 2011</u>).

Mechanically, the drive unit can be realized as a motor-gearbox unit or as an electro-hydraulic system which consists of two cylinders, which are controlled by two valves, determining the direction of rotation. Dependent on the location of the collector in the solar field, the cylinders differ in size. The collectors at the border of the solar field need a stronger hydraulic drive, and consequently bigger cylinders, because they have to withstand higher wind loads than the collectors in the center of the solar field.

In order to know the exact position of the Sun there are two used mechanisms. The first is calculating it through a mathematical algorithm and the second is measuring the sun position by sensors that give a signal to the local controller which operates the tracking system.

Furthermore, there is a sensor that registers the meteorological conditions as the wind speed in order to ensure the collectors protection. In the SEGS plants after 9 m/s the tracking accuracy is compromised but it is still possible to operate the power plant until wind speeds between 16 and 20 m/s. After this value the operating condition is too dangerous and it is preferred to move the collectors to a safety position, which is nearly the vertical position, with a slight inclination of the mirrors to the bottom. During the night, the collectors are also in the safety position.

2.2 Receiver

The receiver of a parabolic trough collector is the tube located in the focus of the parabola that has the function of maximizing the absorption of solar radiation and heating the HTF. The principal requirements of a receiver tube are to improve the radiation absorption and minimize the optimal and thermal losses. For this reason special coatings and thermal insulation are applied.

Currently the principal receiver producers are the German Schott AG, the German Siemens AG and the Italian Archimede Solar Energy (ASE). The first two have developed receivers with oil as HTF; therefore the receivers are designed for an operation temperature of 400°C. On the other hand, ASE has developed a receiver for molten salt as heat transfer fluid, designed for a maximum operation temperature of 580°C.

Figure 25. Receiver tube prototypes. Above left: Siemens. Below left: Archimede. Below right: Schott (source: Gunther et al., 2011).

2.2.1 Receiver components

The receiver structure is projected in order to achieve the maximum radiation absorption and the minimum heat losses. Figure 26 illustrates the specific receiver components
.

Figure 26. Receiver tube components (Source: Gunther et al., 2011).

- **Absorber tube**

The absorber tube maximized the absorption of the solar radiation and minimizes the irradiative heat losses. In order to comply with these specifications, the tube absorptance must be high for the solar spectral range ($250\text{nm} \leq \lambda \leq 2500\text{nm}$), and the emissivity must be low for the infrared range ($3000 \text{ nm} \leq \lambda \leq 50000 \text{ nm}$). Special coatings have been analyzed to reach this goal.

Nowadays absorber tubes are made of three layers, the most external consists of an antireflection ceramic layer like Al2O3 or SiO, the medium layer is made out of a metal and ceramic combination (cermet) and the most internal layer is composed by a reflection layer made out of a metal that is highly reflective in the infrared range, for instance copper, aluminum or molybdenum.
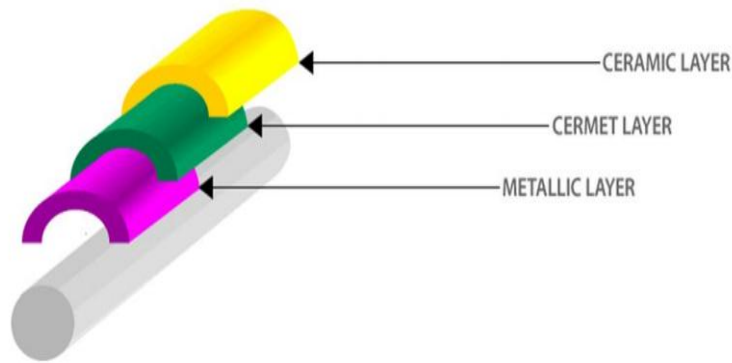
Figure 27. Structure of the absorber tube (Source: Gunther et al., 2011).

The reached values for the absorptance are between 0.95 and 0.96 for the solar spectrum. The emissivity is in the range of 0.1- 0.15 depending on the design temperature. It is important to highlight that the higher the temperature, the more difficult is the design of an efficient selective coating because there is a larger overlap of the thermal emission spectrum and the solar spectrum. Already at 400°C there is a non-negligible spectral overlap in the range of 1500 to 2500 nm.

The absorber tube diameter has to be larger enough for a high intercept factor, which is defined as the ratio between the total reflected radiation and the reflected radiation that hits the absorber tube. On the other hand, the absorber diameter should not be too large to minimize the thermal losses. An optimization procedure has to be carried out in order to find the optimal absorber tube diameter.

Most of the receivers produced by the three mentioned companies have an absorber tube diameter of 70 mm and a glass tube diameter of 125 mm.

- **Glass tube**

The glass tube must separate the absorber tube from the external air in order to reduce the convective and conductive heat losses. Additionally, the gap between the absorber tube and the glass envelope is made under vacuum, so that the convective and conductive heat losses are further reduced.

Usually the glass tube is made out of borosilicate glass, a material characterized by a high solar transmittance, in the order of 0.92. Additionally the glass tube is covered by a special antireflective coating to increase the transmittance by 0.04, from 0.92 to 0.96.

The glass tube also contributes to maintain the emitted thermal radiation by the absorber inside the tube, since the borosilicate glass has a low transmittance in the infrared range. The transmittance of the borosilicate glass is illustrated in Figure 28.
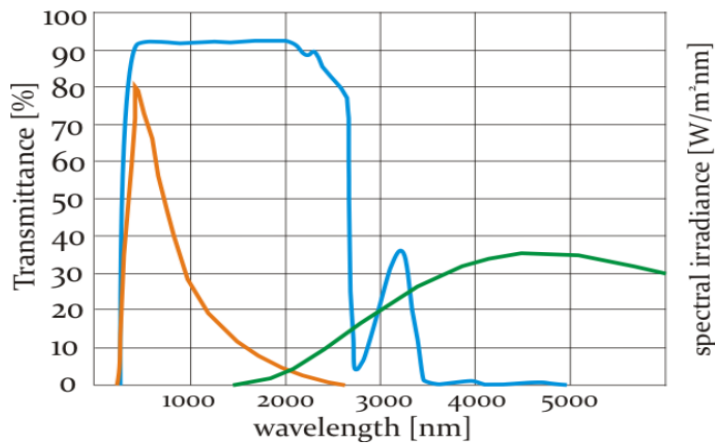
Figure 28. Transmittance of the glass tube (blue line) in the solar spectrum (orange line) and the infrared range (green line) (Source: Gunther et al., 2011).

2.2.2 Receiver efficiency

The receiver efficiency is defined as the fraction of the radiant flux projected onto the receiver that is converted into useable thermal energy. The receiver efficiency decreases with the thermal and optical losses as is illustrated in Figure 29.
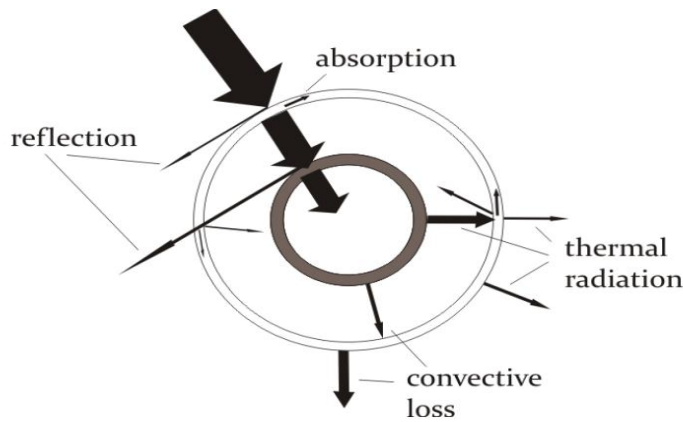
Figure 29. Energy flows at the receiver (Source: Gunther et al., 2011).

- **Optical losses**

The optical losses are produced at the glass tube as well as at the absorber tube. As mentioned the glass tube has a transmittance of 0.96, thereby the rest 0.04 is lost due to the reflection and the absorption. In the same way the absorber tube has absorption of around 0.95, therefore the remaining 0.05 is also lost. Additionally there is a reduction of the active receiver area due to the bellows and the metal shields, this reduction can be assumed as 3.6 % (Siemens). Hence the equation of the fraction of energy lost is as follows:

$$\frac{Q_{loss,opt}}{A_{rec,act}*G_{rec}} = 1 - (1 - 0.04) * (1 - 0.05) * (1 - 0.036) = 12.1\ \% \qquad \textbf{Eq. 10}$$

Where G_{rec} is the irradiance on the active surface of the receiver.

- **Thermal losses**

The thermal losses are generated by the temperature difference between the absorber tube and the surrounding air. From the absorber tube to the glass tube the radiative heat loss dominates because of the high tube temperature and because of the vacuum which minimizes convective and conductive losses. On the other hand, the heat losses from the glass tube to the ambient are mainly convective due to the quite small temperature difference with the environment and to the freely movement of the air around the glass tube.

A quantification of the different heat loss processes and their share in the total heat loss is not possible without taking into consideration several boundary conditions as, most importantly, temperature differences, absolute temperatures, wind conditions and air humidity.

Some experiments at ambient temperature (23 ºC) and without wind have resulted in the following relation (Gunther et al., 2011):

$$\boldsymbol{Q_{loss,therm}} = \boldsymbol{0.26 * \varDelta T + 1.05 * 10^{-8} * \varDelta T^4} \qquad \left(\frac{W}{m}\right) \qquad \textbf{Eq. 11}$$

Where ΔT is the difference between the HTF temperature and the surrounding air temperature.

2.3 Solar field

The solar field results from the arrangement of the collectors in the solar power plant. The orientation, the structure and the size of the solar field will be discussed in this section.

2.3.1 Solar field orientation

A solar field composed by parabolic trough collectors can have any of the following orientations: the North-South alignment with the respective sun tracking from East to West and the East-West alignment with the respective North-South tracking. However the preferred orientation in commercial CSP plants is the North-South alignment, while the East-West alignment has been applied only for experimental purposes.

The advantages and disadvantages of each orientation depend on the power plant latitude. For locations with latitude between 40º and 15º North the following holds:

Table 2. Differences between the East-West and the North-South alignment in locations with latitude within 40º and 15º (source: Gunther et al., 2011).

East-West alignment	North- South alignment
Smaller tracking movements are required during the day.	Higher tracking movements are required during the day.
Lower annual energy yield.	Higher energy yield.
Smaller differences of energy yield between summer and winter. The incidence angles on the collector do not change with the season.	Larger differences of energy yield between summer and winter. The incidence angles in winter are bigger than in summer.
The collector performance over the day is quite uneven. After and before noon the collector performance is reduced due to the large incident angles while in the noon the full aperture always faces the Sun, i.e. the incidence angle is zero.	The collector performance over the day is quite even. Generally, the incident angle is higher at noon than in the morning and evening and tends to compensate, hence, the different DNI conditions.

Figure 30 illustrates the performance of a collector oriented in the North-South alignment and one oriented in the East-West alignment. For a location at 30º North latitude the irradiation on the collector aperture will be illustrate in a summer solstice, equinox and winter solstice. From the area below each curve it is possible to notice that the annual energy yield is larger for the North-South alignment than for the East-West alignment.
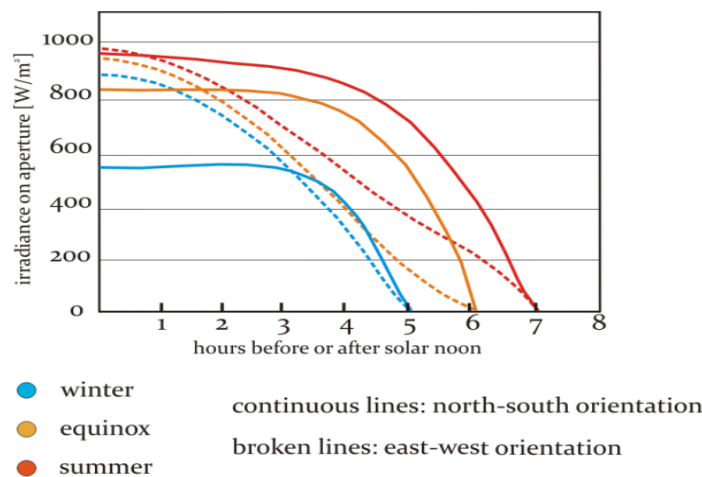
Figure 30. Irradiance on the collector aperture for both parabolic trough orientations, at different seasons (source: Gunther et al., 2011).

27

2.3.2   Typical configuration of the solar field

Solar field are generally structured in a nearly square form with the power block in the center as illustrated in Figure 31. This configuration is mostly chosen in order to keep a reasonable distance between each loop of the solar field and the central power block in order to reduce thermal and pumping losses.

The pipes that lead the HTF from the power block to the solar field and reverse are called heaters. There are two pipes of heater, the cold one and the hot one, if the HTF is leaving the power block passes through the cold heater to reach the solar field while if the HTF is already heated and have to reach the power block it passes through the hot heater.
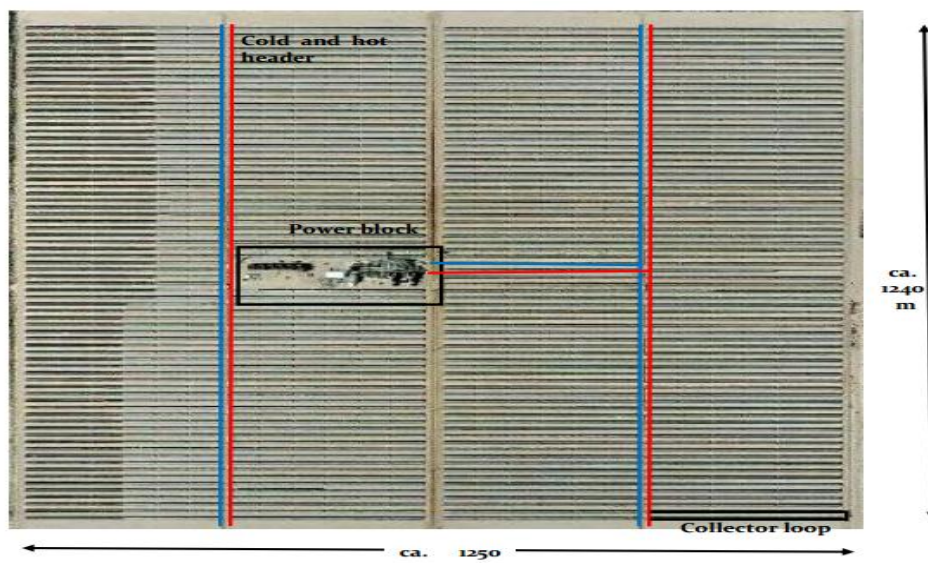
Figure 31. Solar field layout of SEGS VIII and SEGS IV (source: Gunther et al., 2011).

The collector loop is connected, to one end, to the hot heater and, to other end, to the cold heater as illustrates Figure 32.
.
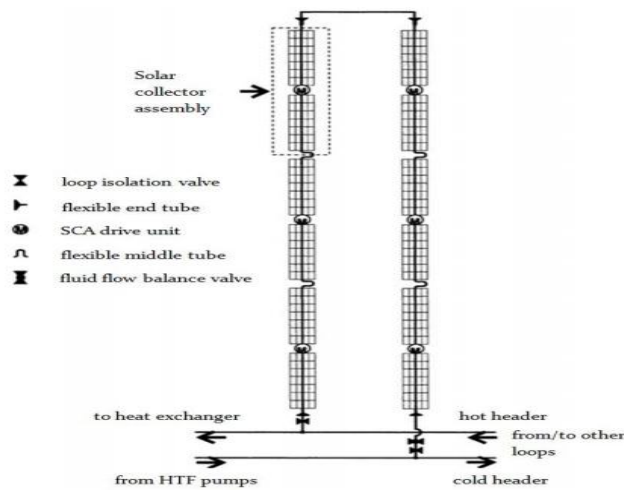
Figure 32. One collector loop, composed by 6 Solar Collector Assemblies, connected to the heaters (source: Gunther et al., 2011).

Usually the length of a loop of collectors is around 600 m. This means that the HTF has to flow this length before reaches its set point temperature.

The distance between collectors' rows needs to be optimally estimates, since if it is too small then the shading effect reduces the solar field performance and if it is too large the cost investment increases as well as the thermal and pumping losses. A good distance is considered as three times the aperture width of the collector (Gunther et al., 2011).

2.3.3 Sizing the solar field

The total solar field ground area is the sum of the total collectors' aperture plus the area between collectors' rows, the area occupied by the pipes, by the power block and by the storage tanks. At the end the solar field ground area amounts to about 3.5 to 4 times the collectors' aperture area. An example is the Andasol plants which have an aperture area of 0.51 km and a power plant ground area of 2 km.

The aperture area has to be carefully estimated, if it is too small the power plant will operate always at partial load, thus decreasing its efficiency, if it is too large will happen more frequently that thermal energy from the solar field cannot be used in the power block and has to be dumped.

The following equation approximates roughly the aperture area for a CSP plant.

$$A_{ap} = \frac{P_{el}*SM}{\eta*G_{b,ap}} \qquad \textbf{Eq. 12}$$

Where P_{el} is the electric power plant capacity, SM the solar multiple, η the solar-to-electric efficiency and $G_{b,ap}$ the direct irradiance (at the design point) on the collector aperture area.

The solar multiple is the factor by which the solar field is amplified. A solar field with SM = 1 has the size to supply the required energy at the design irradiance

conditions. A solar field with SM = 2 has the double solar field size of a power plant with SM = 1 and will supply the required energy when the direct irradiance halves the design point. An economic optimization has to be carried out in order to find the optimal solar multiple.

2.4 Heat Transfer Fluid (HTF)

2.4.1 Synthetic thermal oil

Currently the most widely used HTF is the synthetic oil despite of its high cost and hazardous characteristics. The oil has been used for more than 25 years as HTF in parabolic trough power plants, some examples are the Andasol I, II, III, Nevada Solar One, SEGS, etc.

Typically the synthetic oil used in the CSP plants is Therminol, an eutectic mixture of biphenyl/diphenyl oxide. The oil is considered a suitable heat transferred fluid thanks to its high thermal conductivity, high specific heat and low consumption of pumping due to its low viscosity.

On the other hand, the synthetic oil has some disadvantages like instability at high temperatures. The maximum heating temperature of the oil is typically less than 400 °C; above this temperature thermal cracking occurs. Another problem is that oil must be kept under pressure. At 393 °C the oil has a high vapor pressure and to avoid this, the solar field has to be pressurized between 20 bars and 40 bars, which require a careful design of the parabolic trough collectors. Furthermore it is necessary a system of protection against the oil freezing at a temperature of 15 ° C, which is activated occasionally during the winter nights. Additionally the thermal oil is harmful, toxic, flammable, polluting and quite expensive (2 €/kg, about 5% of the investment costs for the Andasol power plants). Due to its high cost and high vapor pressure it is not convenient as a storage fluid. Thermal oil has to be replaced periodically because of aging processes (i.e. the chemical structure changes over longer time spans) and is environmentally less friendly than some other possible media; thereby, leakages are not only a problem for the plant operation but also for the environment.

2.4.2 Molten salt

Molten salts are very attractive heat transfer fluids as they are generally cheaper than thermal oil and stable up to 500 - 600 ° C (Palmieri, 2010). Consequently the temperature of operation of CSP plants can reach greater values than thermal oil. This increase in operative temperature level is favorable for both the power block and the Thermal Energy Storage as it improves the power block efficiency while the high temperatures in the thermal storage allow accumulating more energy in lower volumes.

Molten salts are non-toxic, non-flammable and does not pollute. Furthermore, the vapor pressure is very low even at high temperatures; therefore, the operative pressure is only a few bars in order to preventing the infiltration of air in the pipes or tanks. The usage of molten salt as HTF also allows the integration of a direct storage system into the power plant.

The main drawback of molten salt is its high freezing temperature, ranging between 120 °C and 220 ºC. Freezing must be avoided in order to prevent damage in other equipment. Furthermore the fusion of the molten salt is quite complex. The CSP plants that use molten salt employ protection systems against freezing and are equipped with molten salt defrost systems. In addition, molten salts are corrosive and may potentially damage valves, pipes, pumps, etc. The materials in contact with the molten salt must be compatible in order to minimize the corrosion. However, the large plants that used molten salts have already proven the feasibility of managing corrosion and freezing issues.

As the freezing temperature of the Hitec solar salt, i.e. a binary mixture of molten salts, is quite high (200 °C), other mixtures of molten salts have been investigated. Hitec and HitecXl are two ternary mixtures of molten salt that include sodium nitrite, calcium nitrate and potassium nitrite (Angelini, 2012). This composition results in a lower freezing temperature, between 120 ° C and 142ºC respectively. Freezing protection is still required, although easier to manage than the Hitec solar salt. The maximum operation temperature of Hitec and HitecXL is 535 ºC and 500 °C respectively, which is lower than the Hitec solar salt (600 °C). But higher than the thermal oil (Angelini, 2012).

2.5   Thermal Energy Storage (TES)

In plants with Thermal Energy Storage heat produced by absorbed solar radiation is collected daytime and stored for a certain number of hours in thermal storage. Heat in the storage is then used to produce electricity nighttime, in cloudy days and to cover max electrical production during peak hours. Commonly the TES system is composed by two tanks, one at high temperature and the other at low temperature.

The storage fluid has to be characterized with a high heat capacity in order to reduce the storage volume. The most common thermal fluid is the Hitec solar salt, a molten salt binary mixture composed by 60% of NaNO3 and 40% of KNO3. Figure 33 shows a two- tanks indirect system, as the HTF and the storage fluid are not the same. Examples of this kind of plant are the Andasol power plants and the Solana Generation Station in Spain, with synthetic oil as HTF and molten salt as storage fluid. If the HTF (typically molten salts) is also used in the storage, the system becomes a two - tanks direct system, as illustrated in Figure 34. An example of this configuration is the Archimede power plant in Italy, the first commercial parabolic trough plant using molten salt as HTF.

Figure 33. Scheme of a CSP plant with 2-tanks indirect system, synthetic oil as HTF and molten salt as storage fluid Source (source: Martini, 2013).

Figure 34. Scheme of a CSP plant with 2-tanks direct system with molten salt as HTF and storage fluid (source: Martini, 2013).

Figure 35. Aerial view of Andasol I (source: Gunther et al., 2011).

2.6 Biomass boiler

2.6.1 Grate-firing system

Grate-firing combustors together with fluidized bed systems are currently the most common types of boilers for biomass combustion. Both boilers have good fuel flexibility and can be fuelled entirely by biomass or co-fired with coal.

Grate-firing was the first combustion system used for solid fuels. Today it is used mainly for burning biomass, but also for smaller coal furnaces. Capacities of grate-fired boilers range from 4 to 300 MWth (especially in the range of 20–50 MWth) in biomass-fired combined heat and power (CHP) plants. The heat release rate per grate area may be up to about 4 MWth/m^2 as a result of high volatile and low ash characteristics of typical biomass fuels (Yin et al., 2008).

2.6.2 Components of grate-fired boilers

Generally modern grate-fired boilers are composed by five key elements: a fuel feeding system, a fuel bed or grate assembly, a primary and secondary air system and an ash removal system (see Figure 36).

In this section the key elements in grate-fired boilers are described.
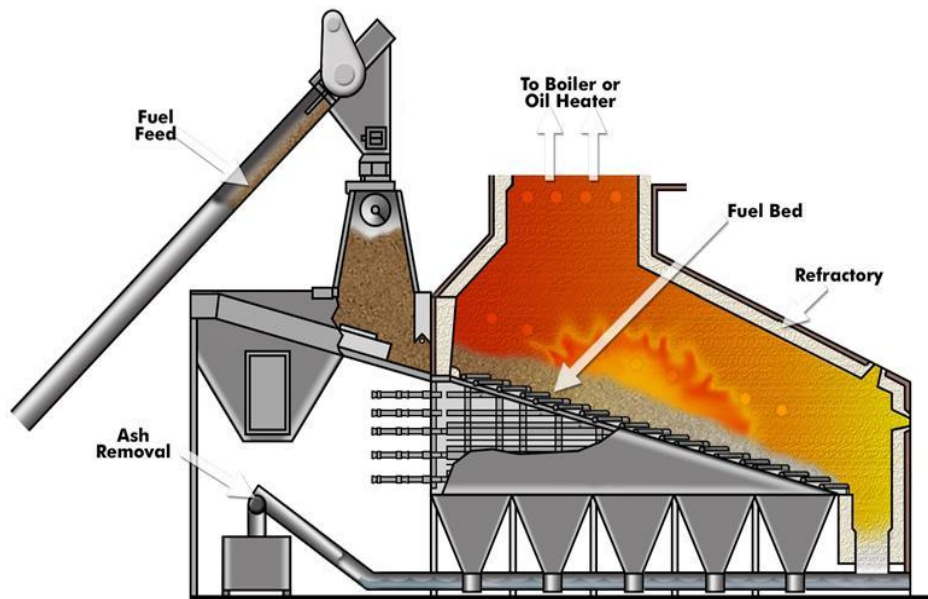
Figure 36. Grate-fired boiler burning biomass (source: http://koilerxm.info/reciprocating-boilers/).

2.6.2.1 Fuel feeding system

In the case of biomass fuels that contain a high fraction of fine particles (i.e. a few millimeters and smaller) the fuel feeding system is composed by a spreader in order to reduce the tendency for fuel separation since the grate is usually only suitable for gross

particles. The heavier and bigger biomass particles fall and combust on the grate surface while the finer particles burn in suspension when they fall against the flowing primary air (Yin et al., 2008).

2.6.2.2 Grate assembly

The grate assembly is the part of the grate-fired boiler where the fuel is transported and mixed with the primary air. The grate has to be cooled; this could be done with air or with water, although is usually preferred with water in order to account with more primary air to the combustion process.

The grates can be distinguished in: stationary sloping grates, travelling grates, reciprocating grates and vibrating grates (Yin et al., 2008).

2.6.2.2.1 Stationary sloping grate

The grate does not move, thereby the fuel burns as it slides down the slope under gravity. The degree of sloping is a relevant characteristic of these grates.

The main disadvantages are related to the difficulty controlling the combustion process as well as the possible risk of avalanching of fuel.

2.6.2.2.2 Travelling grate

In this king of grate the fuel is fed on one side of the grate and is burned during its transport until the ash removal. Unlike stationary sloping grate, travelling grates improve the control and the burnout efficiency due to the small layer of fuel on the grate.

2.6.2.2.3 Reciprocating grate

The reciprocating grate improves once again the fuel burnout efficiency thanks to its better mixing mechanism. The grate transports fuel with forward and reverse movements of the grate rods as combustion proceeds. At the end of the grate the solid particles are released in the ash pit.

2.6.2.2.4 Vibrating grate

Vibrating grate allows a further improvement of the fuel burnout efficiency. This improvement is mainly related to the shaking movement that spreads the fuel evenly in the grate. Additionally vibrating grates have less moving parts than other moveable grates, thereby lower maintenance and higher reliability.

2.6.2.3 Primary air supply system

The primary and secondary air supply system together with the movement of the grate play a fundamental role in the efficiency and the complete combustion. Generally for grate-fired boiler the overall excess air for most biomass fuels is set to 25 % or above. In modern grate-fired systems the ratio between the primary and secondary air tends to be 40/60, instead of 80/20 in older units.

Most of grate-fired boilers may be interpreted as a cross-flow reactor, where biomass is fed in a thick layer perpendicular to the primary flow. The fuel bed consists of

a huge number of solid particles that are piled up on the grate with a characteristic porosity. The preheated primary air passes through the fuel bed from the bottom and enters in the furnace. Additionally the fuel bed is heated by bed radiation, flames and refractory furnace walls until the ignition of the fuel.

The propagation of the ignition front in the bed is of interest since it affects the release of pollutants as well as determines the heat output from a given grate area and the stability of the combustion (Yin et al., 2008).

2.6.2.4   Secondary air supply system

The secondary air supply is the most important element in order to reduce the emissions and to reach the complete combustion. The gases produced by the biomass conversion together with a small amount of entrained fuel particles continue to combust in the grate, in this moment secondary air supply plays an important role mixing and burning.

Usually advanced secondary air-staging is used in modern grate-fired boilers. The main idea of this system is to reduce NO_x formation by reducing oxygen availability in the flame and by lowering flame temperature peaks. In air-staged combustion process, the first air-deficient (i.e., fuel-rich) zone reduces NO_x formation, and the complete combustion is achieved only after the addition of over-fire air in the second zone (i.e., the burnout zone).

Figure 37 illustrates the advanced secondary air supply in the straw-fired vibrating-grate boiler.
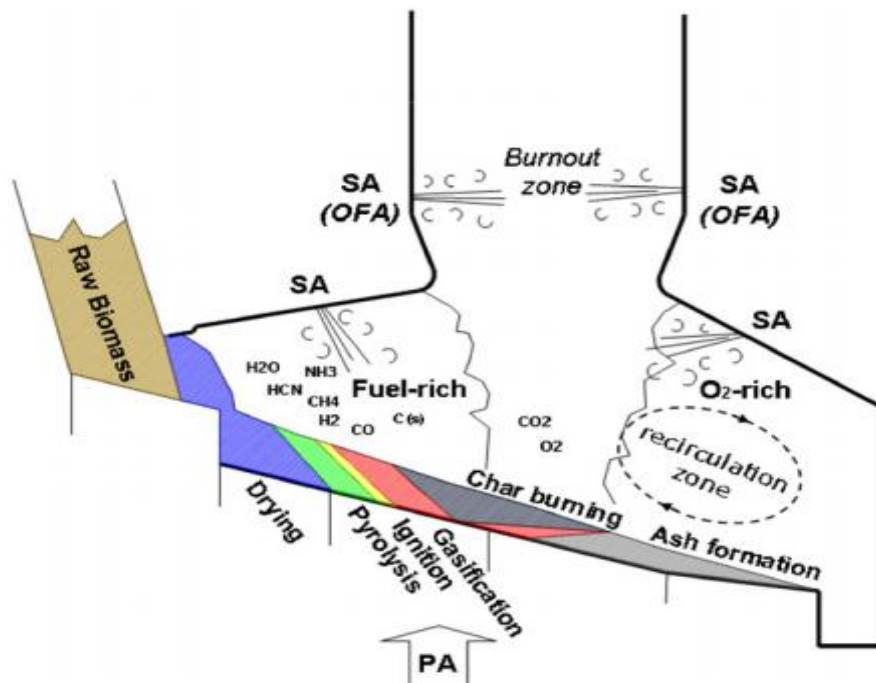
Figure 37. Scheme of the air supply and the resulted different zones in a grate-fired boiler burning biomass (source: Yin et al., 2008).

2.6.3 Key issues associated with grate firing boiler

Some of the issues related to the biomass combustion are similar to those of the coal combustion. However, biomass fuels fall over a very wide range and have different chemical and physical properties which not only result in different combustion and emission characteristics but also cause some practical problems during combustion in different plants.

In this section will be discussed the principal issues related to grate-fired boilers burning biomass.

2.6.3.1 *Primary pollutant formation and control*

Primary pollutants from biomass combustion include NO_x, SO_x, CO, C_xH_y, tar, HCl/Cl_2, PAH, PCDD/PCDF, heavy metals, particulate matter, and incompletely burned char particles. These pollutants can be classified into the following groups:

- Pollutants from incomplete combustion;
- Pollutants from the inorganic species in the biomass fuel.

The **Pollutants from incomplete combustion** tend to be a more prominent topic especially in grate- fired boilers. The comparatively poor mixing, both in the fuel bed and in the freeboard, is the main reason for the incomplete combustion in grate-fired boilers. Since grate-firing systems have relatively low combustion temperatures, good mixing and sufficient residence time of the combustibles at high temperatures are particularly crucial to improve the combustion.

The **Pollutants from the inorganic species in the biomass fuel** are listed in Table 3 with their respective consequences.

Table 3. Inorganic species in the biomass and its consequences.

Inorganic species in the biomass	Products	Consequences
Cl	HCl	Corrosive effect on the metal surfaces in the boiler, acidic pollutant emissions and particulate emissions, improves the formation of PCCD/PCDF.
	Alkali chlorides (e.g., KCl and NaCl)	Corrosive effect on the metal surfaces in the boiler.
N	NOx	Neglected since the lower temperatures in grate- fired boilers.
S	SOx	Corrosive effect on the metal surfaces in the boiler.

2.6.3.2 *Deposit formation and corrosion*

In solid fuel combustion, the particulate matter formed during the process may be deposited on furnace walls and heat-exchanger tubes. As a consequence the heat transfer rate decreases as well as could also give rise to corrosion problem. Actually deposition of particulate matter and corrosion represent the main issues related to the operation of a biomass boiler.

Nowadays biomass-fired furnaces, in particular straw-fired furnaces, are often reported to have severe deposition and corrosion problems compared to coal-fired boilers. The fuel properties together with the boiler design play an important role in the occurrence of ash deposition problems. Usually the probability of deposition increases at higher combustion temperatures or with an aerodynamics that encourages a flame impingement. On the other hand, if the fuel ash chemistry is favorable to the ash formation, then the probability will also be high.

2.6.3.2.1 Possible solutions to the problems of deposition and high temperature corrosion

- Additives

The use of additives can mitigate the high temperature corrosion as well as the deposit formation during biomass combustion. The objective is to raise the melting temperatures of the ash formed during the process in order to avoid ash related problems. Raising the ash melting temperatures can largely increase the potentials for the use of the biomass fuels. Some materials as Al_2O_3, CaO, MgO, $CaCO_3$, $MgCO_3$ and kaolin have been study to raise the melting temperatures of ash, to temperatures higher than those normally encountered in boiler furnaces. It is worth to highlight that additives do not change the first melting temperature of the ash, instead they dilute the ash and thus decrease the percentage of the molten phase in the mixture, which could show as an increase in the measured empirical temperature for the radical deformation of a standard body.

- New alloys or new forms of ceramic composite coating

This solution proposes the use of new alloys or ceramic tiles that are resistant towards chlorine corrosion especially for actual large-scale biomass-fired grate boilers. After some experiments has been observed that selective corrosion increases with respect to the chromium content of the alloy.

Currently a new form of ceramic composite coating has been studied and installed in different boilers after discovering that is effective in preventing corrosion.

- Decrease the surface temperature

Usually biomass-fired grate boilers are characterized by high steam parameters (temperature and pressure) in order to reach high plant efficiencies. As a consequence chlorine-induced high temperature corrosion takes place. However, for small or medium

boilers there is a solution, it is possible to reach high efficiencies at a lower temperature using a modified Rankine cycle.

2.7 Power block

Generally CSP plants operate with a Rankine cycle with water/steam as working fluid in order to convert the thermal into electrical energy. Lastly, in order to improve the thermal to electric conversion process, new fluids have been studied; some of these are organic fluids. The implementation of an organic fluid in the power block is also known as Organic Rankine Cycle.

Advantages and disadvantages of each working fluid will be discussed in this section.

2.7.1 Rankine cycle

A traditional Rankine cycle is defined as a heat engine that transforms thermal energy into mechanical work. The working fluid in a Rankine cycle follows a closed loop and is reused constantly. Figure 38 illustrates a Rankine cycle with regeneration.
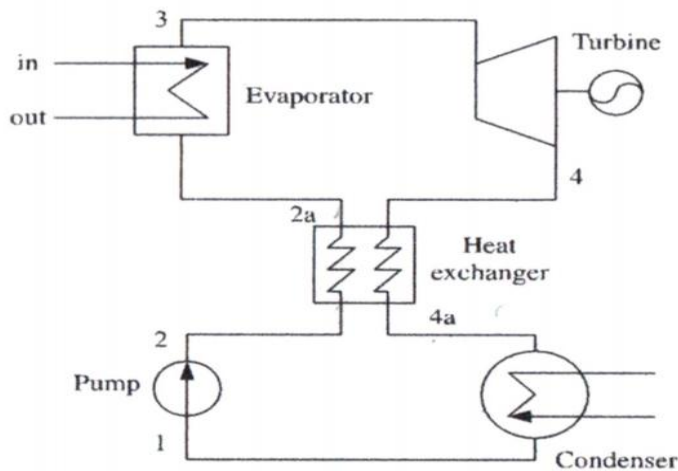
Figure 38. Scheme of a basic Rankine cycle (source: Vandin, 2012).

The cycle is composed by five processes:

- Process 1-2: The working fluid is pumped from low to high pressure. As the fluid is in liquid phase the pump requires low input energy.
- Process 2-2a: The working fluid takes heat from the hot fluid leaving the turbine.
- Process 2a-3: The high pressure liquid enters a boiler where it is heated at constant pressure by an external heat source to become a dry saturated vapor or overheated vapor.

- Process 3-4: The dry saturated vapor expands through a turbine, generating power. This decreases the temperature and pressure of vapor and some condensation may occur.
- Process 4-4a: The expand vapor gives heat to the liquid leaving the pump.
- Process 4a-1: The cycle close when the wet vapor enters in the condenser where it is condensed at a constant pressure to become a saturated liquid.

2.7.2 Organic Rankine Cycle (ORC)

The ORC consists on a conventional Rankine cycle that instead of water uses organic fluids as working fluid. Organic fluids are characterized by a high molecular mass, e.g. hydrocarbons, HCFCs, polysiloxanes or refrigerants.

Another characteristic of organic fluids is the low boiling temperature, very useful in combination with renewable energy power systems such as the solar energy. However, the overheating of the organic fluid at temperatures around 600 K produces chemical instability (Vandin, 2012).

Quoilin et al. (2013) have presented an Organic Rankine Cycle (ORC) plant in combination with the CSP systems. The results show that the ORC is more convenient than steam Rankine cycles in a low-to-medium power range (typically less than a few MWe). For high power ranges, higher than 2 MWe, the steam cycle is generally preferred, except for low temperature heat sources. The ORC manufacturer Turboden (2014) suggests ORC turbines for solar systems with an electrical power between 1 and 10 MWe. Currently the only known operational solar plant with an ORC system is the 1 MWe Saguaro project in Arizona, USA which operates with n-pentane as organic fluid. Canada et al. (2004) have also developed some investigations on the Saguaro project.

For the turbines a critical issue in steam Rankine cycles is the formation of two-phase in the last stages of expansion, as the drops of liquid may cause of structural damage to the blade rotor. To overcome this problem, it is necessary to superheat the steam entering the turbine, i.e. in diagram cycle T- s point 3 is the end point of expansion. This problem of the biphasic fluid in the turbine is absent in the case of the Organic Rankine Cycle, because while the slope of the T-s diagram curve for water is negative, the slope of the curve for an organic fluid is positive, therefore the end point expansion will always be in the area of dry saturated steam preventing the formation of two-phase fluid (Vandin, 2012).

Figure 39 illustrates the performance of the organic fluids and the water in the Rankine cycle.
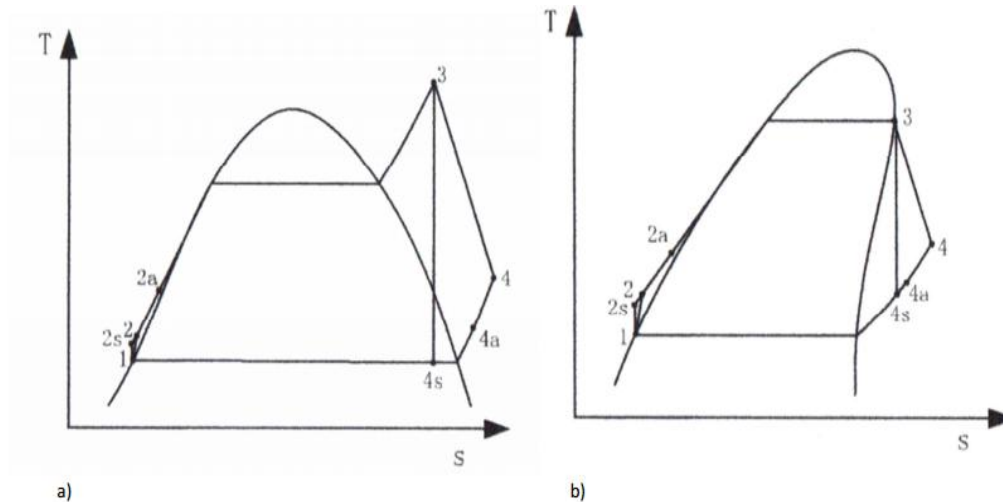
Figure 39. T-S diagram of a Rankine cycle a) Water as a working fluid b) Organic fluid as a working fluid (source: Vandin, 2012).

2.7.2.1 The advantages of the ORC

The main advantages that characterized an ORC system is the increase of the turbine operative life due to the absence of liquid formation in the final stages of expansion and the low mechanical stress due to the low peripheral speed.

The interposition of reducers is not more necessary since the lower rpm of the turbine, and therefore a direct connection turbine-generator is possible.

Additionally, ORC accounts with a higher reliability in comparison with steam cycles, as well as, reduces the maintenance interventions, especially because the working fluid is non-corrosive and keeps clean and lubricate the parts with which it comes in contact.

Unlike traditional steam cycles, ORCs can be operated without the supervision of licensed personnel. The reduce pressure make it safer, as well as, the procedures of startup and stop of the ORC are simpler.

Generally ORC does not required superheaters and decreases the level of noise of the power plant. Furthermore, the performance is good even at partial load.

2.7.2.2 Organic fluids

According the thermal level of the energy source, it is important to choose a suitable organic fluid for the ORC cycle. Since the energy source in the actual system reaches temperatures between 450°C and 550 °C (depending on the molten salt used) the required organic fluid must to be stable at high temperatures.

Nowadays ORC manufacturers are using siloxanes as working fluids in some high temperature applications, as these compounds present the desired technological characteristics for ORC working fluids: low toxicity and flammability, low foul formation over heat transfer surfaces, good material compatibility and good thermal stability.

The siloxanes, more precisely polymethylsiloxanes, or siliconic oils, are linear or cyclic polymers composed of alternating silicone oxygen atoms with methyl groups attached to the silicon atoms. Some of the thermodynamic characteristics of several of these compounds are listed in Table 4.

In this Table the names of the compounds were abbreviated with letters. D_x designates the cyclic molecules and MD_xM the linear molecules, **x** being the number of silicon atoms in the molecule. For example D4 is octamethylcyclotetrasiloxane.

As Table 4 shows the thermal stability of cyclic siloxanes (D_4,D_5,D_6) is better that the linear siloxanes (MM, MDM, MD_2M).

For the present study, the chose working fluid in the ORC cycle was the cyclic siloxane D_6 because its better thermal stability compared with the other cyclic siloxanes.

The maximum temperature in the ORC in the simulation was fixed at 360 °C (see chapter 5).

Table 4. Thermodynamic characteristics of siloxanes (source: <u>Fernandez et al., 2011</u>).

Compound	Molecular Mass, M (kg/kmol)	Critical Pressure, p_c(bar)	Critical Temp., t_c(°C)	Boiling Temp., t_b(°C)	Acentric Factor
MM	162.37752	19.39	245.60	100.52	0.419
MDM	236.531	14.15	290.94	152.53	0.5297
MD_2M	310.685	12.27	326.25	194.35	0.668
D_4	296.61576	13.32	313.35	175.00	0.589
D_5	370.7697	11.60	346.00	210.95	0.6658
D_6	444.924	9.61	372.63	244.99	0.7361

2.8   Efficiency of parabolic trough power plants

2.8.1   Solar to electric efficiency

The solar to electric efficiency is defined as the overall efficiency of the parabolic trough power plant. It is the ratio between the electric power and the direct solar irradiance on the total aperture area of the solar field:

$$\eta = \frac{P_{el}}{A_{ap}*G_{b,ap}} \qquad \textbf{Eq. 13}$$

Where η is the solar to electric efficiency. Additionally this overall efficiency is divided into solar field efficiency and power block efficiency:

$$\eta = \eta_{SF} * \eta_{PB} \qquad \textbf{Eq. 14}$$

The solar field efficiency η_{SF} is the ratio between the HTF heating rate and the direct solar irradiance on the total aperture area of the solar field. The power block efficiency η_{PB} is the ratio between the electric power and the HTF heating rate in the solar field. Both efficiencies are not constant throughout the year. The efficiency of a parabolic trough power plant varies between zero and a certain peak efficiency, which is reached at favorable radiation and other conditions. Table 5 displays the efficiencies values for Nevada Solar One in USA and Andasol I in Spain.

Table 5. Peak and average efficiency of two parabolic trough power plants (source: <u>Gunther et al., 2011</u>).

	Nevada Solar One (2007)	**Andasol I (2009).**
Peak overall efficiency	23	28
Average overall efficiency	12	16
Peak solar field efficiency	66	70
Peak power block efficiency	35	40
Average solar field efficiency		50
Average power block efficiency		30

2.8.2 Solar field efficiency

The losses that affect the solar field efficiency are classified into optical and thermal losses. The optical losses are distinguished by losses due to geometrical inaccuracies, losses due to limited reflectivity, absorptance and transmittance, losses related to beam incidence angle variance and shadowing losses.

2.8.2.1 Optical losses

The **geometrical inaccuracies** in a parabolic trough collector can be subdivided into macroscopic, microscopic, positioning, tracking and orientation errors. Macroscopic errors are those connected with the slope and form of the parabola while microscopic errors are local roughness areas in the mirror that cause a larger spread of the reflected solar radiation. Positioning errors are related with inaccuracies on the mirror positions, as well as, on the receiver position. The tracking and the orientation error can be caused by collector torsion.

       All these inaccuracies produce a reduction of the intercept factor, defined as the measure of the reflected radiation that gets lost because it does not hit the receiver tube. Actual parabolic trough collectors have an intercept factor between 0.96 and 0.97.

       The intercept factor can also be incremented making larger the absorber tube diameter, on the other hand, this leads to higher thermal losses. That is why an economic optimization has to be carried out in order to select the optimal receiver diameter.

The **limited reflectivity, absoptance and transmittance** of the optical components lead to more optical losses.

       According with some parabolic trough producers, the mirror reflectivity ρ is about 0.94, the receiver glass envelope transmittance τ is around 0.96 and receiver tube absorptance α approximates to 0.95. All these values are theoretical. Certainly under real operation conditions this values are lower since mirrors and receivers are never absolutely clean. That is why frequent cleaning plays an important role in the solar field efficiency.

The **variance of the incident angle of the direct radiation on the collector** can be distinguished by its influence on the optical parameters, on the intercept factor and on the row end losses.

The parabolic trough collectors track the sun only in one axis, for this reason the incident angle is not constant throughout the day and the year. The following equation relates the incident angle θ with the solar zenith angle θ_z, the declination δ and the hour angle ω:

$$\cos \theta = \sqrt{\cos^2 \theta_z + \cos^2 \delta * \sin^2 \omega} \qquad \textbf{Eq. 15}$$

- Influence on optical parameters

The optical parameters of the solar field components decrease at incident angles larger than zero. The reduction of the optical efficiency by changes on the reflectivity, transmittance and absorption is accounted by the variance factor ξ_{OP}.

- Influence on the intercept factor

The intercept factor gets influenced by the incident angle since the larger is the incident angle the longer is the way of the beam radiation from the collector to the absorber. A longer way allows the widening of the sunbeams and in consequence the intercept factor gets reduced. The variance factor ξ_{IC} accounts for the reduction of the optical efficiency due to lower intercept factors at larger incident angles.

- Row end losses

When the incident angle is larger than zero the sunbeams that hit the end of the collector rows are lost. This phenomenon is due to at one end of the row the reflected radiation misses the absorber tube and at the other end there is no reflected radiation for the absorber tube. The receiver length that is not illuminated depends on the focal length f and the incidence angle θ.

$$l = f * \text{abs}\,(\tan \theta) \qquad \textbf{Eq. 16}$$

The variance factor that accounts for the optical efficiency reduction due to the row end losses is defined through the following equation:

$$\xi_{CL} = \frac{L-l}{L} \qquad \textbf{Eq. 17}$$

Where L is the collector row length.

The combination of these three incident angle effects leads to the introduction of the Incident Angle Modifier (IAM), defined as the ratio of the optical solar field efficiency at a given incident angle to the optical solar field efficiency at θ = 0 :

$$\textit{IAM} = \xi_{OP} * \xi_{IC} * \xi_{CL} = \frac{\eta_{SF,opt}\,(\theta)}{\eta_{SF,opt}\,(\theta=0)} \qquad \textbf{Eq. 18}$$

Finally the optical losses can be caused **by mutual shading of the collector rows**

As mentioned the estimation of the distance between collector rows is an optimization task. It is recommended to select a distance more or less three times the collector width.

Figure 40 illustrates the approximate losses due to the incident angle and the shadowing losses for a parabolic trough power plant at spring or autumn equinox at latitude of 30° North. The power plant is oriented in the North-South alignment.
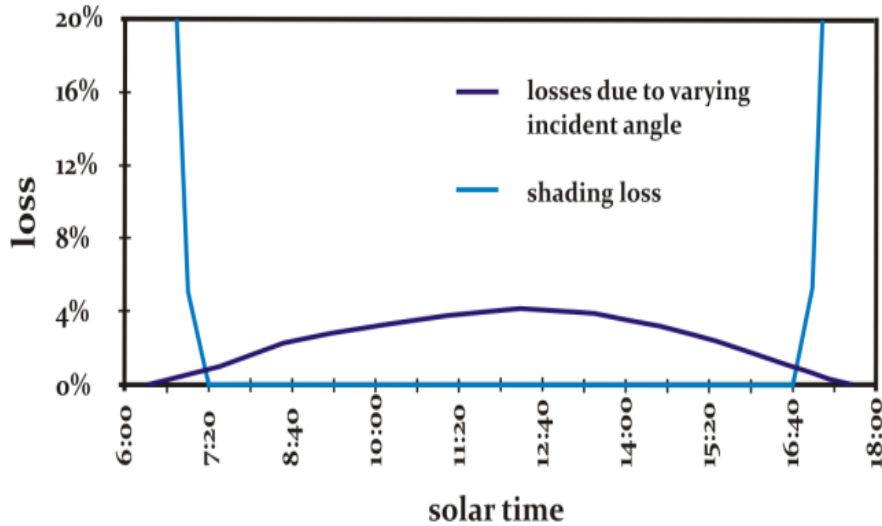
Figure 40. Losses due to varying incident angle and shading in a parabolic trough power plant at spring or autumn equinox and at a latitude of 30º North (source: Gunther et al., 2011).

2.8.2.2 Thermal losses

The thermal losses were described in the section 2.2.2 (receiver efficiency).

2.8.3 Power block losses

The power block losses include thermal to mechanic and mechanic to electric conversion losses, mechanic losses due to friction, thermal losses in the generator and pressure losses in the heat exchangers.

As in any power plant the thermal to mechanic conversion has the biggest influence on the power block losses. According to the second law of thermodynamics the maximum efficiency depends on the involved temperature levels:

$$\eta_{tm,max} = 1 - \frac{T_L}{T_H} \qquad \textbf{Eq. 19}$$

Where T_L is the low temperature level of the process and T_H the high temperature level (the temperatures in K). Assuming a $T_L = 190°C$ and $T_H = 450°C$, the maximum reached efficiency amounts to 36 %. This ideal efficiency can only be achieved by the Cycle of

Carnot; in real operation the heat supply is not isothermal. In this case T_H must be substituted by the medium temperature at which the heat supply is performed.

On the other hand, in real operation the compressor and the turbine are non-isentropic components; therefore the power block efficiency is reduced again. Larger turbines have an isentropic efficiency of about 85 %.

The generator losses (thermal and pressure losses) are quite low. Smaller generators, of 20 MW, reach efficiency close to 97 %, while larger generators, of 50 MW and more reach 98%.

Mechanical losses in larger power block do not exceed 1 %.

2.8.4 Parasitic energy uses

Unlike most power plants, the parasitic energy consumption in parabolic trough power plants is much higher. The electric energy is fed by the power block in order to keep the plant under operation. In parabolic trough power plants there are two mainly loads: the pumping system and the sun tracking system. Typically, for this type of power plants the parasitic energy consumption amounts to around 10 % of the generated power or 2 % of the input power.

Figure 41 describes the energy flow in a parabolic trough power plant. Around 40 % of the direct irradiance on the collector aperture is lost due to the optical and thermal losses in the solar field. Another 42 % is lost in the power block, mainly rejected in the condenser. At the end the gross electric output is about 18 % of the input power. The final useful power is 16 % due to the parasitic energy consumption (2%).
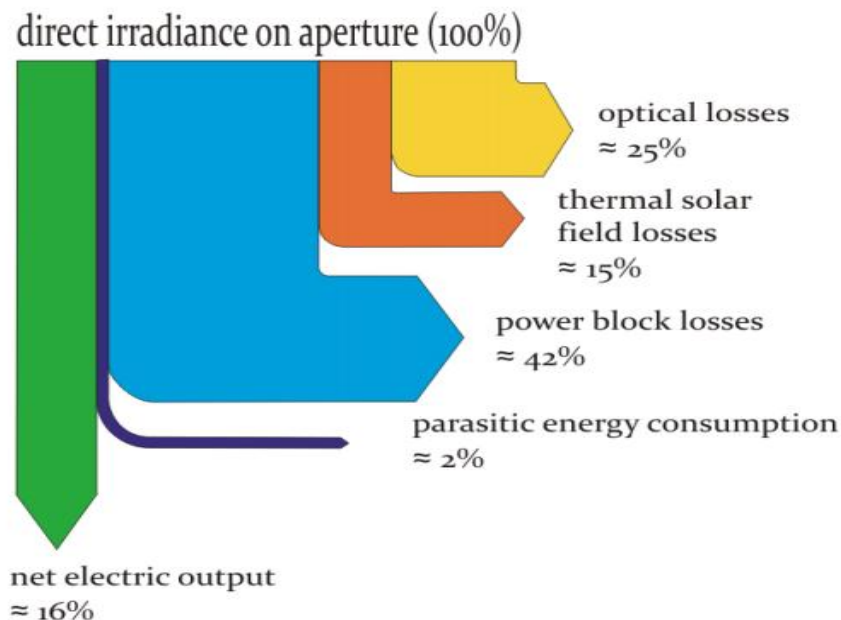
Figure 41. Energy flow in a parabolic trough power plant (source: Gunther et al., 2011).

CHAPTER 3

Site and biomass selection

The site definition of a CSP plant integrated with a biomass boiler is based on two main factors, the solar irradiation and the availability of biomass in the location.

3.1 Solar irradiation availability

Figure 42 illustrates the solar irradiation availability in Italy, being the South and the islands the most suitable locations for the CSP plant. In this regions the global horizontal solar irradiation in a year is between 1600 kWh/m^2 and 1800 kWh/m^2 in, while in the rest of the Country, especially in the Northern area, the annual irradiation varies from 900 kWh/m^2 until 1600 kWh/m^2. This solar distribution drives the choice of the location of the solar power plant in one of the following regions: Puglia, Basilicata, Calabria, Campania, Sicilia and Sardegna.
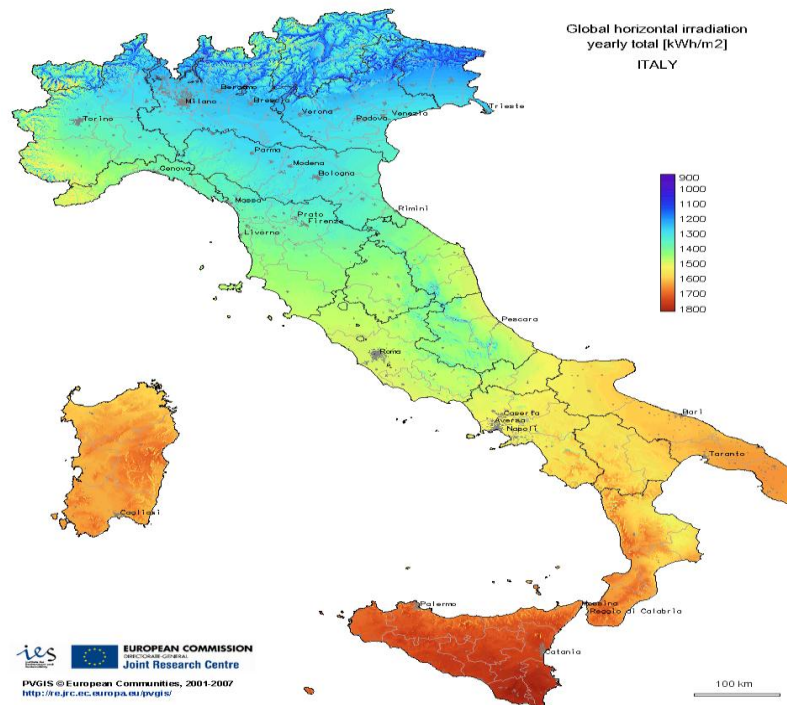
Figure 42. Global horizontal irradiation in a year in Italy

Once defined the region for the location of the solar power plant, the next step is to analyze the availability of biomass resources.

3.2 Biomass selection

3.2.1 Biomass chemical and physical characteristics

The selection of the biomass is carried out through the comparison of the following parameters:

- Gross Calorific Value (GCV)
- Humidity in the collection (%)
- Ash concentration (%)

A suitable biomass must be characterized by a large GCV, low moisture content, as well as a low percentage of ashes. The higher limits of the composition of the biomass have been set according to actual biomass boilers requirements: 60 % at most of moisture and 6% at most of ashes composition.

According to Table 6, the biomass in Italy which comply with these requirements are the corn cobs as well as the vine and olive residues.

Table 6. Physical and chemical characteristics of the main residual biomass in Italy (source: <u>Van Loo et al., 2008</u>)

Biomass	Gross Calorific Value (MJ/kg d.b.)	Humidity in the collection (%)	Ash (% d.b.)
Herbaceous			
Wheat straw	17.5-19.5	10-20	2-10
Rye straw	17.5-19.5	10-20	2-10
Barley straw	17.5-19.5	10-20	2-10
Oats straw	17.5-19.5	10-20	2-10
Rice straw	17- 18.4	20-30	10-15
Corn cobs	*16.8-18*	*30-55*	*2-3*
Corn stalks	16.8-18	55-66	2-7
Tree pruning			
Vine residues	*16-19*	*18-55*	*2-5*
Olive residues	*17-19*	*45-60*	*1.5-6*
Fruit trees residues	18-18.5	35-45	10-12
Dregs	11.46	55-65	5

d.b. = Dry Basis.

3.2.2 Biomass availability

According to Table 7 the olive residues has the higher annual production with 543 kt/year especially in the region of Puglia, the vine residues follows it with 250 kt/year and finally the corn cobs has the lower availability with 31 kt/year.

Table 7. Availability in the South and in the islands of Italy of the more suitable residual biomass for the boiler (source: ENAMA, 2011).

Regions	Corn cobs	Vine residues	Olive residues
Puglia	1	103	236
Basilicata	2	4	19
Calabria	6	8	118
Campania	20	18	45
Sicilia	0	92	100
Sardegna	2	25	25
TOTAL (kt/year)	**31**	**250**	**543**
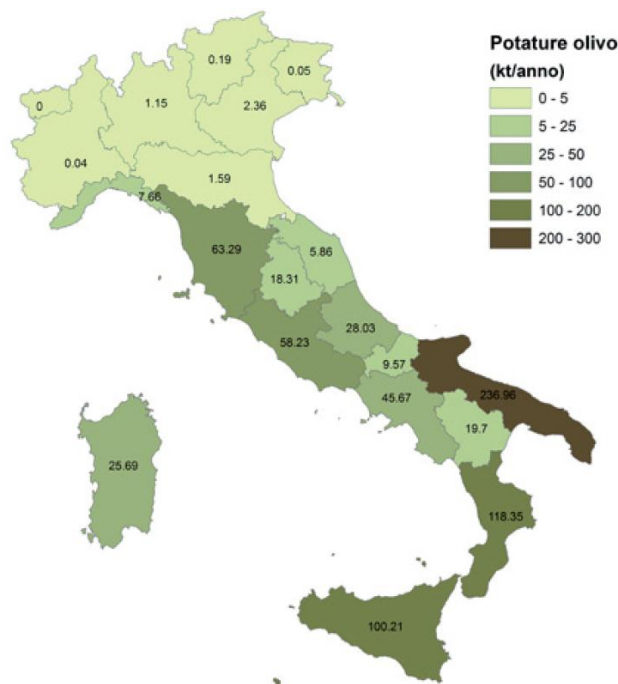
Figure 43. Olive wood annual availability in Italy (source: ENAMA, 2011)

The selected biomass is the olive residues from the natural pruning due to its large availability.

Once defined the biomass for the power plant the next step is to make a more detailed analysis of the thermal properties. According to Van Loo et al. (2008) the Gross calorific value (GCV) and the Net calorific Value (NCV) can be estimated through the following two equations, where the main variables are based on the biomass chemical concentration.

$$GCV = 0.3491 * X_C + 1.1783 * X_H + 0.1005 * X_S - 0.0151 * X_N - 0.1034 * X_O - 0.0211 * X_{ash} \quad \textbf{Eq. 20}$$

$$NCV = GCV * \left[1 - \frac{w}{100}\right] - 2.444 * \frac{w}{100} - 2.444 * \frac{h}{100} * 8.936 * \left[1 - \frac{w}{100}\right] \quad \textbf{Eq. 21}$$

Where:

- GCV: Gross Calorific Value in MJ/kg.
- NCV: Net Calorific Value in MJ/kg.
- Xi: Content of carbon (C), hydrogen (H), sulphur (S), nitrogen (N), oxygen (O) and ash in wt% (d.b.).
- w: Moisture content of the fuel in wt % (w.b.).
- h: Concentration of hydrogen in wt % (d.b.).
- 2.444: Enthalpy difference between gaseous and liquid water at 25°C.
- 8.936: M_{H2O} / M_{H2}; the molecular mass ratio between H_2O and H_2.

The olive wood chemical composition is derived from ENAMA (2011) in order to estimate the GCV and the NCV. The following table shows the different components present in the olive wood in a weight percentage.

Table 8. Chemical composition of the olive wood (source: ENAMA, 2011)

Olive wood residual biomass (wt %)						
C	H	S	N	O	Ash	Moisture
49.0 – 55.0	5.4 – 7.2	0.03 – 0.09	0.7 – 2.0	34.1 - 44.9	2.0 – 7.0	53.0 - 63.0

The Net Calorific Value displayed in Table 9 is the real biomass calorific value since it considers the moisture content in the olive residues. This NCV will be the calorific value employed for the calculation of the annual biomass requirement.

Table 9. GCV and NCV of olive wood calculated with

Gross Calorific Value (GCV) [MJ/kg d.b]	Net Calorific Value (NCV) [MJ/kg w.b]
18.7-23.6	7.6 – 9.8

w.b. = wet basis

Table 10 shows the theoretical annual request of olive residues in the power plant operating at full rate capacity. This value amounts to about 16 kt/year and the region of Puglia produces around 230,000 t/year; therefore, the supply of biomass can be guaranteed as well as the feasibility of an eventual future expansion of the power plant.

Table 10. Annual demand of olive wood for a production of 5 MWt

Power of the plant (MWt)	Lavorative Time (h/year)	Energy required (MWh/year)	NCV (MWh/t)	Biomass demand (kt/year)
5	8760	43800	2.7	16.1

3.2.2.1 *Chemical additives to the olive tree for growing*

The quantity of nitrogen, potassium and phosphorous contained in the olive wood is around 7g, 1g and 5g per kg of wood (<u>Caruso, 2013</u>). Furthermore it is worth to consider the addition of these chemicals for tree growing purposes. The nitrogen, potassium and phosphorous added for tree growing purposes together with the original quantities already in the tree, the total amount of these chemical compounds is around of 14g, 2g and 10g per kg of wood. In the present study these chemical substances used for the growing process are neglected.

Additionally the phytosanitary defense of the olive tree also concerns the use of chemicals substances. Most of these insecticides are not considered suitable for the combustion by the fact that can release toxics products at high temperatures, however, the use of these chemical substances is at most twice a year, also in minimal quantities in order to have no impact on the olive and oil production, that is why these substances are not a concern for the thermal process (<u>Piano di sviluppo rurale, 2000</u>).

3.3 Final site and biomass selection

The selected location for the CSP plant is the region of Puglia in Italy. This region is the one with the best combination of favorable solar irradiation and available residual biomass.

The defined biomass for the integration boiler is the olive pruning since this it is one of the main biomass resources in Puglia. The availability of olive residues in this region is estimated in 236 kt/year (see Figure 43) while the annual biomass requested by the plant, operating at design conditions amounts to about 16 kt/year. Therefore it is possible to suppose that the biomass demand of the CSP plant can be fully satisfied locally. Furthermore the quality and composition of the biomass is within the limits imposed by the biomass boiler technology and it does not present significant issues due to chemical contaminants.

CHAPTER 4

Energy simulation of the power plant

The simulation of the power plant is performed in order to make detailed predictions about its annual performance.

For the simulation of parabolic trough solar technologies a number of performance and economic software tools are currently available. For the present study the employed models are TRNSYS and Sam Advisor Model (SAM), the latter used in order to validate the results obtained with TRNSYS.

4.1 Software employed

4.1.1 Solar Advisor Model (SAM)

The Solar Advisor Model was developed by NREL, partnering with the U.S. Department of Energy Solar Energy Technologies Program and Sandia National Laboratories. This software is based on a comprehensive solar system that allows users to investigate the impact of variations in physical, economical, and financial parameters to better understand their impact on the system performance.

Some of the achievable results with SAM related to the cost and performance of a solar system include: the hourly, monthly and annual system energy output, the peak and annual system efficiency, the levelized cost of electricity (LCOE), the net present value, the system capital costs and the system operating and maintenance (O&M) costs (Wagner et al., 2011).

4.1.2 TRNSYS

TRNSYS is a simulation program dedicated to dynamic systems in the fields of building simulation and renewable energy engineering, including the parabolic trough solar technology. This software was initially developed in 1975 by the Laboratory of Solar Energy of the University of Wisconsin, Madison (United States) partnering with the Solar Energy Applications Laboratory in the University of Colorado (United States). Since then, TRNSYS has been in continually development thanks to the teamwork of various institutions such as the Solar Energy Laboratory, University of Wisconsin-Madison, the Scientifique et Technique du Batiment Centre in France, Transsolar Energietechnik GmBH in Germany and the Thermal Energy Systems Specialists in Wisconsin.

Currently TRNSYS accounts with a graphical interface, with a library of about 80 standard components, and other libraries that offer around 300 components and has users and distributors around the world (France, Germany, Spain, USA, Japan) (Moreno, 2010).

4.2 Comparison between TRNSYS and SAM

SAM is a simulation software based on a TRNSYS model engine. SAM, as well as TRNSYS makes performance predictions derived from system design parameters that the user specify as inputs of the model. The additional quality of SAM is that estimates the cost of energy for grid connected projects based on installation and operating costs.

The first step for the creation of a SAM file is to choose a technology and financing option for the project. SAM automatically populates input variables with a set of default values for the type of project. In the case of TRNSYS before the creation of the entire model the user needs to study each suitable component available in the TRNSYS' libraries, identify the possibility to connect it with the rest of the system and then enter the inputs for each component.

Like TRNSYS, SAM requires a weather data file in order to describe the renewable energy resource and weather conditions at a project location. Depending on the chosen location it is possible to select a weather data file from a list, download one from the Internet, or create the file using available data.

In contrast with SAM, TRNSYS accounts with more degrees of freedom, allowing the user to simulate any required system at the desired conditions. On the other hand, SAM only allows modeling the parabolic trough system integrated with fossil-fired backup boilers instead of biomass boilers.

One advantage of SAM in comparison with TRNSYS is that can perform the optimization of the solar field size and the thermal storage capacity. For instance, if the user desired to obtain the optimal solar field size SAM performs several simulations with different size in order to find that one with the lower LCOE (Levelized Cost of Energy).

SAM makes hourly calculations of a power system electric output, generating a set of 8,760 hourly values that represent the system electricity production over a single year. With TRNSYS the time step can be controlled by the user as well as the obtained results.

SAM displays modeling results in tables and graphs, ranging from the metrics table that displays levelized cost of energy, first year annual production, and other single-value metrics, to tables and graphs that show detailed annual cash flows and hourly performance data.
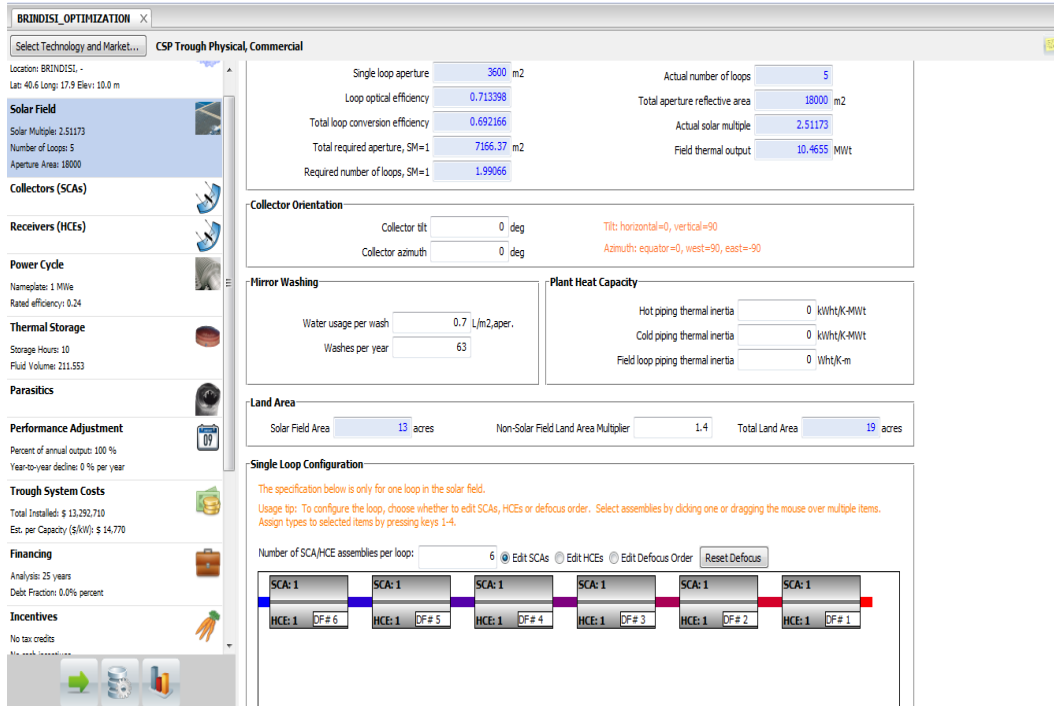
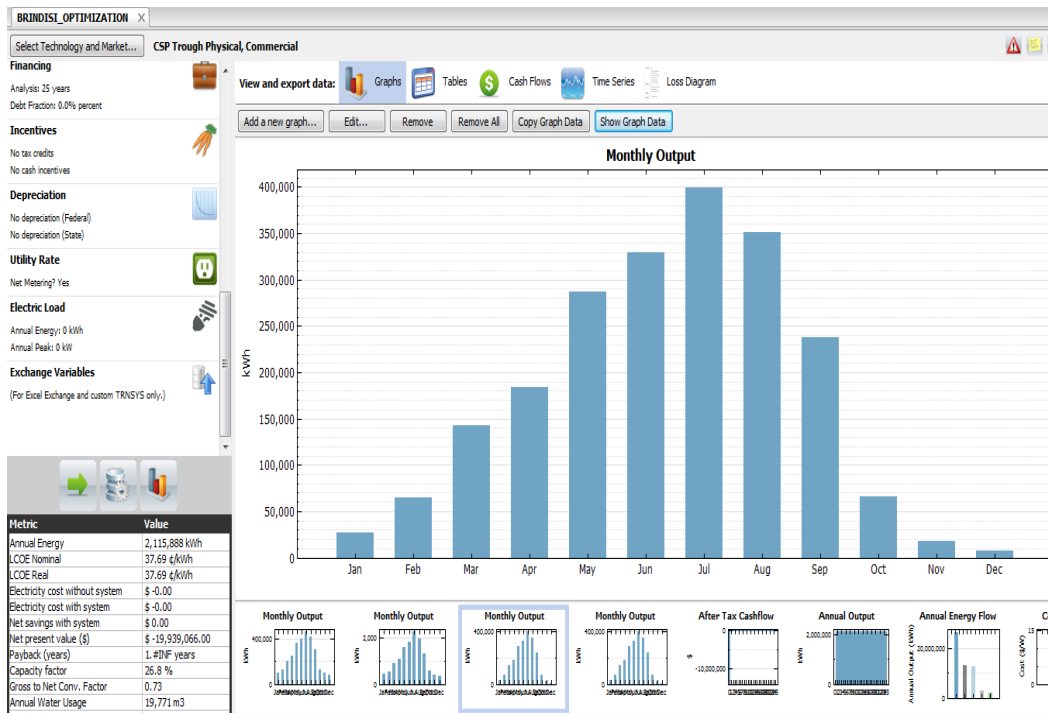**Figure 44. Solar Advisor Model input pages (source: SAM).**

Figure 45. Solar Advisor Model results page (source: SAM).

4.3 The TRNSYS model

The simulation with TRNSYS is based on the modeling and connection of the different components until the construction of the power system. The TRNSYS standard library has provided the majority of the required components, those which are not available in this library are modeled in a different way. In the case of the biomass boiler, the modeling of this component is performed with MATLAB, and then it is integrated into the energy system. In order to perform the simulation of the parabolic collector it is required the use of a special library that accounts with the appropriate component for the representation of this concentrating collector. This library is the "TESS library" or "Thermal Energy System Specialist library" and the component is recognized by TRNSYS as type 1257 (Parabolic trough collector).

For further details about the components refer to TRNSYS documentation (Solar Energy Laboratory, 2007).

4.3.1 Solar field simulation

The solar field system is modeled through the connection of the following components:

- an array of parabolic trough collectors : Type 1257
- a weather component : Type 15-6
- a HTF temperature controller : Type 22
- a pump : Type 110
- an auxiliary heater : Type 6

In this section will be described the most relevant parameters and functions of each component.

The scheme with the corresponding links is as follows:
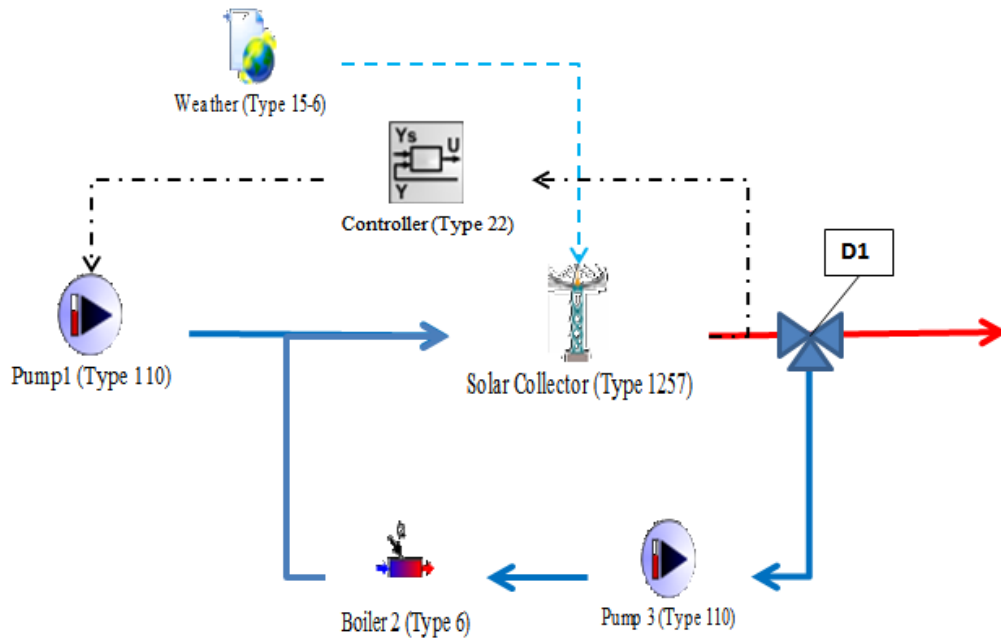
Figure 46. Scheme of the solar field system.

4.3.1.1 *Parabolic trough collectors (Type 1257): <u>solar collector</u>*

Type 1257 models an array of parabolic trough collectors. In contrast to other parabolic trough models, type 1257 accounts for change in fluid properties with temperature.

The Compound Parabolic Concentrator (CPC) or type 74 available in the standard library of TRNSYS is a parabolic concentrator as well; however it differs in some parameters from type 1257.
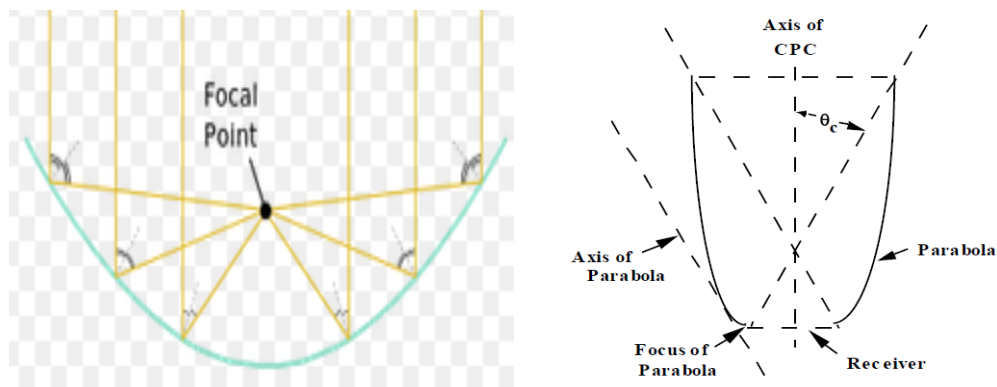
Figure 47. Parabolic concentrators. In the left: Parabolic trough collector. In the right: Compound parabolic concentrator (source: <u>Solar Energy Laboratory, 2007</u>).

Table 11 . Comparison between the parabolic trough (Type 1257) and the compound parabolic concentrator (Type 74).

Parabolic trough collector (TYPE 1257)	Compound Parabolic Concentrator (CPC) (TYPE 74)
The receiver or heat collector element (HCE) is a tube.	The receiver or heat collector element (HCE) is a plate.
Accounts for change in mass flow due to property change with temperature.	Fixed mass flow.
Accounts for change in the heat loss coefficient due to change with temperature.	Fixed heat loss coefficient.
Accounts for change in enthalpy, internal energy and density with temperature.	Fixed fluid specific heat.

4.3.1.1.1 Inputs of type 1257

The parameters required in order to model the parabolic trough collector can be subdivided into:

- Geometrical parameters
- Array configuration
- Optical and thermal losses
- Heat transfer fluid properties : Density, enthalpy, internal energy

The **geometrical parameters** of the parabolic trough collector include the aperture width and length of the collector and the diameter of the receiver tube. According to some investigators the aperture width and length of most actual collectors amounts to about 6 meters and 100 meters respectively. Assuming an aperture width of 6 meters the collector focal length must be close to 1.75 meters (Gunther et al., 2011).

Geometrical parameters also include the diameter of the absorber tube. The inner diameter adopted is 64 mm like the absorber diameter of the parabolic trough power plant "Archimede" (NREL, 2014).

The **array configuration** regards the specification of the number of collectors in series per loop. According to existing parabolic trough power plants the common length of a loop is around 600 m. If the length of each collector is 100 m, the number of collectors results equal to 6 (Gunther et al., 2011).

The **optical and thermal losses** are specified through the Incident Angle Modifier coefficients and the heat loss coefficients.

As mentioned, the incident angle modifier is an efficiency reduction factor that accounts for the collector optical losses as a function of the incident angle. The following equation described the empirical formula employed by TRNSYS to calculate the incident angle modifier factor. The coefficients for this equation are derived from the field tests of the SEGS LS2 collectors for air & vacuum tubes (Dudley et al. 1994).

$$IAM = b_0 * cos(\theta) + b_1 * \theta + b_2 * \theta^2 \quad (Adim) \qquad \text{Eq. 22}$$

Where θ is the incident angle in radians

Table 12. Incidence Angle Modifier equation coefficients b₀, b₁, and b₂ specified as inputs on the collector parameters (source: <u>Dudley et al., 1994</u>).

IAM coefficients for air & vacuum tube		
b₀	**b1**	**b2**
1	0.000884	-0.00005369

The heat loss coefficients account for the thermal losses due to a temperature difference between the receiver tube and the ambient. The following equation is the empirical formula employed by TRNSYS to calculate the heat losses (<u>Dudley et al. 1994</u>). The coefficients for this equation were derived from the parabolic trough receiver tests for air & vacuum tubes.

$$Heat\ loss = a_0 + a_1 * T_r + a_2 * T_r^2 + a_3 * T_r^3 + DNI * (a_4 + a_5 * T_r) \ \left(\frac{kJ}{hm}\right) \text{ Eq. 23}$$

Where T is the temperature of the Tube (HCE) in ºC.
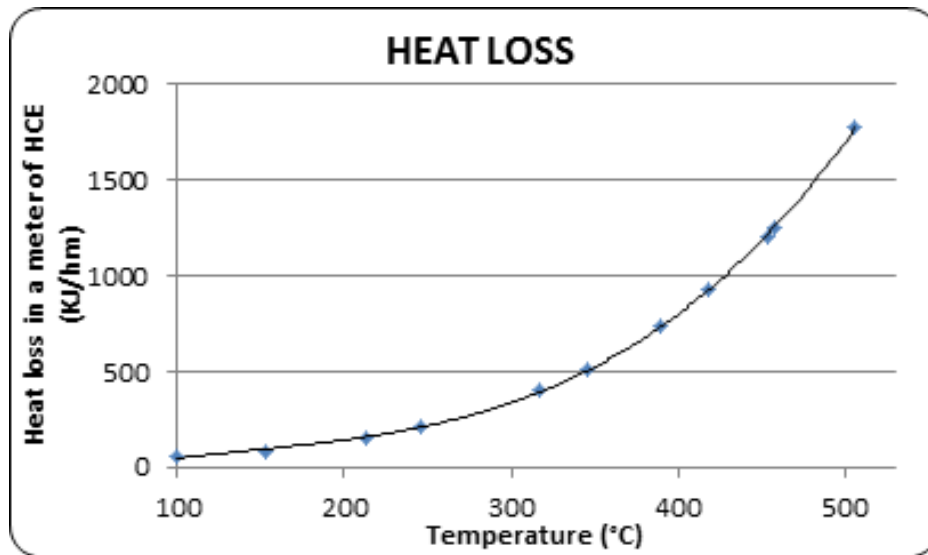
Figure 48. Heat loss in a meter of receiver tube in function of the receiver tube temperature

According to Figure 48, the heat loss curve is described by the following equation

$$Heat\ loss = 3e - 5\ T_r^3 - 0.0121 T_r^2 + 2.6226 T_r - 122.98 \qquad \text{Eq. 24}$$

Table 13. Heat loss equation coefficients a$_0$, a$_1$, a$_2$, a$_3$,a$_4$ and a$_5$ specified as inputs on the collector parameters

Heat loss coefficients for air & vacuum tube					
a$_0$	a1	a2	a$_3$	a4	a5
-122.980	2.620	-0.012	0.000	0.000	0.000

The polynomial function that describes the fluid density in function of the temperature is as follows:

$$Density = r_0 + r_1 * T_f + r_2 * T_f^2 + r_3 * T_f^3 \quad \left(\frac{kg}{m^3}\right) \qquad \textbf{Eq. 25}$$

Where T_f is the temperature of the HTF in °C.

The density coefficients for the Hitec solar salt and the Hitec XL are derived from the HTF data of SAM.
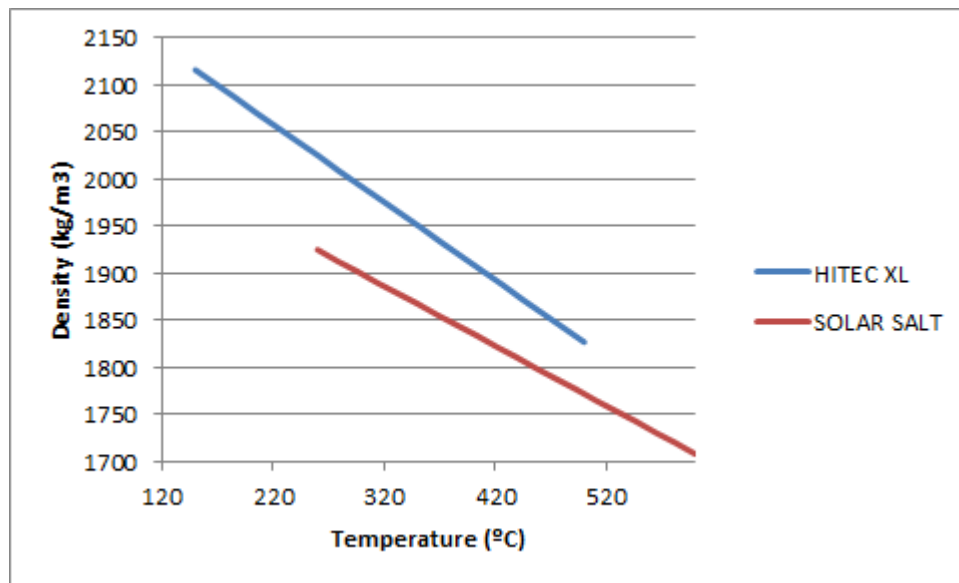
Figure 49. Density as a function of the molten salt temperature (source: SAM).

According with the previous plots, the density of both molten salts changes with temperature following a linear tendency:

$$\rho_{ss} = -0.636 * T_f + 2090 \qquad \textbf{Eq. 26}$$

$$\rho_{XL} = -0.8266 * T_f + 2240 \qquad \textbf{Eq. 27}$$

Where ρ_{ss} is the solar salt density and ρ_{XL} the Hitec XL density in kg/m^3.

Table 14. Density equation coefficients r₀, r₁, r₂ specified as inputs on the collector parameters.

Density coefficients					
Hitec Solar Salt			Hitec XL		
r_0	r1	r2	r_0	r1	r2
2090	-0.64	0	2240	-0.82	0

The polynomial function that describes the fluid enthalpy is as follows:

$$Enthalpy = h_0 + h_1 * T_f + h_2 * T_f^2 \qquad \left(\frac{kJ}{kg}\right) \qquad \text{Eq. 28}$$
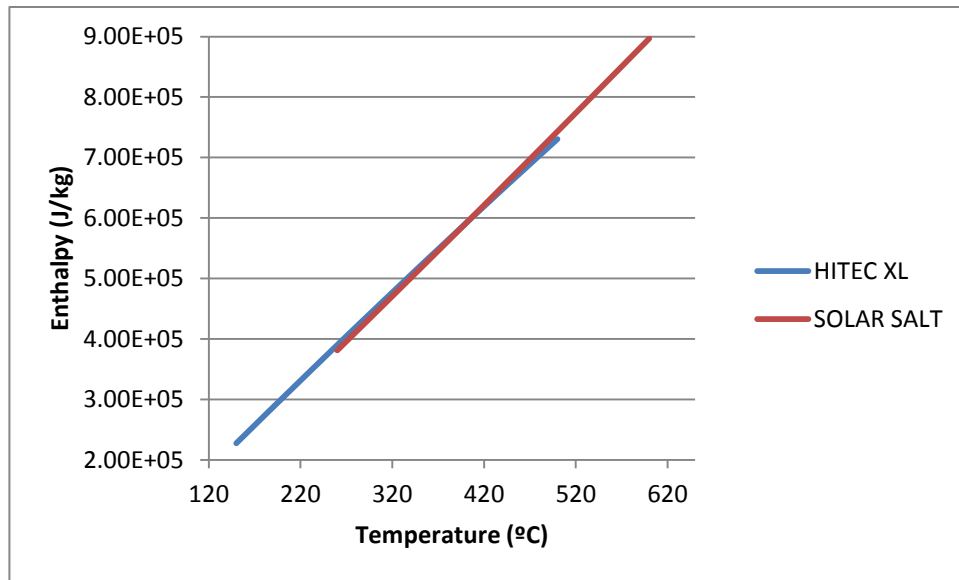
Figure 50. Enthalpy as function of the molten salt temperature (source: SAM)

According with the previous plots, the density of both molten salts changes with temperature following a linear tendency:

$$H_{ss} = 1484 * T_f \qquad \left(\frac{J}{kg}\right) \qquad \text{Eq. 29}$$

$$H_{XL} = 1479 * T_f \qquad \left(\frac{J}{kg}\right) \qquad \text{Eq. 30}$$

Where H_{ss} is the solar salt enthalpy and H_{XL} the Hitec XL enthalpy.

Table 15. Enthalpy equation coefficients h$_0$, h$_1$ and h$_2$ specified as inputs on the collector parameters.

Enthalpy coefficients					
Hitec Solar Salt			Hitec XL		
h$_0$	h1	h2	h$_0$	h1	h2
0	1.484	0	0	1.479	0

The polynomial function that describes the fluid internal energy is as follows:

$$Internal\ Energy = u_0 + u_1 * T_f + u_2 * T_f^2 \qquad \left(\frac{KJ}{Kg}\right) \qquad \textbf{Eq. 31}$$

The coefficients for this equation were derived from (Ferri et al., 2008).

As the heat calorific value at constant volume (Cv) and the heat calorific value at constant pressure (Cp) are similar for liquid substances the internal energy coefficients adopted for both molten salts are assumed analogous.

Table 16 . Internal energy equation coefficients u$_0$, u$_1$ and u$_2$ specified as inputs on the collector parameters.

Internal energy coefficients					
Hitec Solar Salt			Hitec XL		
u$_0$	u1	u2	u$_0$	u1	u2
372.7	1.5	0.0	372.7	1.5	0.0

4.3.1.2   Weather component (Type 15-6): <u>Weather</u>

Type 15-6 provides the hourly weather data for the required location, in this case the city of Brindisi in Italy. The data source employed in the simulation is Meteonorm, which includes more than 1000 locations in more than 150 countries.

4.3.1.2.1   Inputs of type 15-6

The parameters required in order to model the weather component linked to the parabolic trough collector can be subdivided into:

- Tilted Surface radiation mode
- Collector tracking mode
- Collector angles

There are 4 different **tilted surface radiation modes** available to calculate the radiation components on a tilted surface. The Isotropic Sky Model assumes that the diffuse radiation is uniformly distributed over the complete sky dome; this is the model that has been used by default in previous versions of TRNSYS. The Hay and Davies Model accounts for both circumsolar and isotropic diffuse radiation; under clear sky conditions

there is an increased intensity of diffuse radiation in the area around the sun (circumsolar diffuse). The Reindl Model adds a horizon brightening diffuse term to the Hay and Davies model while the Perez Model accounts for circumsolar, horizon brightening, and isotropic diffuse radiation.

The documentation of TRNSYS recommends for general use any of the anisotropic sky models (Hay and Davies, Reindl, and Perez, et al.) because these provide far better estimates of the total radiation on a tilted surface in comparison with isotropic sky model (Solar Energy Laboratory, 2007).

For the present simulation, the Reindl model is chosen for been a detailed model and for its simpler computational model compared to the others models.

The collector **tracking mode** can be:
1: fixed surface (no tracking).
2: the surface rotates about a vertical axis in order to track the sun.
3: the surface rotates about a fixed (user-defined) axis.
4: the surface 2-axis tracks such that the beam radiation is always normal to the surface.

For the present CSP system was adopted the third tracking mode with a North – South alignment with the respective East-West tracking.

The **collector angles** include the slope of surface and the azimuth of surface. In the case of the adopted tracking mode the slope of surface refers to the slope of the axis around which the collector rotates. Since the collector fixed axis was defined as parallel to the ground (horizontal) this value is null. On the other hand, the azimuth angle of the surface was set equal to zero because the collector fixed axis was specify facing towards the South, in the case of Italy towards the Equator.

4.3.1.3   *Feedback Controller (Type 22): controller 1*

The feedback controller operates only during sunny days in order to keep the outlet temperature of the array of collectors at the set point value. The manipulate variable in this case is the mass flow rate of the pump 1. The on /off signal of the controller is given by the solar beam useful radiation, if the latter is larger than a set value then the signal controller is set to 1, i.e. the controller is on. Type 22 models an iterative feedback controller.

4.3.1.4   *Auxiliary heater (Type 6): boiler 2*

Unlike the feedback controller the auxiliary heater enters in operation exclusively during times of extended shutdown or cool night time temperatures in order to keep the molten salt temperature over its freezing temperature. Type 6 models a typical fossil fuel auxiliary heater and if the temperature falls below the minimum allowable value, heat is added to the system in order to maintain the temperature at the minimum value. This heating system is implemented in the TRNSYS simulation only for practical purposes because a physical CSP works with a different arrangement; in actual operating CSP plants there is electric heat trace equipment that provides supplemental heat to the HTF

directly in the solar field. This heating energy is then tracked and reported as a parasitic loss.

4.3.1.4.1 Auxiliary heater size

The auxiliary heater size was calculated through the following two equations. Eq. 32 is an empirical equation derived from (Gunther, 2011) that considers thermal losses in the receiver tube depending on the temperature difference between the absorber tube and the surrounding air. The heat conduction is assumed as negligible. Eq. 33 calculates the design boiler thermal output to ensure the molten salt freezing protection in the trough parabolic collectors.

$$\textit{Thermal losses} \; = \; \mathbf{0.26} * (T_r - T_{sur}) - \mathbf{1.05} * \mathbf{10^{-8}} * (T_r - T_{sur}) \; \left(\frac{W}{m}\right) \quad \textbf{Eq. 32}$$

$$\textit{Boiler thermal output} = \textit{Thermal losses} * L_r \; \; (W) \qquad \textbf{Eq. 33}$$

Where
- T_r : Minimum receiver temperature.
- Tsur: Minimum surrounding air temperature in the year, in the case of Brindisi is around -1°C.
- L_r : Receiver length in one array of collectors (600 m).

4.3.2 Thermal Energy Storage (TES)

The Thermal energy storage system is modeled through the connection of the following components:

- A variable tank volume : Type 39;
- an auxiliary heater : Type 6;
- three diverters : Type 11f;

In this section will be described the most relevant parameters and functions of each component.

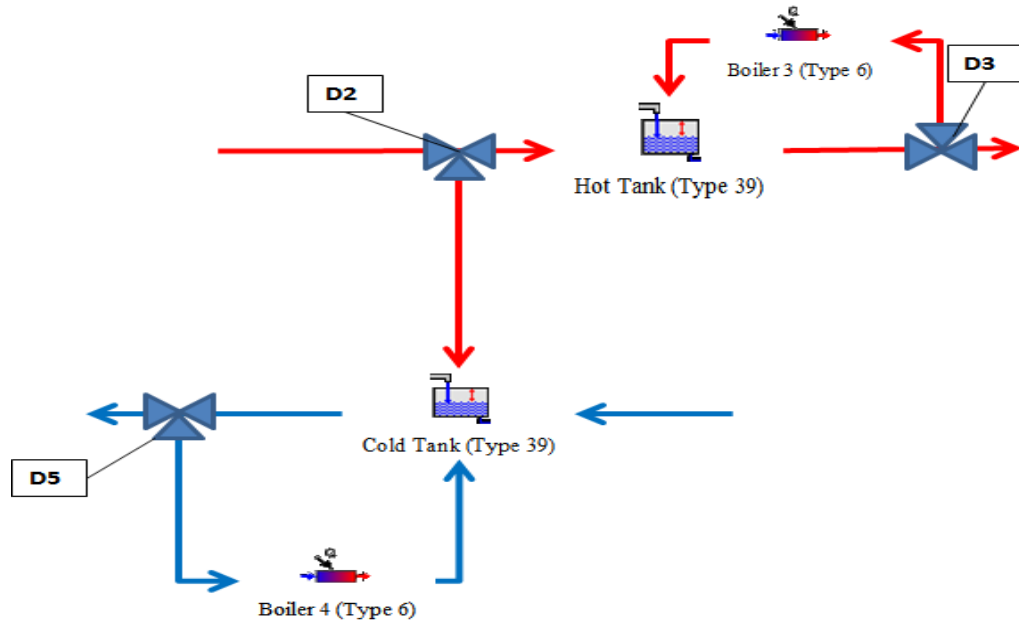The scheme with the corresponding links is as follows:

Figure 51. Scheme of the Thermal Energy Storage system.

4.3.2.1 Variable tank volume (Type 39): hot tank and cold tank

This component models a fully-mixed tank with a constant cross-sectional area that contains a variable quantity of fluid.   In its simplest form, a single flow enters from a hot source and a single flow stream exits to a load.   Since the incoming and outgoing flows need not be equal, the level of fluid in the tank can vary.   The level is allowed to vary between user specified high and low level limits.   If the lower limit is reached, the load flow necessary to maintain this level is output rather than the desired load flow.   If the volume of fluid exceeds the upper limit, then the excess incoming fluid stream is diverted from the tank.

4.3.2.1.1 Storage size

The storage size is usually measured with the Full load hours of TES.   This magnitude indicates the number of hours that thermal storage can supply energy to operate the power cycle at its full design point output.   According with existing CSP plants integrated with TES, the thermal capacity is between 7.5 and 9 hours.   On the other hand, the CSP plants under development are projecting higher storage capacities (NREL, 2014).   For the present simulation the thermal storage capacity is set at 10 h in order to improve the solar field energy contribution.

The procedure for the estimation of the storage size was derived from the Technical manual for the SAM (Wagner, 2011) where is assumed that both storage tanks have the same geometry:

$$\textbf{\textit{Thermal storage capacity}} = \frac{Nominal\ power * Full\ load\ hours}{\eta_{ORC}} \quad (\textbf{\textit{MWht}}) \quad \textbf{Eq. 34}$$

$$Volume_{useful} = \frac{thermal\ storage\ capacity}{Cp_{HTF} * \rho_{HTF} * \Delta T_{HTF}} * 3600 \quad (m^3) \qquad \text{Eq. 35}$$

$$Volume_{total} = Volume_{useful} + Volume_{unusable} \quad (m^3) \qquad \text{Eq. 36}$$

Where

- η_{ORC}: Organic Rankine Cycle efficiency at nominal power.
- Cp_{HTF}: average heat calorific value of the storage fluid (MJ/kgK).
- ρ_{HTF}: average density of the storage fluid (kg/m³).
- ΔT_{HTF}: temperature difference between the inlet and outlet source fluid in the heat exchanger (K).

4.3.2.2 Diverter (Type 11f): D2

Type 11f is included in the Thermal Energy Storage system in order to keep the hot tank temperature around the user specified set point. D2 was located before the hot tank inlet access to divert the flow to the cold tank in the hours when the flow temperature was lower than a set value.

4.3.2.3 Auxiliary heater (Type 6): boiler 3

As illustrates Figure 51 each tank in the system is provided with an auxiliary heater. Boiler 3 has the task of heating the hot storage tank and Boiler 4 of keeping the cold storage tank at the minimal allowable temperature.

The auxiliary heater of the hot tank performs two different functions depending on the available solar energy. During sunny days it operates in order to keep the hot tank temperature around its design temperature value and during times of extended shutdown or night time it is employed to maintain the molten salt temperature over its freezing temperature.

4.3.2.4 Auxiliary heater (Type 6): boiler 4

Unlike the boiler of the hot tank, the auxiliary heater of the cold tank operates exclusively to ensure the molten salt freezing protection. The minimum temperature allowable was the fluid freezing temperature plus 50 °C of safety margin.

Boiler 2, Boiler 3 and Boiler 4 are implemented in TRNSYS to simulate the heat equipment that provides supplemental heat to the HTF directly in the storage tank. This heating energy is then tracked and reported as a parasitic loss.

4.3.2.4.1   Boiler 3 and Boiler 4 size

The maximum capacity of the boilers is calculated based on the volume of the storage tanks and the storage fluid temperature. Since the temperature inside each storage tank differs, the maximum capacity of the boilers will be different.

$$Boiler\ size\ =\ U * A * \left(T_{sf} - T_{sur}\right) \qquad (W) \qquad \text{Eq. 37}$$

Where:

- U: Thermal loss coefficient (W/m^{2}K)
- A: The storage external surface (m^2)
- T_{sf} : storage fluid temperature inside the tank (ºC)

4.3.3 Biomass boiler model

The biomass boiler is integrated to the power plant in the solar field cycle. The boiler is modeled with MATLAB, therefore it is required another component in order to implement the link between TRNSYS and MATLAB. This component is Type 155.

Biomass boiler (Type 155)

Figure 52. Type 155 of the Standard library of TRNSYS.

4.3.3.1 Biomass Boiler Model (MATLAB): *biomass boiler*

A 5 MW biomass boiler is modeled with MATLAB and then linked, through the Type 155, to the rest of the components of the energy system.

The model can be subdivided in the three boiler operating phases: startup, normal operation and stand-by mode. The required condition to make the startup is that the molten salt level in the hot storage is lower than a set value. Once the combustion process reaches the operative conditions, the biomass boiler enters in the normal operation phase. At hours when solar energy satisfies the whole energy demand, the boiler enters in the stand-by mode. In the section 4.3.3.3 are described these phases in more detail.

The MATLAB code is annexed in Appendix C.

4.3.3.2 Inputs of the MATLAB model

The main inputs required in the biomass boiler model include:

- Chemical composition (C, H, S, N, O, ash) and moisture content of the biomass.
- The temperature and mass flow rate of the inlet flow.
- The hot storage volume.

All the inputs except for the biomass properties are recalculated at each time step.

4.3.3.3 Biomass boiler operation

According to personnel communication with a biomass boiler manufacturer, a 5 MWth biomass boiler requires about 1 hour to supply its nominal power output from stand-by mode. As the simulation operates with a time step equal to 1 hour, the considered time of the boiler startup is 1 hour as well. During this phase, the biomass fuel is introduced in a

quantity equivalent to nominal conditions (100%). Once the boiler is on, it can modulate in a range between 100 % and 20 % of its nominal power.

In the case that the boiler is not required because solar energy is enough to meet the energy demand, the biomass boiler enters in stand-by mode, reducing the biomass input to 5% of that required at nominal power. During the stand-by mode the introduced air is minimized and the biomass boiler temperature is kept at 400ºC.

4.3.3.4   *Biomass boiler efficiency*

Figure 53 illustrates the biomass boiler partial load efficiency curve considered in the model (green curve). The efficiency decreases as the percentage of nominal power does. The fouling effect is considered as a reduction coefficient equal to the 5% of the boiler efficiency (Shah et al., 2003).
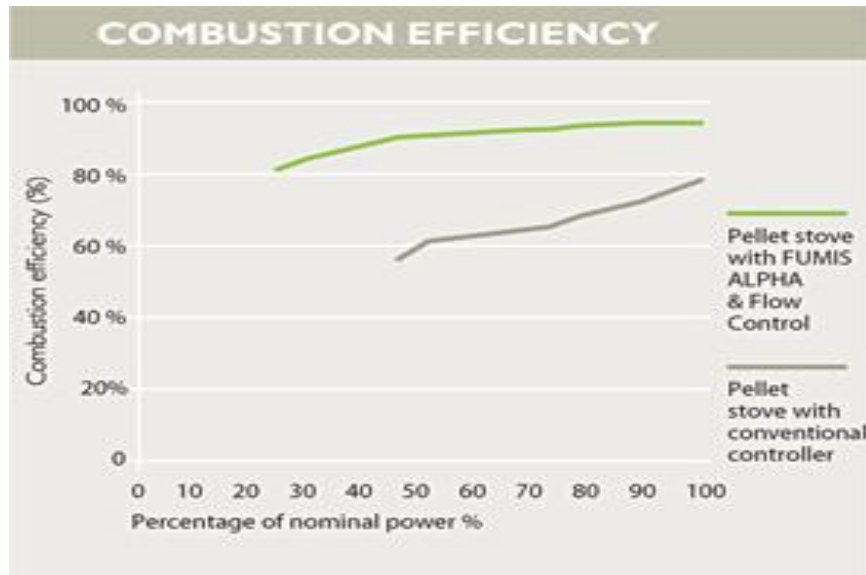

Figure 53. Biomass boiler partial load efficiency (source: Fumis by ATech Electronics).

4.3.3.5   *Biomass boiler and hot storage tank relation*

The biomass boiler thermal output is modeled according to the molten salt level in the hot tank (TES). The regulation system is implemented during the charging and the discharge of the hot storage tank. The Matlab code that describes this regulation system is annexed in the Appendic C.

4.3.3.5.1   Hot tank charging mode

The charging mode starts when the hot storage tank reaches its minimum volume and ends when the tank reaches 50 % of its useful volume. During this time the outlet mass flow rate is equal to zero and the entire energy demand is supplied by the biomass boiler.

66

When the tank volume is within 50 % and 100% of its useful volume the biomass boiler and the storage tank operate together in order to satisfy the energy demand. The relation between the biomass boiler and the tank storage volume is complementary, i.e. when the tank volume increases the boiler output decreases (see Figure 54).

4.3.3.5.2 Hot tank discharging mode

The discharging mode starts when the hot storage tank volume reaches the maximum volume. During this phase the biomass boiler enters in stand-by mode keeping this stage for almost all the discharge time. The biomass boiler enters in operation when the thermal output in the hot tank is just enough to provide 1 hour of full design power cycle operation. The biomass boiler is started up in advance in order to complete the transition phase between the standby mode and the normal operation without stopping the power supply to the ORC cycle (see Figure 55).
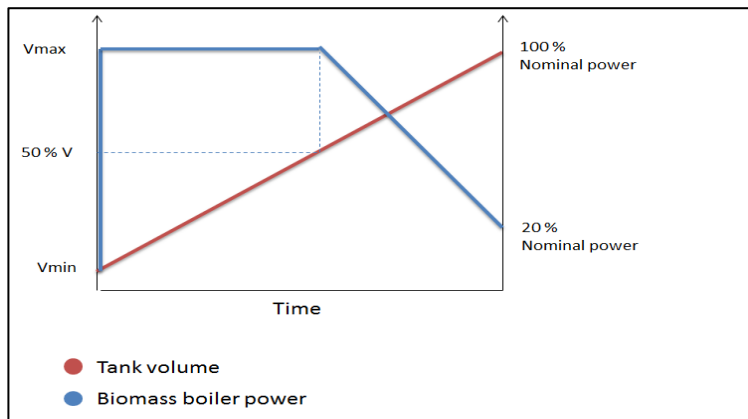

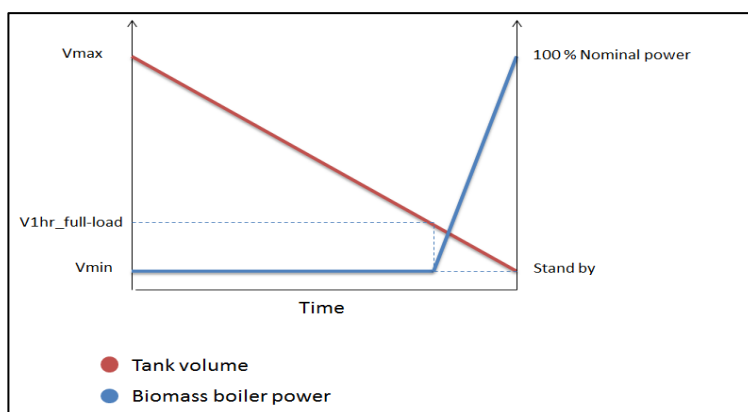**Figure 54. Hot tank charging mode**

Figure 55. Hot tank discharging mode

4.3.3.6   Biomass storage sizing

The biomass storage is design over the basis that the time between a delivery and the next is equal to 4 days. According to this assumption the biomass storage must be projected to contain the required biomass for 4 days at full operation and 4 days at standby mode.

According to Van Loo et al. (2008)**¡Error! No se encuentra el origen de la eferencia.** olive residues have a bulk density that amounts to 650 kg/m^3. Taking as reference this density it is possible to calculate the biomass storage dimension.

Table 17. Biomass storage volume.

Useful volume (m^3)	Emergency volume (m^3)	Total storage volume (m^3)
259.5	14.0	273.5

4.3.4   Power block simulation

The power block is simulated in a simplified way. The key components are:

- an evaporator of the cycle (Type 5b);
- a temperature controller (Type 22);
- an electrical load profile of the consumers (Type 14h).

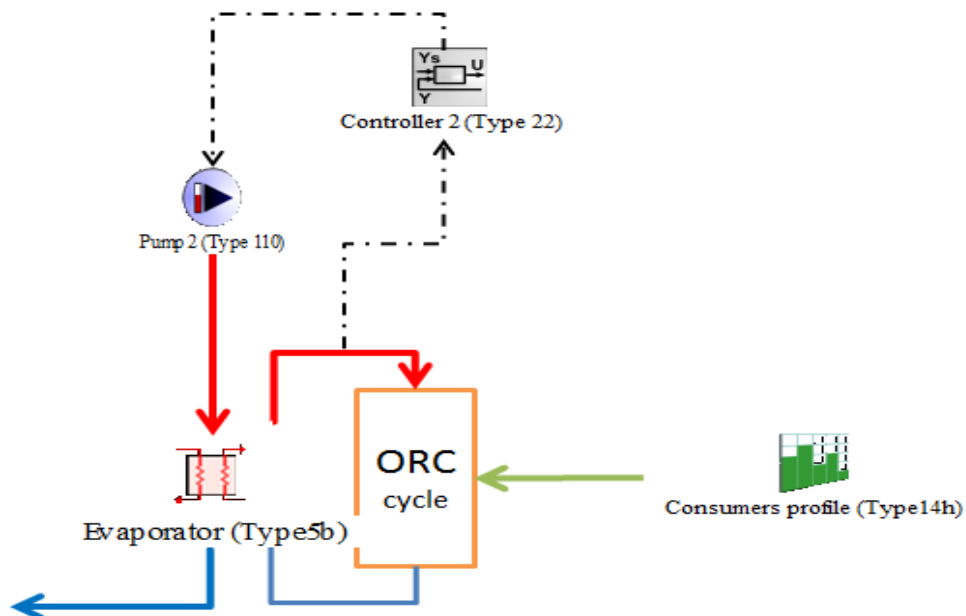The scheme with the corresponding links is as follows:

Figure 56. Scheme of the power block system

4.3.4.1   Evaporator (Type 5b): _Evaporator_

This component is a heat exchanger. In the source side flows the hot molten salt coming from the thermal storage, while in the load side flows the organic fluid coming from the ORC cycle.

The selected organic fluid is a cyclic siloxane (D_6) as this compound presents the desired technological characteristics for ORC working fluids: low toxicity and flammability, low foul formation over heat transfer surfaces, good material compatibility and good thermal stability (Fernandez et al., 2011).

The mass flow rate of the organic fluid is calculated through the following equations:

$$\eta_{ORC} = C_{partial,load} * \eta_{ORC,100\%} \qquad \qquad \textbf{Eq. 38}$$

$$Qev = \frac{P_{ORC}}{\eta_{ORC}} \qquad (\textbf{MW}) \qquad \textbf{Eq. 39}$$

$$m_{D6} = \frac{Q_{ev}}{Cp_{D6}*\Delta T_{D6}} \qquad \left(\frac{\textbf{Kg}}{\textbf{s}}\right) \qquad \textbf{Eq. 40}$$

Where:

- m_{D6}: the organic fluid mass flow rate (kg/s).
- Q_{ev}: Thermal power required by the ORC cycle (MW).
- cp_{D6}: average heat calorific value of the organic fluid (MJ/kgK).
- ΔT_{D6}: the temperature difference between the inlet and outlet organic fluid in the heat exchanger (K).
- P_{ORC}: Electric demand derived from the consumption profile (MW).
- η_{ORC}: The ORC efficiency.
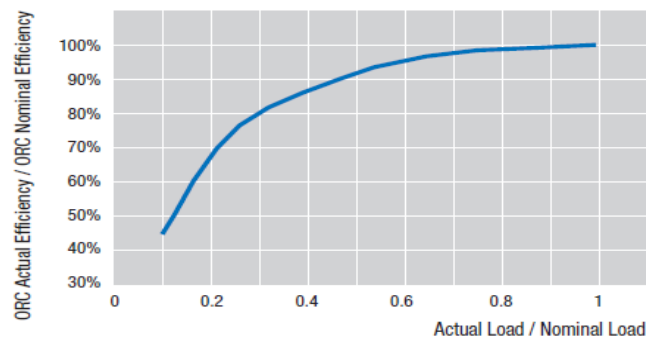- $C_{partial,load}$: The ORC partial load coefficient (see Figure 57).

Figure 57. ORC partial load efficiency (source: PW Power Systems, 2013).

4.3.4.2 Feedback Controller (Type 22) : *controller 2*

The controller 2 is added to the system in order to keep the outlet temperature of the organic fluid leaving the generator around the set point temperature, as well as, to avoid the overheating of the organic fluid, causing its decomposition. For this purpose the controller manipulates every hour the quantity of molten salt entering into the generator.

4.3.4.3 Load profiles (Type 14h): *consumers profile*

Type 14h allows the user to fix an hourly load daily profile which is adopted during the 365 days of the year. Three load profiles are simulated with TRNSYS:

- Profile 1: considers a constant electric load, with the assumption that the excess power is sold to the grid;
- Profile 2: considers a time dependent electric load, with nighttime load (from 8 pm until 8 am) equal to half the daytime load (from 8 am until 8 pm).
- Profile 3: This profile does not consider the electrical load; instead it considers the thermal load of the user. This profile is analyzed since the bigger part of the produced energy by the ORC cycle is composed by thermal energy, and the cogeneration systems are generally designed in order to follow the thermal load.

The third profile is derived from the daily curve of thermal energy demand in a winter day for the residential sector (Macchi et al., 2005).
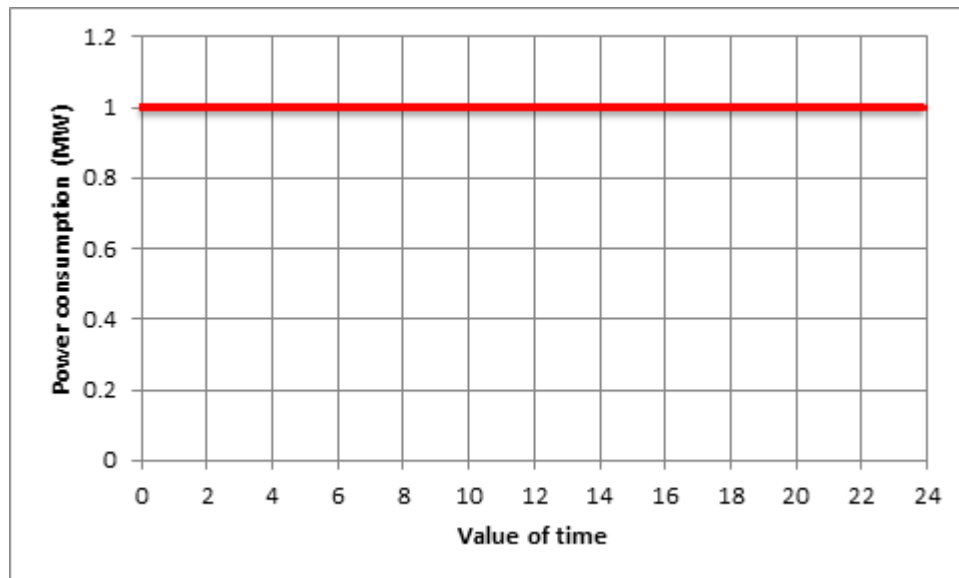
Figure 58. Constant electrical load (Profile 1).
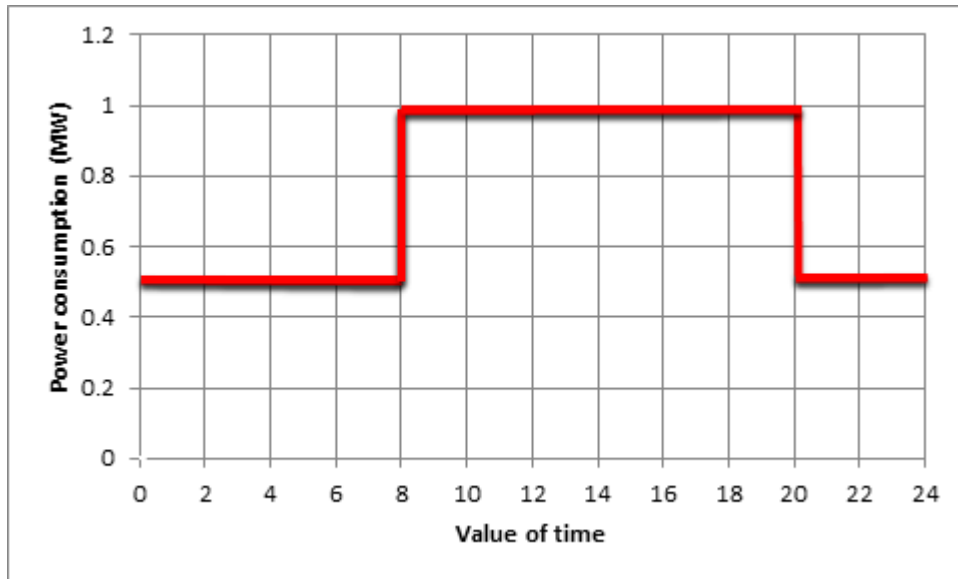
Figure 59. Time dependent electrical load (Profile 2).
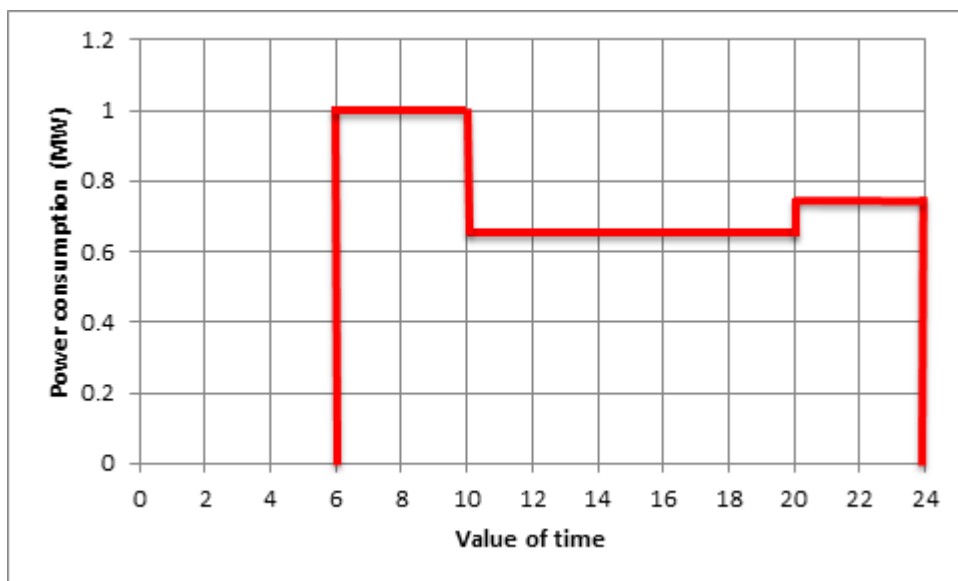
Figure 60. Thermal load profile (Profile 3).

4.3.5   Complete system

In order to simulate the entire generation system it is necessary to link the subsystems described. The simplified scheme is shown in Figure 61 while a screenshot of the simulation in TRNSYS is displayed in

Figure 62.
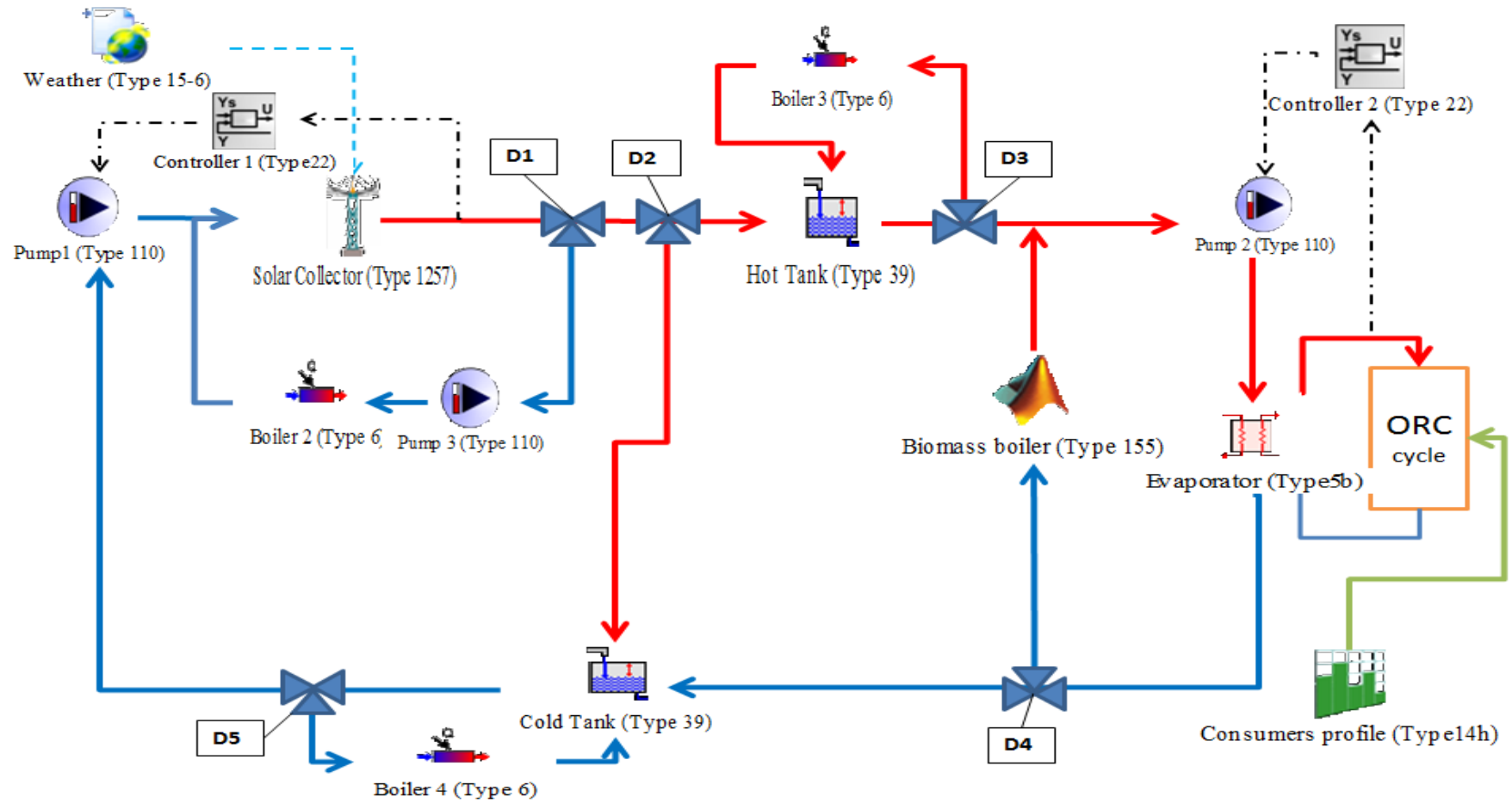
Figure 61. Scheme of the energetic system.
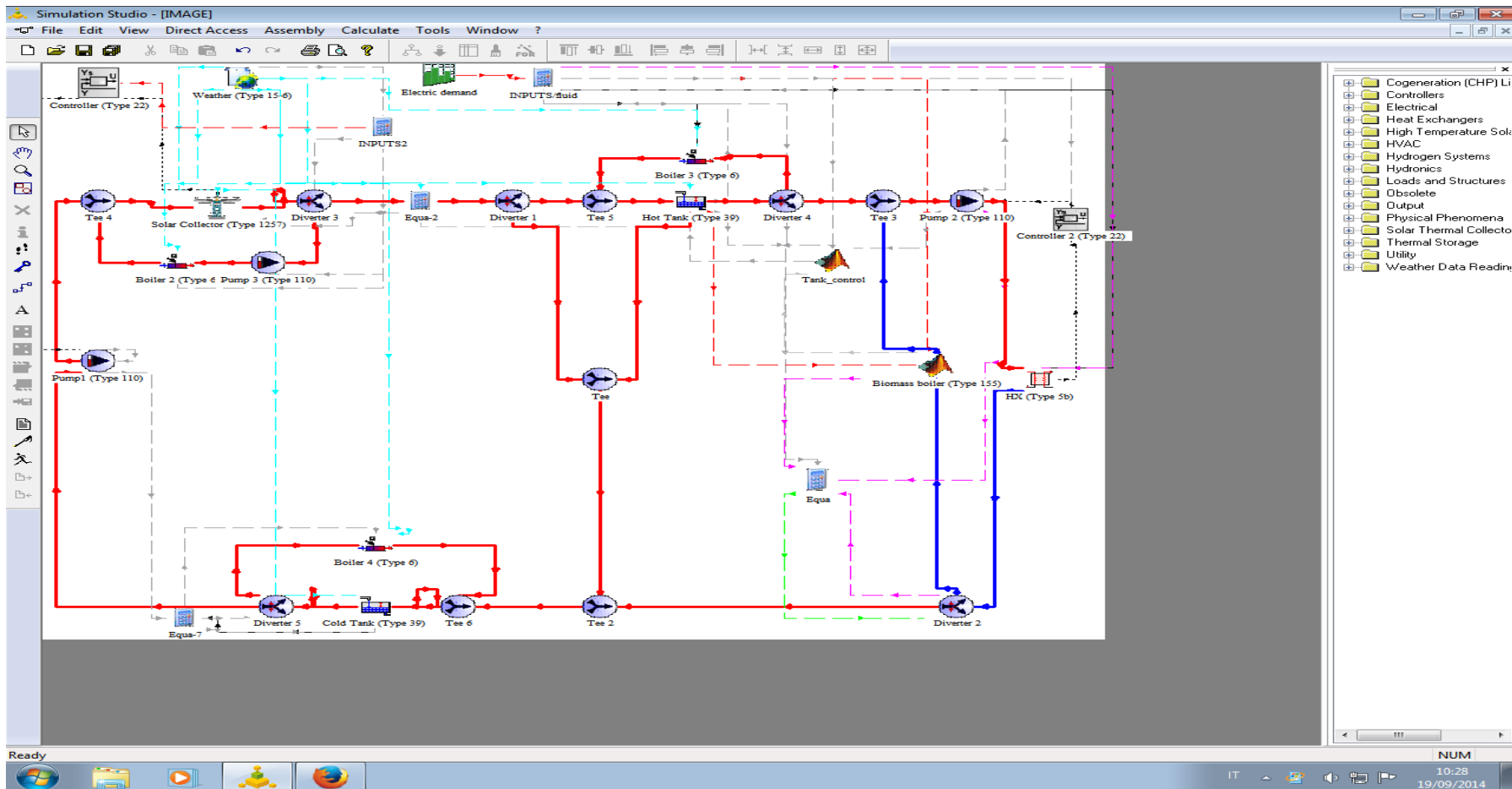
Figure 62. Scheme in TRNSYS of the energetic system.

4.4 Inputs of the TRNSYS and SAM simulation

Geographical

- Location: Brindisi –Italy.

Solar field

- Solar field orientation: North – South alignment.
- Nº collectors in one loop: 6.
- Collector aperture area: 600 m.
- Solar field inlet temperature: 200 ºC.
- Solar field outlet temperature: 450 ºC.
- HTF: Hitec XL.

Power block

- Power block capacity: 1MWe.
- ORC fluid: D_6 (cyclohexasiloxane).
- ORC lower temperature: 190ºC.
- ORC higher temperature: 360 ºC.

Table 18. Cyclohexasiloxane properties (source: Fernandez et al., 2011).

| Cyclohexasiloxane (D6)	
Type of fluid	silicone oils
Molecular mass (kg/ kmol)	444.9
Critical pressure (bar)	9.6
Critical temperature (ºC)	372.6
Boiling temperature (ºC)	244.9
Cp (kJ/kgK)	1.6

Thermal Storage

- Storage capacity: 10 hours.
- Storage useful volume: 214 m^3.
- Storage minimum volume: 10 m^3.
- Storage total volume: 234 m^3.
- Storage fluid: Hitec XL.

CHAPTER 5

Simulation results

5.1 Comparison of the energy performance with different sizes of the solar field

The power plant has been simulated with the inputs specified in the previous chapter. The simulation is carried out with a constant power demand (see Figure 58). For each simulation, the number of loops in the solar field has been changed, starting from zero up to 15 loops. As mentioned in the TRNSYS model description, one loop of the solar field includes 6 collectors in series and the loops operate in parallel.

Figure 63 displays the thermal energy coming from the solar field and thermal storage (blue line) and the biomass consumption of the boiler (red line) for the different number of loops:
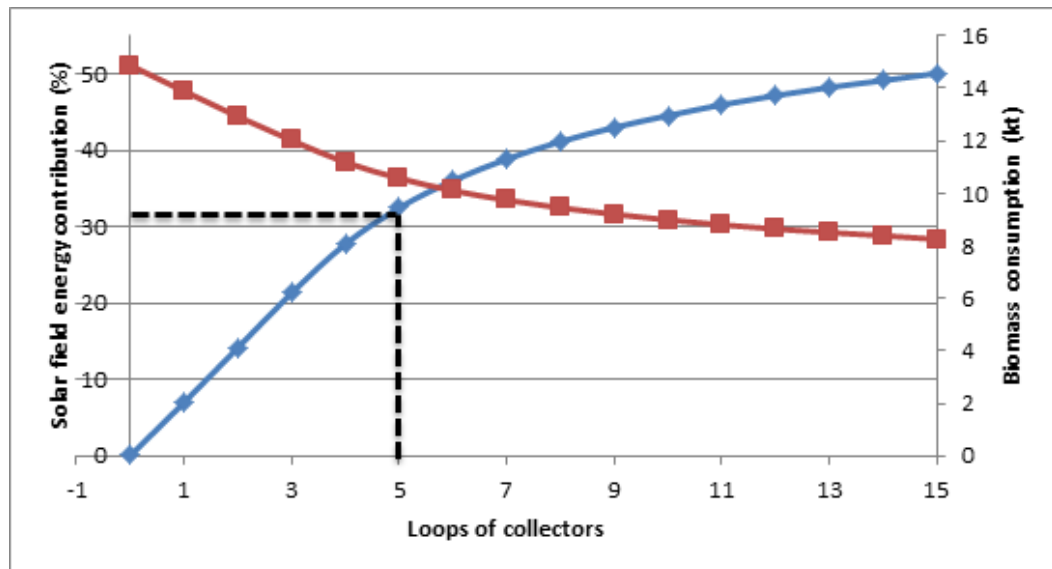
Figure 63. Percentage of the thermal energy to the power block coming from the solar field and TES (blue line) and biomass consumption (red line).

As expected when the number of loops of collectors increases the contribution of the solar field rises as well as the biomass consumption falls. The relation between the size of the solar field and the solar energy contribution follows a linear tendency when the number of loops goes from zero loops to about 5 loops, i.e., when the number of collectors duplicates its power contribution doubles as well. On the other hand, when the number of collector loops exceeds 5 loops, the blue line follows again an almost linear tendency, but in this case the slope is quite lower.

It is worth to highlight that from 5 collector loops and up, the increase of the number of collectors becomes unprofitable. The explication of this performance is that

during times when there is enough solar resource and the solar field is too large, the produced thermal energy will be more than the power block and the storage tank can handle.

In general, there is a meaningful relation between the solar field size and the rest of the components (power block, thermal storage, etc.). Therefore, it is important to select a correct configuration in order to provide sufficient thermal energy to the power block at its rated capacity and at the same time to reduce the dumped energy.

For the currently 1 MWe parabolic trough power system integrated with 10 h thermal storage, the most convenient solar field size is found to be 5 loops of collectors, in consequence the solar field thermal energy contribution will be slightly more than 30 %.

The required area for the power plant is around 7.8 ha. Figure 64 illustrates the possible configuration of the parabolic trough power plant.
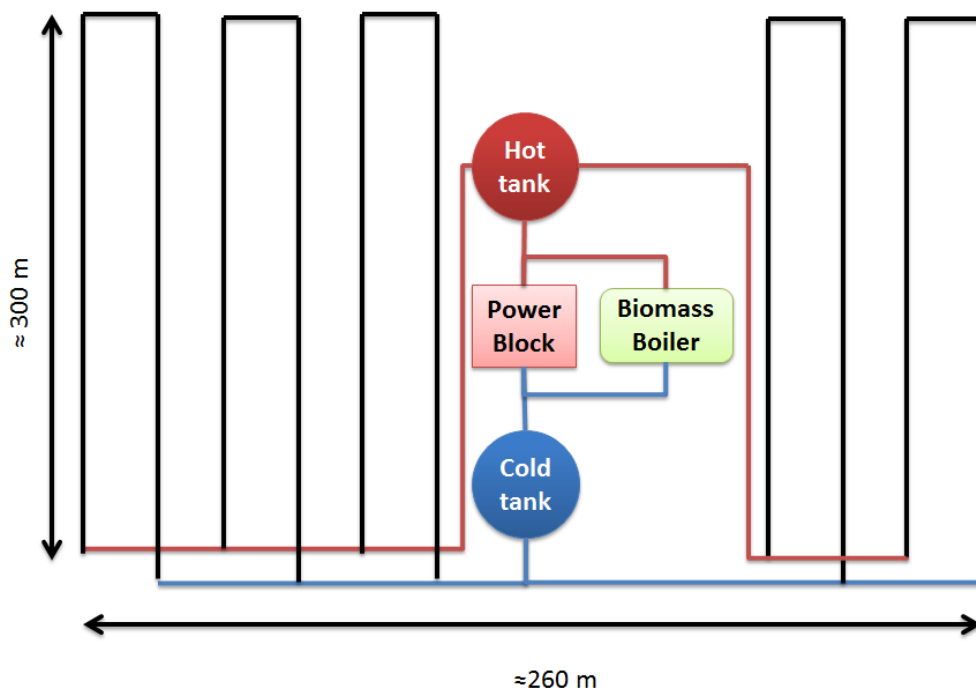
Figure 64. Surface of the solar field.

5.2 Comparison of energy performance with different heat transfer fluids.

Once determined the size of the solar field, the simulation focuses on the HTF. The HTF employed until now, the Hitec XL, is substituted by the Hitec solar salt, a binary molten salt mixture. So far Hitec solar salt is the most popular storage fluid in the CSP plants. This comparison is done in order to determine which of both fluids is most suitable for the parabolic trough power plant.

Table 19 displays the molten salt properties.

Table 19. Hitec solar salt and Hitec XL chemical and physical properties (source: <u>Kerney & Assoc et al., 2001</u>).

	SOLAR SALT	HITEC XL
Type of fluid	Nitrate salt	Nitrate salt
Composition	60% $NaNO_3$, 40 % KNO_3	48% $Ca(NO_3)_2$, 7% $NaNO_3$, 45% KNO_3
Freezing temperature	238	120
Maximum optimal temperature	593	500
Average Cp (kJ/kgK)	1.50	1.43
ρ (kg/m^3)	1872.5	1957.3

The inlet and outlet temperature of the HTF in the solar field is modified due to the different range of temperature operation between both heat transfer fluids. The inlet and outlet temperature of the HTF in the solar field will be 290 ºC and 550ºC respectively. The rest of the inputs remain unchanged.

Figure 65 displays the thermal energy supply by the solar field and the thermal storage system for each type of HTF. According to this plot the thermal energy from the solar field and the TES to the power block is higher when the power plant operates with the Hitec XL. The reason of this result is directly related to the maximum molten salt operating temperature. A higher operating temperature, as the case of the Hitec solar salt, produces higher thermal losses in the receiver tube and in the storage tank.
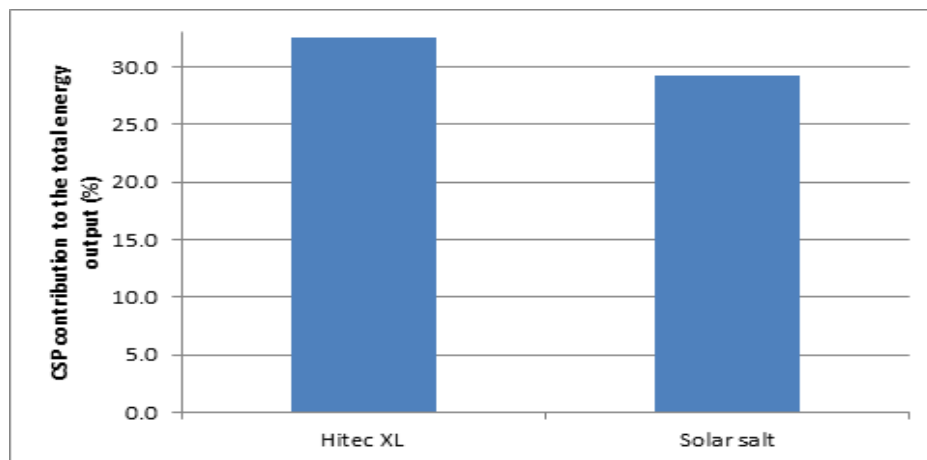

Figure 65 : Percentage of the thermal energy contribution of the solar field and thermal storage operated with Hitec XL and Solar Salt as HTF.

Figure 66 illustrates the parasitic losses in the parabolic trough power system for the two different heat transfer fluids. If Hitec XL is employed, the parasitic losses amount to about 900 MWh, this value reaches almost the double when the Solar Salt is employed. The explanation of this result is again the maximum operating temperature of the HTF. At a lower operation temperature the required energy to keep the thermal storage in the set point temperature is lower.
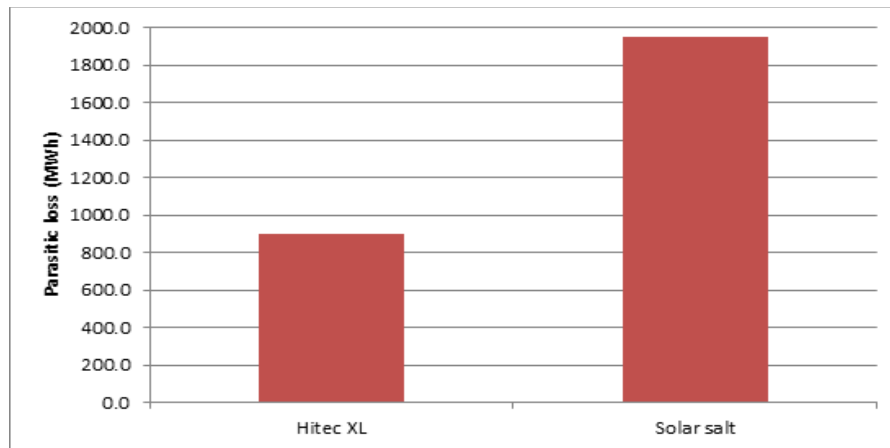
Figure 66 : Parasitic losses in the parabolic trough power plant employing Hitec XL and Solar Salt as HTF.

To sum up, the most suitable HTF for the actual parabolic trough power system is the Hitec XL.

5.3 TRNSYS final results

Once established the optimal solar field size and the most suitable HTF, the results of the simulation with TRNSYS are discussed in this section.

The following figures show the operational temperatures of the most relevant components in the system, the annual electric and thermal output of the parabolic trough power plant, the biomass boiler relation with the storage volume, the molten salt mass flow rate, and the dimension of the biomass feedstock for the selected load profiles.

5.3.1 Operating temperatures in the solar field, the power block generator and the biomass boiler

The following figures illustrate the temperatures related to the most pertinent components of the system: the solar field, the power block generator and the biomass boiler.

5.3.1.1 Inlet and outlet temperature of the HTF in the solar field

Figure 67 and Figure 68 illustrate the hourly temperature of the HTF temperature during January and July. As mentioned, the operating temperature of the HTF in the solar field ranges from 200 ℃ to 450 ℃. However the maximum temperature is only reached in the

hours of high solar radiation, while during nighttime or in cloudy or rainy hours the HTF temperature reaches its minimum value, and is kept by the backup system.

As expected, the maximum temperature is achieved for more hours during the month of July, with around 90 % of the daily hours, than during the month of January, with about 50 % of the daily hours.

On the other hand, the HTF temperature at the inlet of the solar field, represented by the red curve in Figure 67 and Figure 68, is equal or greater than 200 ºC in both months. According to Figure 67 and Figure 68, this temperature varies between 200 ºC and 300 ºC. The reason of this variation is that when the HTF does not reach a set temperature when it leaves the solar field, it is diverted into the cold tank, thus the cold tank temperature varies. The HTF that enters into the solar field comes from the cold tank.

It was already mentioned the importance of maintaining the molten salt temperature always over its freezing point temperature. As shown Figure 67 and Figure 68, this requirement is always accomplished.
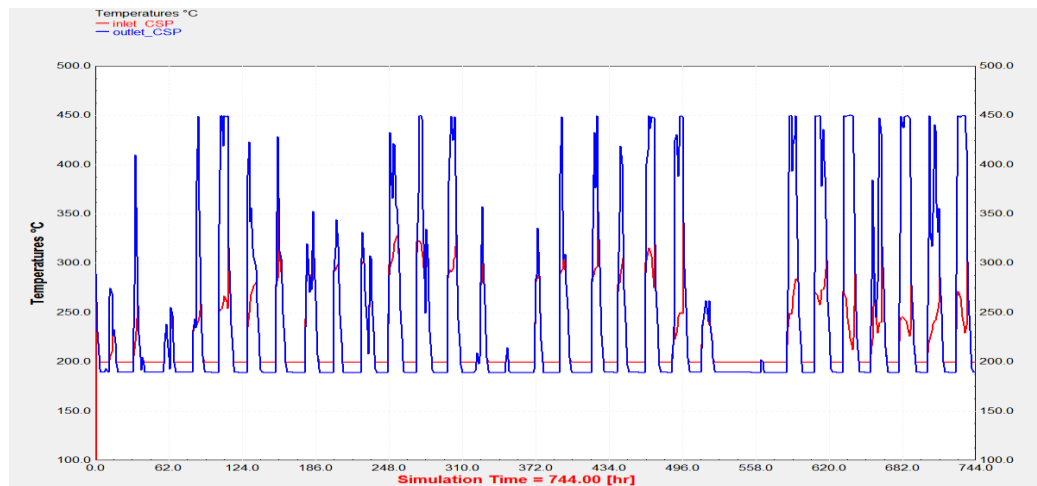
Figure 67. Inlet temperature (red curve) and outlet temperature (blue curve) in the solar field in January (created with TRNSYS).

79
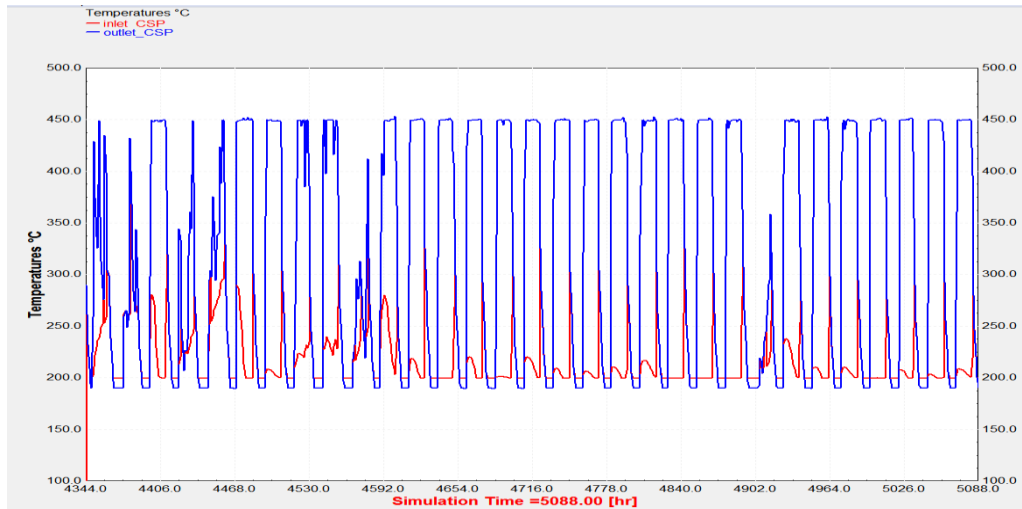
Figure 68. Solar field inlet and outlet temperature in July.

5.3.1.2 Inlet and outlet temperature of the source and load side of the power block generator.

The HTF flows in the source side of the generator, while in the load side flows the fluid to be heated, in this case the organic fluid.

As illustrates Figure 69, the molten salt enters at 450 ℃ into the heat exchanger and leaves at almost 200 °C (red and blue line respectively). In the load side the organic fluid enters at 190 °C and exits at its set point temperature, controlled by the feedback controller, at 360 °C (pink and orange line respectively). This tendency is maintained throughout the year, since the simulated load profile is constant.

Both fluids comply with their design temperature.

Figure 69. Inlet and outlet temperature in the source and load side in the power block generator.

80

5.3.1.3 Inlet and outlet temperature of the HTF in the Biomass boiler

Figure 70 shows the temperature of the HTF at the inlet (red line) and outlet (blue line) of the biomass boiler. As expected, when the boiler is operating under design conditions the Hitec XL enters at 200 ºC and leaves at 450ºC. Instead, when the boiler enters in stand-by mode the inlet and outlet HTF temperature are equal.
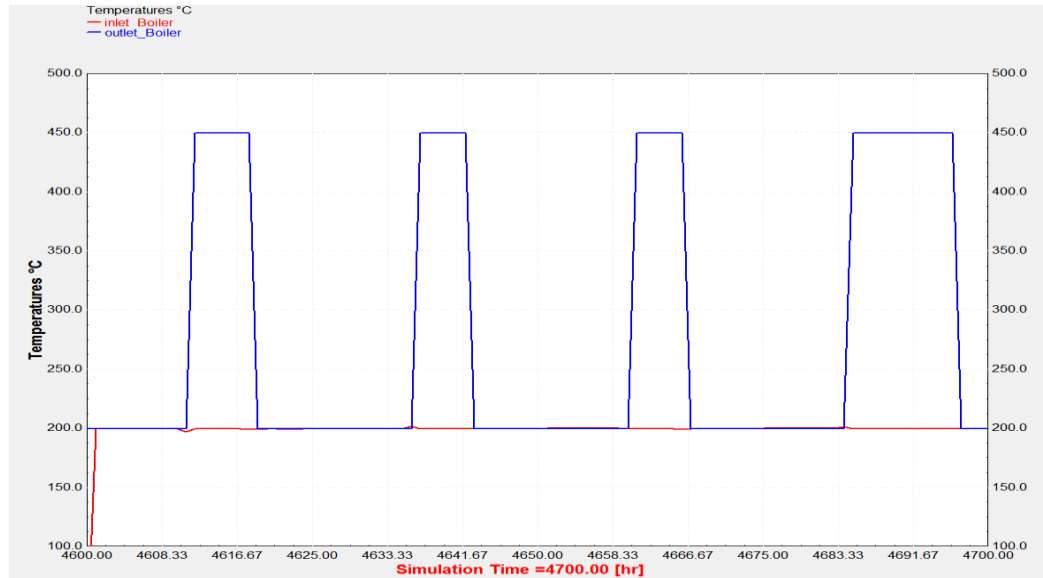
Figure 70. Inlet and outlet temperature of the Hitec XL in the biomass boiler (blue and red line respectively).

5.3.2 Electrical output and thermal energy available in the condenser

As mentioned, the simulation of the power plant is carried out for three different load profiles, profile 1, profile 2 and profile 3.

Figure 71, Figure 72 and Figure 73 display the thermal energy transferred by the HTF to the power block (pink line), the thermal energy rejected by the condenser (blue line) and the gross electric output produced by the turbine of the power block (red line) for each profile.

For all the simulations the thermal energy to the power block at full rate capacity amounts to around 4.2 MWth, while the rejected thermal energy in the condenser is slightly more than 3 MWth and the gross electrical output reaches 1 MWe.
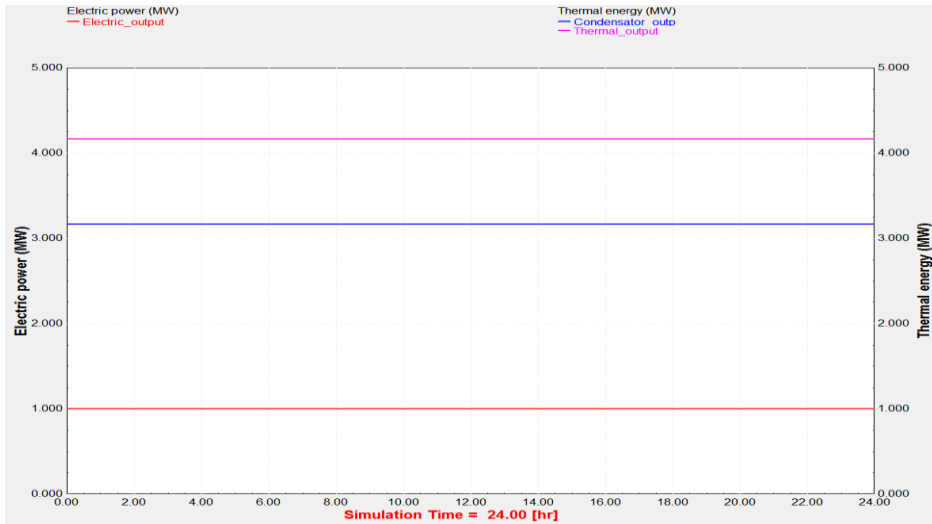
Figure 71. Energy output of the power plant with the Profile 1.
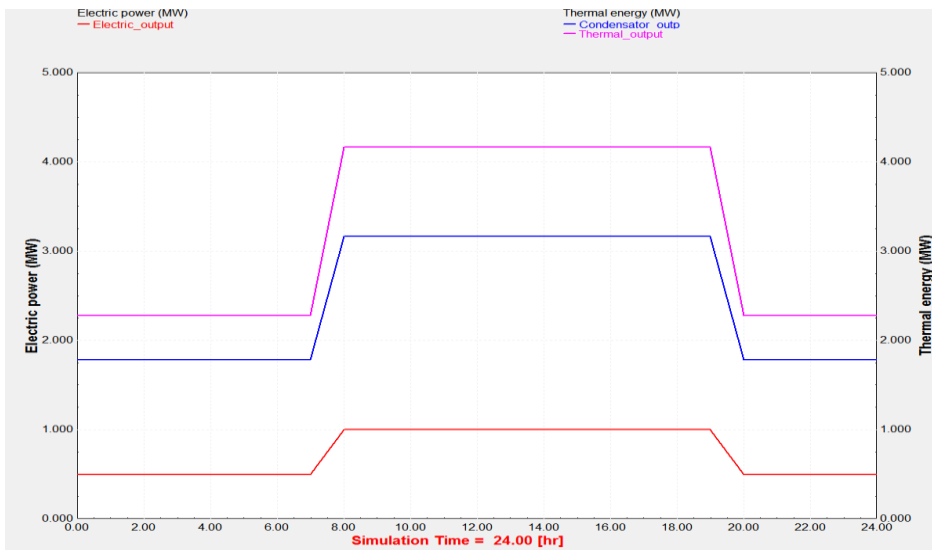
Figure 72. Energy output of the power plant with the Profile 2.
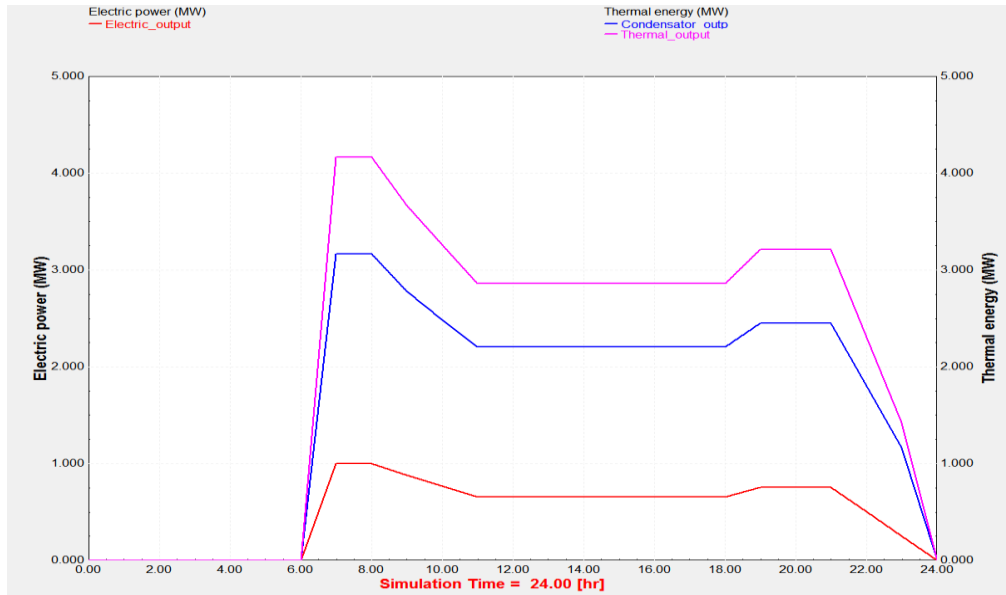
Figure 73. Energy output of the power plant with the Profile 3.

Table 20. Results of the annual simulation with each load profile.

	Profile 1	Profile 2	Profile 3
Annual gross electric power (MWh).	8743.5	6554.2	4361.3
Annual thermal energy rejected in the condenser (MWh).	27761.2	21694.1	14454.3
Annual biomass demand (kt).	10.6	7.4	4.5
Volume of the biomass storage (m^3).	273.5	273.5	273.5

5.3.3 Mass flow rate operating at different load profiles

The molten salt mass flow rate in the principal components of the power plant is described according the three load profiles and the month of the year.

Figure 74 and Figure 75 illustrate the trend of the mass flow rate in a day of January and July respectively operating with a constant profile (Figure 58). According to Figure 74 the molten salt mass flow rate required by the power block operating at 1 MWe is around 12 kg/s, while the molten salt mass flow rate from the solar field is slightly lower than 2.5 kg/s. The missing flow is provided by the storage tank until 8 am and from 8 am to midnight the molten salt stops flowing in the solar field, instead it is heated by the biomass boiler. On the other hand, during the day of July (see Figure 75)

83

more than half of the time the mass flow rate from the biomass boiler is zero i.e. the thermal energy to the power block comes from the hot storage tank.

Figure 74. Solar field outlet flow rate (red line), hot tank outlet flow rate (green line), flow rate in the biomass boiler (blue line), load flow rate in the evaporator (Orange line). Based on profile 1 in a day of January.
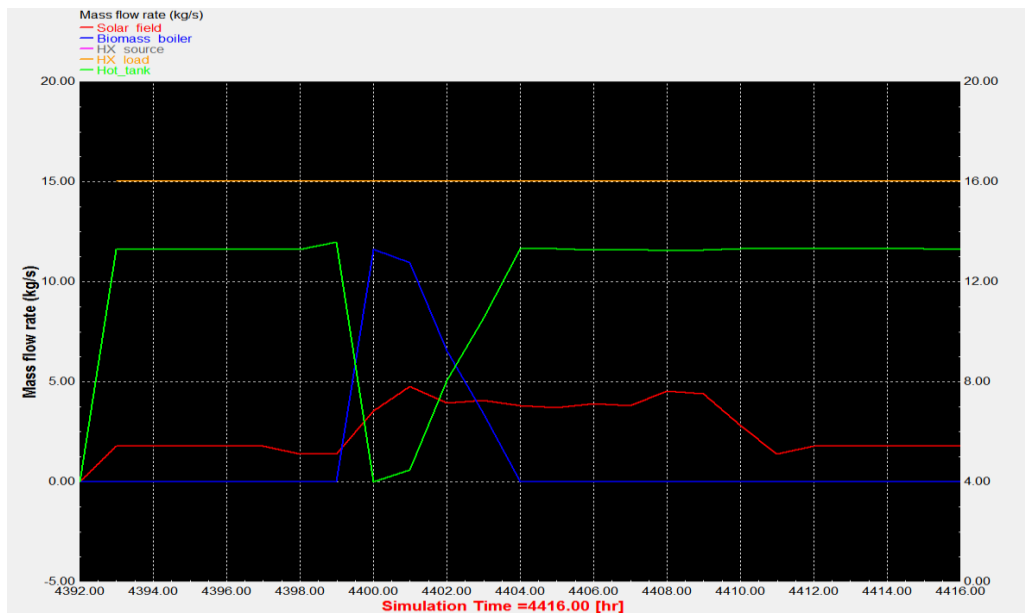
Figure 75. Solar field outlet flow rate (red line), hot tank outlet flow rate (green line), flow rate in the biomass boiler (blue line), load flow rate in the evaporator (Orange line). Based on profile 1 in a day of July.

When the power plant operates under a non-constant profile (see Figure 59 and Figure 60) and during the month of July, the molten salt that flows to the power block comes 100 % of the time from the storage tank, i.e. the boiler is in stand-by mode (see Figure 77 and Figure 79).
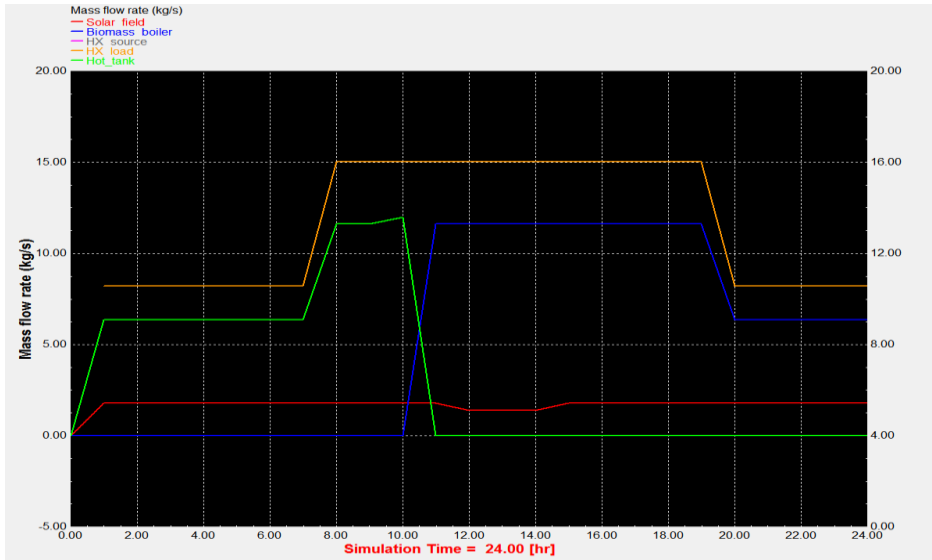
Figure 76. Solar field outlet flow rate (red line), hot tank outlet flow rate (green line), flow rate in the biomass boiler (blue line), load flow rate in the evaporator (Orange line). Based on profile 2 in a day of January.
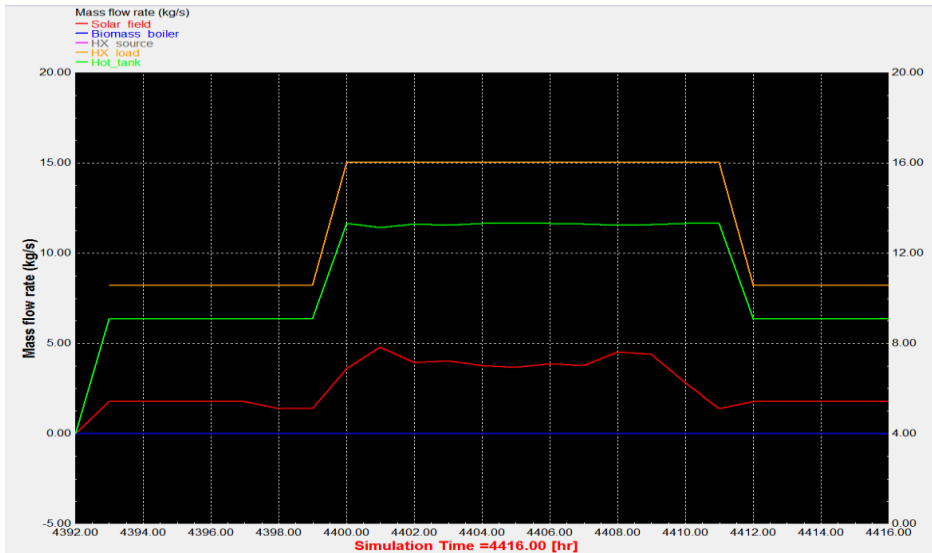
Figure 77. Solar field outlet flow rate (red line), hot tank outlet flow rate (green line), flow rate in the biomass boiler (blue line), load flow rate in the evaporator (Orange line). Based on the profile 2 in a day of July.

85
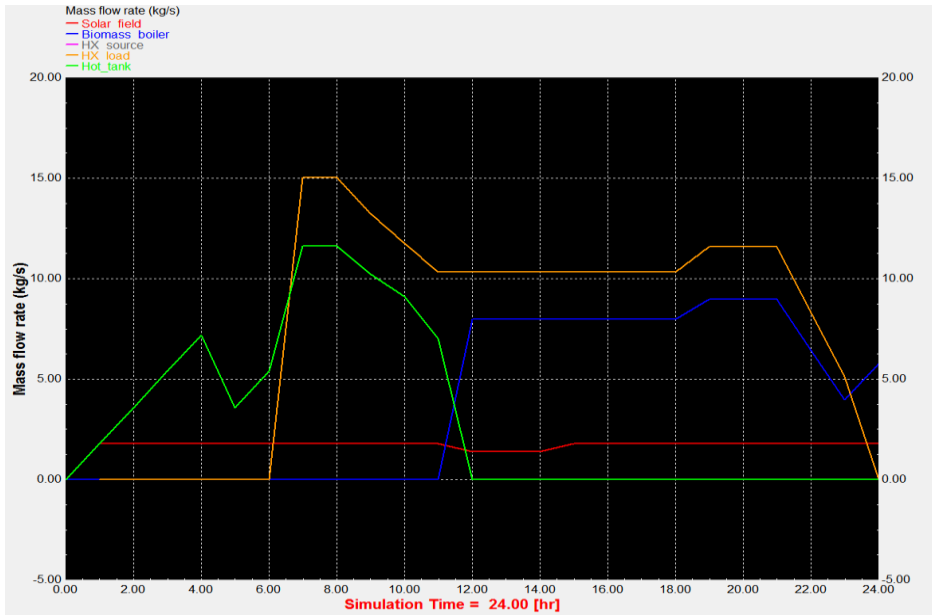
Figure 78. Solar field outlet flow rate (red line), hot tank outlet flow rate (green line), flow rate in the biomass boiler (blue line), load flow rate in the evaporator (Orange line). Based on the profile 3 in a day of January.
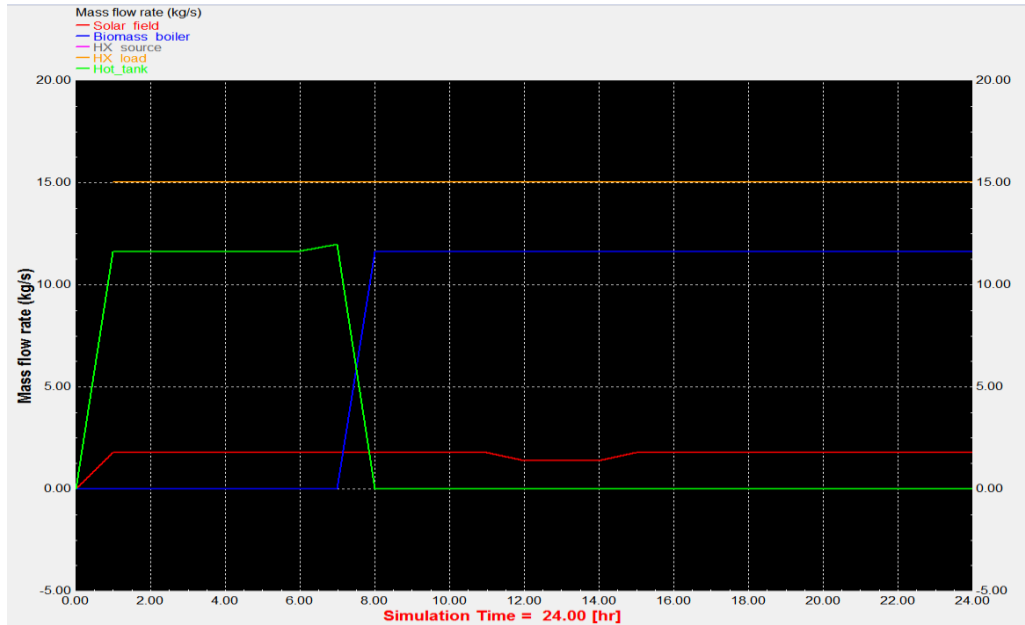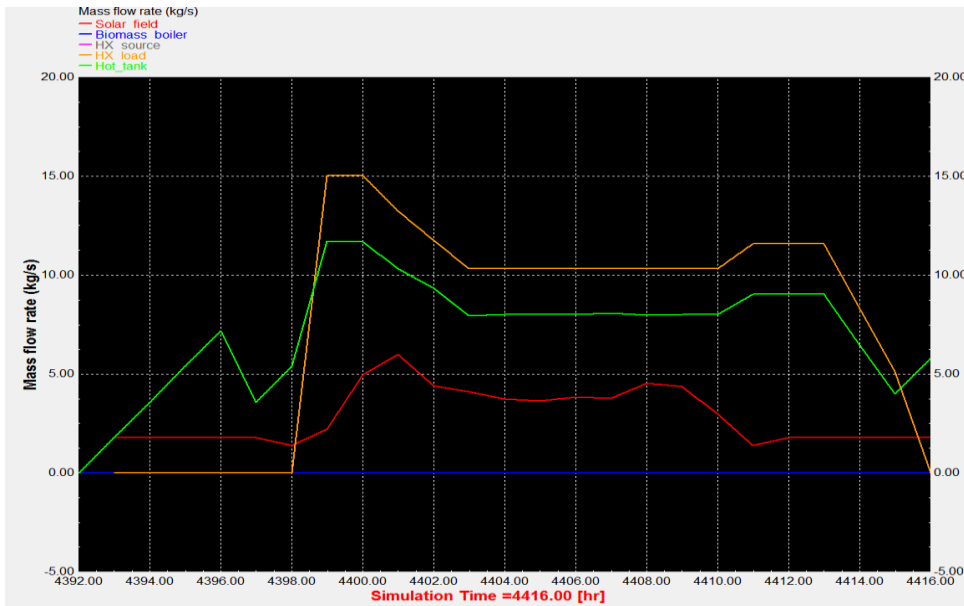

Figure 79. Solar field outlet flow rate (red line), hot tank outlet flow rate (green line), flow rate in the biomass boiler (blue line), load flow rate in the evaporator (Orange line). Based on the profile 3 in a day of July.

5.3.4 Relation between the biomass boiler thermal output and the molten salt level in the hot tank volume

Figure 80 displays the variation of the biomass boiler thermal output and the hot storage volume in the same period of time. When the hot tank volume exceeds about 150 m^3, the 70 % of the total useful volume, the boiler enters in stand-by mode. The opposite occurs when the hot tank volume is close to its minimum volume (see Figure 54 and Figure 55).
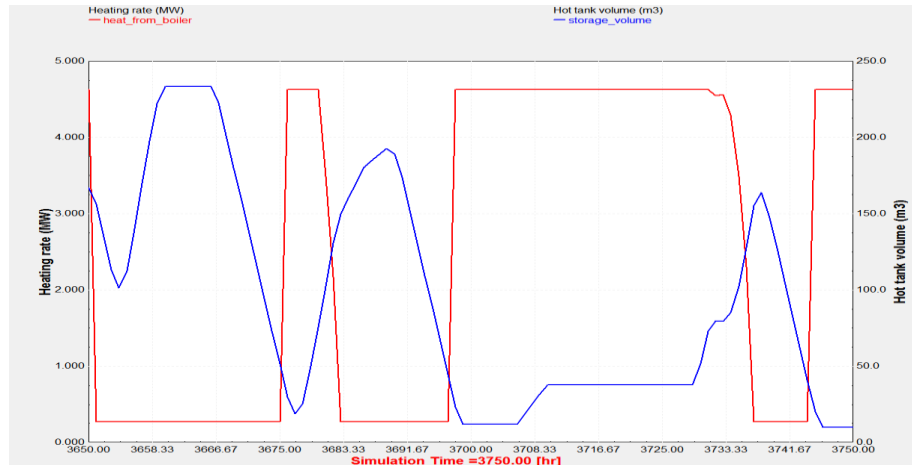
Figure 80. Relation between the biomass boiler thermal output (red line) and the hot tank volume (blue line).

5.4 Comparison of the results obtained with TRNSYS and SAM

Before the comparison of the results obtained with SAM and TRNSYS, it is worth to specify that the weather data used in the simulation with SAM is derived from the Energy Plus website in EPW format, therefore, differs quite bit from the TRNSYS weather data derived from Meteonorm. Figure 81 shows the Direct Normal Irradiation (DNI) for the city of Brindisi derived from each weather data.
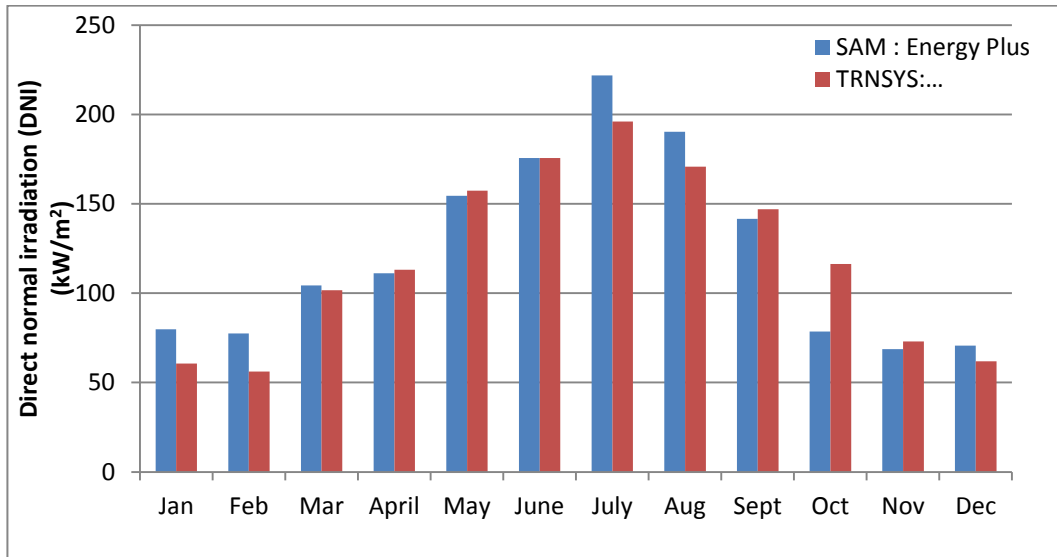
Figure 81. Direct Normal Irradiation in the city of Brindisi from Energy Plus and Meteonorm weather data (source: Energy Plus, Meteonorm).

The simulation with SAM is performed with a solar field of 5 loops and a constant profile of 1 MWe of electrical load. The other inputs are the same as indicated in section 4.4 "Inputs of the TRNSYS and SAM simulation"

Figure 82 illustrates the trend of the thermal energy coming from the solar field and TES to the power block when the number of collector loops in the solar field increases, in order to verify the optimal size of the solar field. As demonstrated in Figure 63 the relation between the area of the solar field and the solar energy contribution follows a linear tendency when the number of loops goes from zero loops to about 5 loops, after this point, from 5 collector loops and up, the increase of the number of collectors becomes unprofitable.
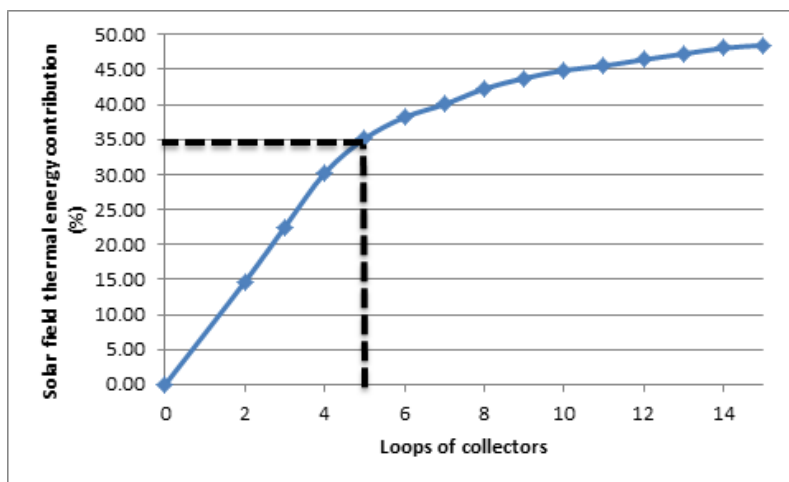
Figure 82. Percentage of the thermal energy to the power block coming from the solar field and thermal storage.

Figure 83 illustrates the electric output from the power plant without the integration boiler, obtained through both models, TRNSYS and SAM.

In the case of the results generated with TRNSYS, the electric power presents almost a symmetrical tendency throughout the year. From January to July the electric output grows following almost a linear tendency. The electric generation reaches its maximum value in the month of July with around 450 MWhe and then starts falling from July until the end of the year.

The results obtained with SAM are not so far from those obtained with TRNSYS. In this case also the electric output grows from January to July following almost a linear tendency. The electric generation reaches its maximum value in the month of July with around 460 MWhe and then starts falling from July until the end of the year.

In general, the trend of the monthly electric output is coherent with the monthly solar irradiation available in the city of Brindisi, according to the weather data adopted for each model (see Figure 81). This is why in some months like October the difference in the electric output is more evident ($\Delta = 66.3$ %). If the weather data for both simulations were the same it is to be expected that the results would be in accordance.
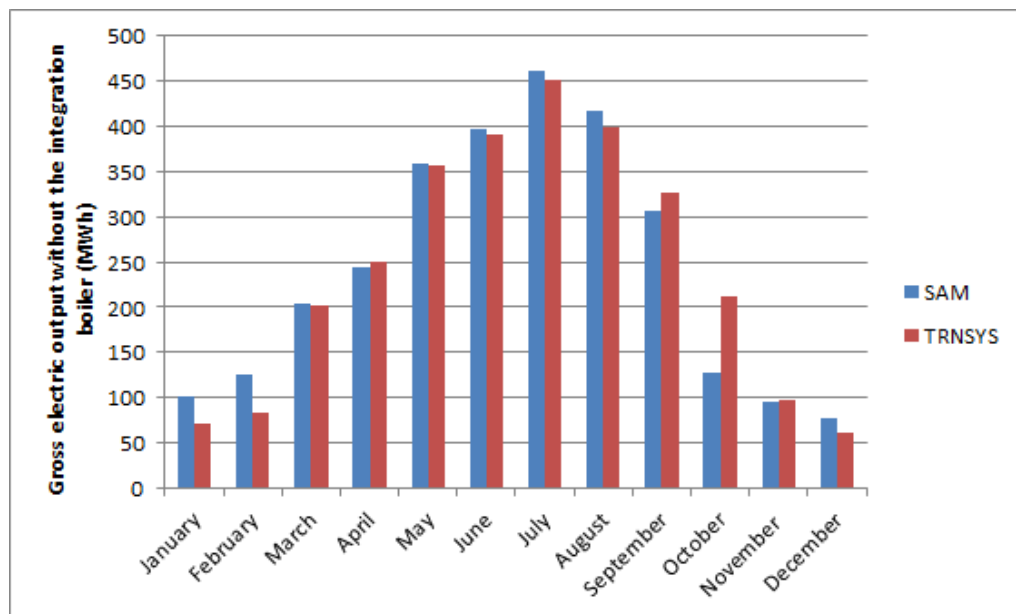
Figure 83. Gross electric output of the power plant without the integration boiler.

Table 21. Gross electric output of the power plant without the integration boiler in SAM and TRNSYS.

Month	Gross Electric Output (MWh) monthly		
	SAM	**TRNSYS**	**Δ (%)**
January	101.0	71.3	-29.4
February	124.7	83.0	-33.4
March	204.4	201.6	-1.4
April	243.1	249.5	2.6
May	357.8	356.1	-0.5
June	396.5	391.6	-1.2
July	461.2	450.7	-2.3
August	418.1	399.5	-4.4
September	306.8	326.5	6.4
October	127.2	211.5	66.3
November	95.3	96.8	1.6
December	76.9	61.0	-20.7

Figure 84 shows the performance of the power plant with and without the integration boiler.

According with this plot, the gross electric output is slightly lower than 3000 MWhe with both simulation programs. This means that a parabolic trough power plant with 10 h thermal storage (without the boiler) can operate at full load only 3000 hours in the year. In the case of the simulation performed with SAM the gross electric output is quite greater due to the higher DNI considered.

Adding the integration boiler, the generated gross electric output increases in around 200 % in both simulations, thereby pushing it to 8760 MWhe. In this case the electrical output becomes identical for both simulations, because regardless of the available solar energy, the boiler will always fill the missing energy in order to supply the energy load.
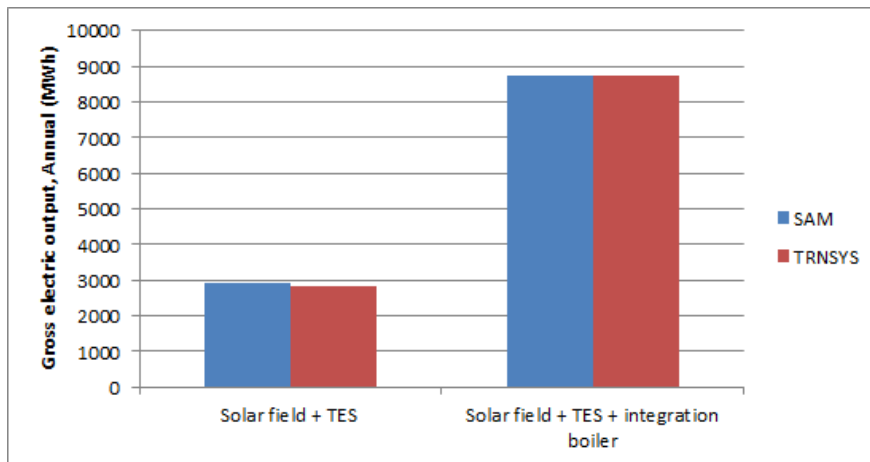
Figure 84 : Gross electric output of the power plant without and with the integration boiler.

Table 22. Gross electric output of the power plant without and with the integration boiler.

Gross electric output (MWh)	SAM	TRNSYS	Δ (%)
Solar field + TES	2912.9	2848.2	-2.2
Solar field + TES + integration boiler	8760.0	8760.0	0.0

Figure 85 and Figure 86 illustrate the energy flow in the power plant operating at constant profile without the integration boiler, modeled with SAM and TRNSYS respectively. As mentioned when the power plant operates without the boiler the optical and thermal losses in the solar field reduced the input incident radiation between 40 % and 50 %. After this lost the next large energy lost is in the thermal to electrical conversion, where around a 70 % of the input energy in the power block is rejected in the condenser. Finally the average net solar to electrical efficiency of the power plant amounts to between 5.5% and 8 % according TRNSYS and SAM respectively (see Table 23).

The integration of the parabolic trough power plant with the boiler has the potential to increase the average power plant efficiency by up to 122 %, thereby the efficiency reaches 12 % and 14 % with TRNSYS and SAM respectively (Assuming in both simulation software the same biomass consumption) (see Table 24).

Generally small CSP plants are characterized by low solar to electrical efficiencies. For example the actual operating Saguaro power plant, with 1 MWe of installed capacity has an efficiency of about 7.5 %.
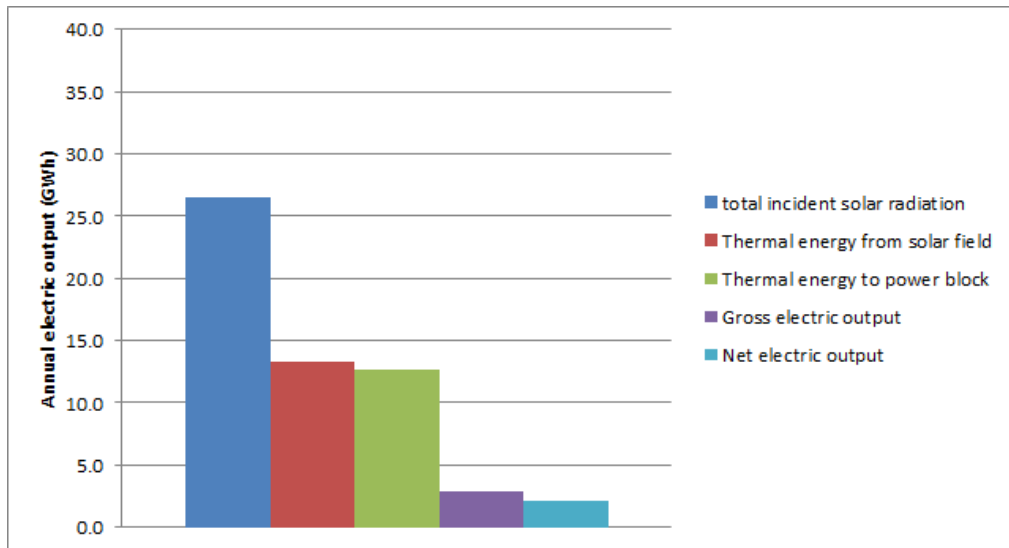
Figure 85. Energy flow in the power plant without boiler (source: SAM). Cambiar a GWh
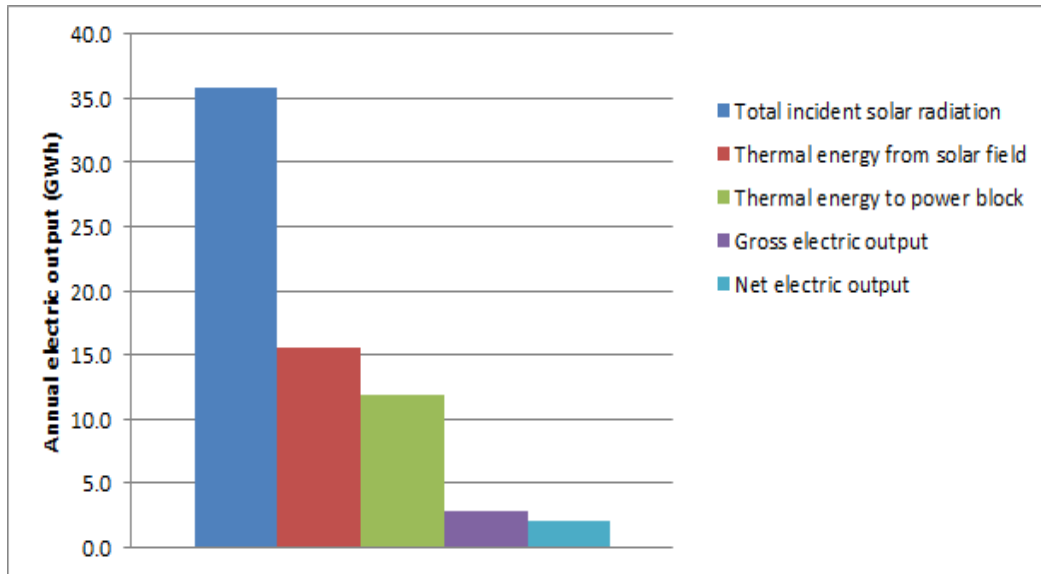
Figure 86. Energy flow in the power plant without boiler (source: TRNSYS).

Table 23. Energy flow and efficiency of the power plant without the integration boiler

	SAM	TRNSYS	Δ (%)
Total incident solar radiation (GWh) annual	26.5	35.8	34.9
Thermal energy from solar field (GWh) annual	13.2	15.5	16.9
Thermal energy to power block (GWh) annual	12.7	11.9	-6.6
Gross electric output (GWh) annual	2.9	2.8	-2.2
Net electric output (GWh) annual	2.1	1.9	-7.8
Average net solar to electrical efficiency (%)	8.0	5.5	-31.6
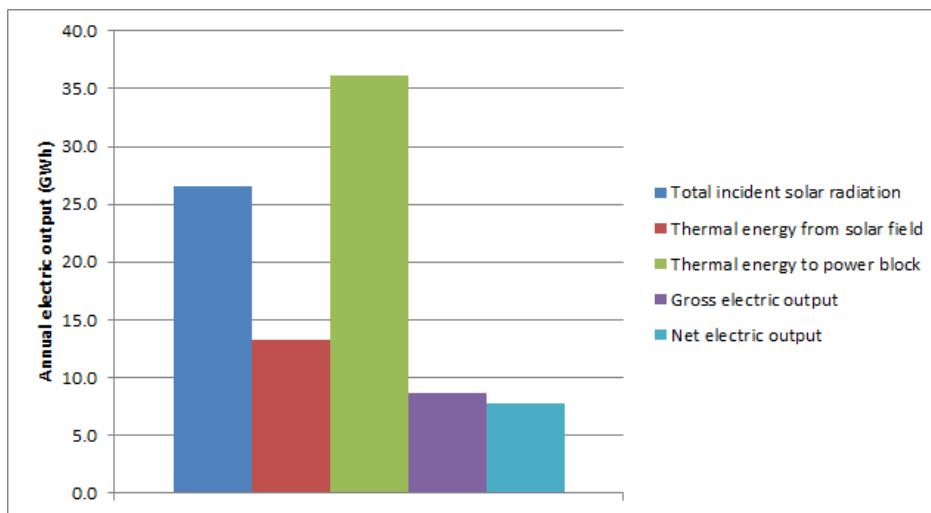
Figure 87. Energy flow in the power plant with boiler (source: SAM).
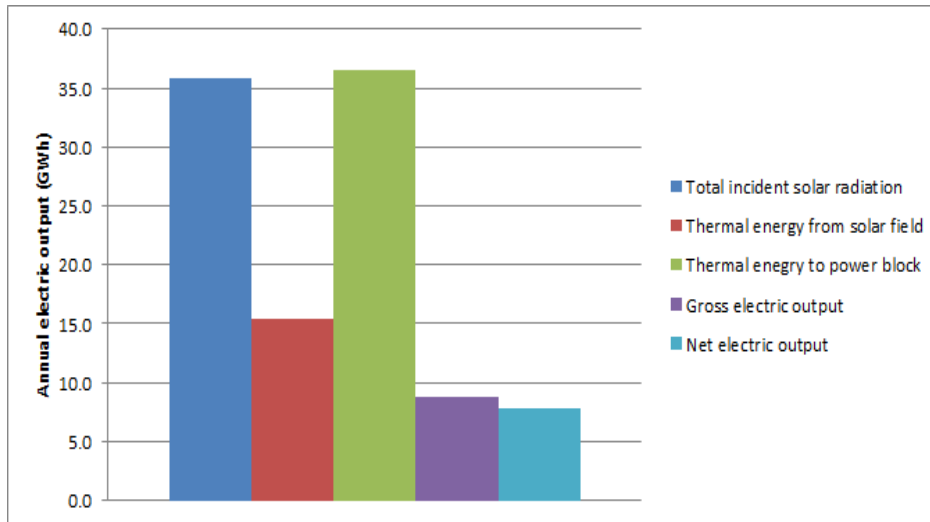
Figure 88. Energy flow in the power plant with boiler (source: TRNSYS).

Table 24. Energy flow and efficiency of the power plant with the integration boiler

	SAM	TRNSYS	Δ (%)
Total incident solar radiation (GWh) annual	26.5	35.8	34.9
Thermal energy from solar field (GWh) annual	13.3	15.5	16.5
Thermal energy to power block (GWh) annual	36.1	36.5	0.9
Gross electric output (GWh) annual	8.7	8.7	0.3
Net electric output (GWh) annual	7.8	7.9	1.1
Average net solar + biomass to electrical efficiency (%)	12.2	14.0	-13.3

93

CONCLUSIONS

Concentrating Solar Power (CSP) is currently an appealing technology for the energy production from renewable sources and the reduction of CO_2 emissions. This technology can take full advantage from the integration with other renewable energy sources and with thermal storage systems, which partially solve the intermittent operation of actual solar thermal plants, increasing its final output and efficiency.

The potential application of a parabolic trough power plant in the region of Puglia in Italy has been quantitatively investigated by using a simulation approach. The evaluation was done through two different software tools: TRNSYS and Solar Advisor Model (SAM).

The developed model in TRNSYS is able to predict the performance of a parabolic trough system integrated with a molten salt thermal storage and a biomass boiler for energy integration. This model can be modified according the requirements of the user load, while SAM is able to simulate the performance of a parabolic trough system integrated with thermal storage and fossil fuel boilers. The TRNSYS energy model is more flexible than the SAM model, which in turn is very useful for detailed economic analyses.

The results obtained with TRNSYS and those obtained with SAM do not differ significantly. However some discrepancies were found and mainly relate to the fact that the weather data for both simulations were taken from different sources.

The CSP integrated only with the thermal storage, i.e. operating in solar mode, can provide the installed capacity of 1 MWe during around one third of the year. Adding the integration boiler it is possible to guarantee the continuous 1 MWe rated capacity, also when solar radiation is not available and when the thermal energy storage is not sufficient. Operating the integrated power plant the annual generation increases up to 8760 MWhe, thereby around 70% of the annual output derives from the biomass resource.

The integration of the parabolic trough power plant with the biomass boiler has the potential to increase the average net solar to electrical efficiency by up to 100 %, thereby pushing it to about 14 %.

The results obtained in this thesis have revealed the feasibility of the integration of CSP with thermal storage and biomass boilers. This result is based on the undeniable suitability of controlling the biomass boiler thermal output with the molten salt level in the hot tank storage, therefore avoiding intermittent starts up and shutdowns in the boiler.

Another advantage of operate a parabolic trough plant integrated with biomass boiler is that regardless the quantity of thermal energy coming from the solar field, the missing energy will be provided by the boiler.

Suggestions for future works include the development of the proposed system in a larger scale, in order to evaluate the trend of the efficiency in function of the installed capacity. Moreover, the economic analysis of the integrated system plays a relevant role in order to assess its actual feasibility.

REFERENCE LIST

Abantia. (2012). *Termosolar Borges la primera planta termosolar comercial en el mundo hibridada con biomassa.* Retrieved March 2014, from http://www.abantia.com/media/upload/pdf//01_abantia_termosolarborgescast _editora_57_127_1.pdf

Angelini, G. (2012). *Numerical modelling of molten-salt thermocline storage systems: feastibility and criteria for performance improvement.* Politecnico di Milano.

Angrisani, G., Bizon, K., Chirone, R., Continillo, G., Fusco, G., Lombardi, S., et al. (2013). Development of a new concept solar-biomass cogeneration system. *Energy Conversion and Management (75)*, 552-560.

Canada, S., Cohen, G., Cable, R., Brosseau, D., & Price, H. (2004). Parabolic Trough Organic Rankine Cycle Solar Power Plant. *Solar Energy Technologies Program Review Meeting*, (p. 5). USA.

CARBON TRUST. (2007). *Biomass fuel procurement guide.* Retrieved June 2014, from http://www.carbontrust.com/media/88607/ctg074-biomass-fuel-procurement-guide.pdf

Caruso, G. (2013). *Efficiente, economica ed ecocompatibile. Le tre "E" della concimazione dell'olivo.* Retrieved May 2014, from http://www.teatronaturale.it/strettamente-tecnico/l-arca-olearia/15924-efficiente-economica-ed-ecocompatibile-le-tre-e-della-concimazione-dell-olivo.htm

DESERTEC-UK. (2009). *CSP pictures*. Retrieved April 2014, from http://www.trec-uk.org.uk/resources/pictures/stills4.html

Dominguez, R., Conejo, A., & Carrion, M. (2014). Operation of a fully renewable electric energy system with CSP plants. *Applied Energy (119)*, 417-430.

Dudley, V., Kolb, G., Sloan, M., & Kearney, D. (1994). *Test results, SEGS LS-2 Solar Collector.* USA.

Duffie, J., & Beckman, W. (2013). *Solar Engineering of Thermal Processes.* USA: John Wiley & Sons, Inc.

ENAMA. (2011). *Caratteristiche tecniche delle biomasse e dei biocombustibili.* Italy.

ENAMA. (2011). *Disponibilità delle biomasse.* Italy.

Fernandez, F., Prieto, M., & Suarez, I. (2011). Thermodynamic analysis of high-temperature regenerative organic rankine cycles using siloxanes as working fluids. *Energy (36)*, 5239-5249.

Ferrer, M. (2012). *Design of a solar thermal power plant.* Universidad Politécnica de Cataluña.

Ferri, R., Cammi, A., & Mazzei, D. (2008). Molten Salt mixture properties in RELAP5 code for thermodynamic solar applications. *International Journal of Thermal Sciences*, 1-12.

Fumis by ATech electronics. (n.d.). *Biomass boilers efficiency*. Retrieved May 2014, from http://www.fumis.si/en/fumis-advantages

Gómez, J., Calvet, N., Starace, A., & Glatzmaier, G. (2012). Ca(NO3)2—NaNO3—KNO3 Molten Salt Mixtures for Direct Thermal Energy Storage Systems in Parabolic Trough Plants. *Journal of Solar Energy Engineering (135)*.

Gunther, M., Joemann, M., & Csambor, S. (2011). *Parabolic Trough Technology.* Germany.

Los Angeles Times. (2013, February). *Large-scale solar farm technology.* Retrieved April 2014, from http://graphics.latimes.com/towergraphic-la-me-solar-desert-tg/

Macchi, E., Campanari, S., & Silva, P. (2005). *La microcogenerazione a gas naturale.* Milano: Polipress.

Martini, P. (2013). *Archimede Solar Energy.* Retrieved March 2014, from http://climatepolicyinitiative.org/sgg/files/2013/11/Session_C_P2_ASE-CPI-martini.pdf

Moreno, J. (2010). *Analisis Termodinamico y simulación de una planta termosolar de colectores cilindro parabólicos.* Universidad de Piura.

Narváez, F., & Monroy, C. (2013). Feasibility of a Solar-Thermal Plant Hybridized with Biomass from Olive Oil Waste in Southern Spain. *The First LACCEI International Symposium on Mega and Micro Sustainable Energy Projects*, (p. 8). Cancun.

National Renewable Energy Laboratory. (2014). *Solar spaces*. Retrieved March 2014, from http://www.nrel.gov/csp/solarpaces/by_status.cfm

Nixon, J., Dey, P., & Davies, P. (2012). The feasibility of hybrid solar-biomass power plants in India . *Energy (46)*, 541-554.

NREL, MWE, Kerney & Assoc, Sandia Natl. Lab, Flabeg Solar International, KJC Operating Co, et al. (2001). *Engineering evaluation of a Molten Salt HTF in a Parabolic Trough Solar Field.* Retrieved August 2014, from http://www.nrel.gov/csp/troughnet/pdfs/ulf_herrmann_salt.pdf

Palmieri, S., & Fabrizi, F. (2010). *Studio di fattibilità relativo alla installazione di un modulo CSP a sali fusi integrato con sistema di gassificazione di biomasse nel*

Comune di Loiano. Retrieved April 2014, from
http://www.centrocisa.it/materiale/Pubblicazioni/termodinamico.pdf

Peterseim, J., Tadros, A., Hellwig, U., & S., W. (2014). Increasing the efficiency of
parabolic trough plants using thermal oil through external superheating with
biomass. *Energy Conversion and Management (77)*, 784-793.

PW Power systems. (2013). *Organic Rankine Cycle Technology.*

Quoilin, S., Van Den Broek, M., Declaye, S., Dewallef, P., & Lemort, V. (2013). Techno-
economic survey of Organic Rankine Cycle (ORC) systems. *Renewable and
Sustainable Energy Reviews (22)*, 168–186.

Ragheb, M. (2011). *Solar thermal power and energy storage historical perspective.*
Retrieved March 2012, from http://www.solarthermalworld.org/node/3303

Regione Puglia assessorato agricoltura, f. a. (2000). *Piano di sviluppo rurale. Norme per
la buona pratica agricola.* Italy.

Sandia Laboratory. (2008). *Stirling Energy Systems set new world record for solar-to-grid
conversion efficiency.* Retrieved April 2014, from
https://share.sandia.gov/news/resources/releases/2008/solargrid.html

Shah, R., & Sekulic, D. (2003). *Fundamentals of Heat Exchanger Design.* USA: John Wiley
& Sons.

Solar Energy Laboratory, U. o. (2007). *TRNSYS 16 mathematical reference.* USA.

Turboden. (2014). *Turboden Solar Thermal Power Applications.* Retrieved April 2014,
from http://www.turboden.eu/en/public/downloads/12-COM%20P-23-
rev.7.pdf

Van Loo, S., & Koppejan, J. (2008). *The Handbook of Biomass Combustion and Co-firing.*
London.

Vandin, F. (2012). *The tesla turbine in small size cogeneration.* Universita degli studi di
Padova.

Wagner, W., & Gilman, P. (2011). *Technical Manual for the SAM Physical Trough Model.*
Colorado.

Yin, C., Rosendahl, L., & Kaer, S. (2008). Grate-firing of biomass for heat and power
production. *Progress in Energy and Combustion Science (34)*, 725-754.

APPENDIX A

PARABOLIC TROUGH POWER PLANTS IN OPERATION IN 2014

Plants	Country	MWe	HTF	Storage	Power block	Backup
Arcosol 50	Spain	50	Oil	Molten salt (7.5 hours)	Steam	Fossil fuel
Andasol I,II,III	Spain	50	Oil	Molten salt (7.5 hours)	Steam	Fossil boiler
Archimede	Italy	5	Molten salt	molten salt (8 hours)	Steam	None
Arenales	Spain	50	Oil	molten salt (7 hours)	Steam	Fossil boiler
Aste 1A, 1B	Spain	50	Oil	molten salt (8 hours)	Steam	Fossil boiler
Astexol II	Spain	50	Oil	molten salt (8 hours)	Steam	Fossil boiler
Borges Termosolar	Spain	22.5	Oil	None	Steam	Biomass
Casablanca	Spain	50	Oil	Molten salt (7.5 hours)	Steam	Fossil boiler
Enerstar	Spain	50	Oil	None	Steam	Fossil boiler
Extresol I, II, III	Spain	50	Oil	Molten salt (7.5 hours)	Steam	Fossil boiler
Genesis Solar Energy project	USA	250	Oil	None	Steam	None
Godawari	India	50	Oil	None	Steam	None
Guzman	Spain	50	Oil	None	Steam	Fossil boiler
Helioenergy I, II	Spain	50	Oil	None	Steam	Fossil boiler
Helios I, II	Spain	50	Oil	None	Steam	None
Holaniku	USA	2	Oil	2 hours	Steam	None
Ibersol	Spain	50	Oil	None	Steam	Fossil boiler
ISCC Ain Beni Mathar	Morocco	20	Oil	None	Steam	None
ISCC Hassi R'mel	Algeria	25	Oil	None	Steam	None
ISCC Kuraymat	Egypt	20	Oil	None	Steam	None

La Africana	Spain	50	Oil	Molten salt (7.5 hours)	Steam	None
La Dehesa	Spain	50	Oil	Molten salt (7.5 hours)	Steam	Fossil boiler
La Florida	Spain	50	Oil	Molten salt (7.5 hours)	Steam	Fossil boiler
La Risca	Spain	50	Oil	None	Steam	Fossil boiler
Majadas I	Spain	50	Oil	None	Steam	None
Manchasol I, II	Spain	50	Oil	Molten salt (7.5 hours)	Steam	Fossil boiler
Martin Next generation	USA	75	Oil	None	Steam	None
Moron	Spain	50	Oil	None	Steam	Fossil boiler
National Solar Thermal power	India	1	Oil	None	Steam	None
Nevada Solar one	USA	72	Oil	Molten salt (0.5 hours)	Steam	Fossil boiler
Olivenza 1	Spain	50	Oil	None	Steam	Fossil boiler
Orellana	Spain	50	Oil	None	Steam	None
Palma del rio I, II	Spain	50	Oil	None	Steam	None
Saguaro	USA	1	Oil	None	ORC (n-pentane)	None
Shams 1	United Arab Emirates	100	Oil	None	Steam	Fossil boiler
Solaben 1,2,3,6	Spain	50	Oil	None	Steam	Fossil boiler
Solacor 1, 2	Spain	50	Oil	None	Steam	Fossil boiler
Solana Generating Station	USA	250	Oil	Molten salt (6 hours)	Steam	Fossil boiler
SEGS I	USA	13.8	Oil	Molten salt (3 hours)	Steam	None
SEGS II, III, IV, V, VI, VII	USA	33	Oil	None	Steam	Fossil boiler
SEGS VIII, IX	USA	89	Oil	None	Steam	Fossil boiler
Solnova I, III, IV	Spain	50	Oil	None	Steam	Fossil boiler

Termesol 50	Spain	50	Oil	Molten salt (7.5 hours)	Steam	Fossil boiler
Termosol 1,2	Spain	50	Oil	Molten salt (9 hours)	Steam	Fossil boiler
Thai Solar one	Thailand	5	Water	None	Steam	None

FRESNEL POWER PLANTS IN OPERATION IN 2014

Plants	Country	MWe	HTF	Storage	Power block	Backup
Puerto Errado 2	Spain	30	Water	0.5 hours	Steam	None
Liddell Power Station	Australia	9	Water	None	Steam	Fossil boiler
Kimberlina Solar Thermal Power Plant	USA	5	Water	None	Steam	None
Puerto Errado 1	Spain	1.4	Water		Steam	None

SOLAR TOWER POWER PLANTS IN OPERATION IN 2014

Plants	Country	MWe	HTF	Storage	Power block	Backup
Ivanpah Solar Electric	USA	377	Water	None	Steam	Fossil backup
Gemasolar Thermosolar Plant	Spain	20	Molten salt	15 hours	Steam	Fossil backup
Planta Solar 20 (PS20)	Spain	20	Water	1 hour	Steam	Fossil backup
Sierra SunTower	USA	5	Water	None	Steam	None
Lake Cargelligo	Australia	3	Water	Graphite solar storage	Steam	None
ACME Solar Tower	India	2.5	Water	None	Steam	None
Jülich Solar Tower	Germany	1.5	Air	1.5 hours	Steam	None
Greenway CSP Mersin tower plant	Turkey	1.4	Water	3 hours	Steam	None

APPENDIX B

SOLAR SALT PROPERTY TABLE

T	Cp	Density	Viscosity	Kin. Viscosity	Conductivity	Enthalpy
[C]	[kJ/kg-K]	[kg/m^3]	[Pa-s]	[m^2-s]	[W/m-K]	[J/kg]
260	1.488	1925	0.004343	2.26E-06	0.4924	380994
277.9	1.491	1913	0.003818	2E-06	0.4958	407643
295.8	1.494	1902	0.003361	1.77E-06	0.4992	434348
313.7	1.497	1890	0.002967	1.57E-06	0.5026	461109
331.6	1.5	1879	0.002629	1.4E-06	0.506	487924
349.5	1.503	1868	0.002344	1.26E-06	0.5094	514794
367.4	1.506	1856	0.002106	1.13E-06	0.5128	541719
385.3	1.509	1845	0.00191	1.04E-06	0.5162	568700
403.2	1.512	1834	0.001751	9.55E-07	0.5196	595735
421.1	1.515	1822	0.001624	8.91E-07	0.523	622825
438.9	1.518	1811	0.001523	8.41E-07	0.5264	649971
456.8	1.522	1799	0.001445	8.03E-07	0.5298	677172
474.7	1.525	1788	0.001383	7.73E-07	0.5332	704428
492.6	1.528	1777	0.001332	7.50E-07	0.5366	731738
510.5	1.531	1765	0.001289	7.30E-07	0.54	759104
528.4	1.534	1754	0.001247	7.11E-07	0.5434	786525
546.3	1.537	1743	0.001201	6.89E-07	0.5468	814001
564.2	1.54	1731	0.001147	6.62E-07	0.5502	841532
582.1	1.543	1720	0.001078	6.27E-07	0.5536	869119
600	1.546	1708	0.000992	5.80E-07	0.557	896760
800	1.546	1708	0.000992	5.80E-07	0.557	896761

HITEC XL PROPERTY TABLE

T	Cp	Density	Viscosity	Kin. Viscosity	Conductivity	Enthalpy
[C]	[kJ/kg-K]	[kg/m^3]	[Pa-s]	[m^2-s]	[W/m-K]	[J/kg]
150	1.494	2116	0.06561	3.1E-05	0.519	227320
168.4	1.489	2101	0.04444	2.12E-05	0.519	254792
186.8	1.483	2086	0.03134	1.5E-05	0.519	282162
205.3	1.477	2070	0.02284	1.1E-05	0.519	309428
223.7	1.472	2055	0.01711	8.32E-06	0.519	336589
242.1	1.466	2040	0.01311	6.43E-06	0.519	363645
260.5	1.46	2025	0.01024	5.06E-06	0.519	390592
278.9	1.454	2009	0.00814	4.05E-06	0.519	417430
297.4	1.448	1994	0.006564	3.29E-06	0.519	444158
315.8	1.442	1979	0.005363	2.71E-06	0.519	470773
334.2	1.436	1964	0.004431	2.26E-06	0.519	497275
352.6	1.429	1949	0.0037	1.9E-06	0.519	523663
371.1	1.423	1933	0.003117	1.61E-06	0.519	549934
389.5	1.417	1918	0.002648	1.38E-06	0.519	576087
407.9	1.41	1903	0.002267	1.19E-06	0.519	602121
426.3	1.403	1888	0.001954	1.04E-06	0.519	628034
444.7	1.397	1872	0.001695	9.05E-07	0.519	653826
463.2	1.39	1857	0.001479	7.96E-07	0.519	679494
481.6	1.383	1842	0.001297	7.04E-07	0.519	705037
500	1.376	1827	0.001143	6.26E-07	0.519	730454
700	1.376	1827	0.001143	6.26E-07	0.519	730455

APPENDIX C

MATLAB CODE OF THE BIOMASS BOILER

```
mFileErrorCode = 100


%---------------- BIOMASS PROPERTIES--------------------

% XC = Content of carbon in the fuel in wt%
% XH = Content of hydrogen in the fuel in wt%
% XS = Content of sulphur in the fuel in wt%
% XN = Content of nitrogen in the fuel in wt%
% XO = Content of oxygen in the fuel in wt%
% XASH = Content of ashes in the fuel in wt%
% W = Moisture content of the fuel in wt% (w.b.)
% NCV = net calorific value in MJ/kg fuel (w.b.)
% GCV = gross calorific value in MJ/kg fuel (d.b.)

XC = 55;
XH = 7.2;
XS = 0.092;
XN=1.94;
XO = 38;
XASH=4;
W=50;


GCV = 0.3491*XC + 1.1783*XH + 0.1005*XS - 0.0151*XN - 0.1034*XO -
0.0211*XASH;
NCV = GCV*(1-W/100) - 2.444*W/100 - 2.444*XH/100*8.936*(1-W/100);



%-------------------- BOILER PROPIERTIES--------------------

% fouling = fouling coefficient
% eta_average = Average efficiency of the biomass boiler
% time_refill = Time between each refill of biomass , 4 days in
hours

fouling = 0.05;
eta_average = 0.85 - fouling;
time_refill = 24*4;


mFileErrorCode = 120


%-------------------- INPUTS------------------------

% Inputs that vary over time:
```

```
% T15 = Actual HFT temperature at the inlet of the boiler
% m15 = Actual HTF mass flow rate in the boiler
% Tank_volume = actual volume of the hot tank in m3
% Constant inputs:

% V_1hour_tank = The hot tank volume required for the boiler
startup in m3
% V_off_boiler = The hot tank volume required for the boiler
stand-by mode in m3
% mnom_MS = HTF flow rate at full load in kg/h
% cp_MS = Heat calorific value of the HTF in MJ/kg/K
% T16_design = Design temperature of the HTF at the outlet of the
boiler
% T15_design = Design temperature of the HTF at the inlet of the
boiler

T15 = trnInputs(1);
m15 = trnInputs(2);
Tank_volume = trnInputs(3);
V_1hour_tank = trnInputs(4);
V_off_boiler = trnInputs(5);
mnom_MS = trnInputs(6);
cp_MS =trnInputs(7);
T16_design =trnInputs(8);
T15_design =trnInputs(9);


mFileErrorCode = 140


%----------------------FIRST CALL OF THE SIMULATION-------

% i = Indicates the boiler operation mode (on: i = 1, stand-by: i
= 0)
% Boiler_on = Counts the number of startup of the boiler
% mstoc_useful = the storage biomass for 4 days of full operation
in kg
% mstoc_stand_by = the storage biomass for 4 days of boiler stand-
by in kg
% mfuel_stand_by = biomass consumption in the stand-by mode in
kg/h
% Qfluid_max = Maximum heat transfer rate required by the HTF in
MW


if ((trnInfo(7) == 0 ) && (trnTime - trnStartTime <1e-6))

    i=0;
    Boiler_on=0;
    Time = -1;
    time=-1;
```

```
        mstoc_useful = Qfluid_max/NCV/eta_average * 3600 *
time_refill;
        mstoc_stand_by = 0.05 * Qfluid_max/NCV * 3600 * time_refill;
        mfuel_stand_by = 0.05 * Qfluid_max/NCV * 3600;
        time2 = trnTime;
        Qfluid_max = mnom_MS * cp_MS * (T16_design-T15_design);
        mnom_MS = mnom_MS/3600; % HTF flow rate at full load in kg/s


end
    mFileErrorCode = 160


%----------------------BIOMASS REFILL----------------------

if (trnTime - time2 == time_refill)

    mstoc_useful = Qfluid_max/NCV/eta_average * 3600 *
time_refill;
    mstoc_stand_by = 0.05*Qfluid_max/NCV * 3600 * time_refill;
    time2 = trnTime;


end

 mFileErrorCode = 165


% ----------------------BOILER START UP-------------------

% Qfluid = heat transferred to the HTF in MW
% Qboiler = Inlet heat in the boiler in MW
% mfuel = Fuel consumption in kg/s

 if ((Tank_volume <= V_1hour_tank) && (i==0)&& (trnTime>time))

        Qfluid = 0;
        Qboiler = Qfluid_max;
        mfuel = Qboiler/NCV;
        i=i+1;
        Time = trnTime;
        Boiler_on = Boiler_on + 1;

     if mstoc_useful < mfuel*3600

           mfuel =  storage
(mstoc_useful,mstoc_stand_by,Qfluid_max ,NCV);
           i=0;
           Qfluid =0;
           Boiler_on = Boiler_on-1;
           yy=0;

     end
```

```
        Qboiler = mfuel * NCV;
        mash = XASH/100 * mfuel;
        Qloss = 0;
        yy=0;
        T16 = T15;

  End

      mFileErrorCode = 170


    %--------------------NORMAL OPERATION------------------------

    % Pload = Partial load, ratio between the heat transfer required
    by the HTF and the maximum output of the boiler
    % eta = Biomass boiler partial load efficiency
    % mash = Quantity of ashes produced by the combustion in kg/s
    % Qloss = Losses of the boiler in MW
    % T16 = HTF temperature at the outlet of the boiler in °C

    if ((trnTime > Time) && (i==1) )

        yy=1;
        Qfluid = m15/3600 * cp_MS * (T16_design - T15);
        Pload= Qfluid/Qfluid_max;
        eta = efficiency (Pload) ;
        Qboiler = Qfluid/eta;
        mfuel = Qboiler/NCV;

      if mstoc_useful < mfuel*3600

          mfuel = storage
      (mstoc_useful,mstoc_stand_by,Qfluid_max,NCV);
          i = 0;
          Qfluid = 0;
          yy = 0;

      end

      Qboiler = mfuel * NCV;
      mash = XASH/100 * mfuel;
      Qloss =(1-eta)* Qboiler;
      T16 = T16_design;

    end

      mFileErrorCode = 180
```

```
% ---------------------------SHUT DOWN------------------------

if ((Tank_volume>=V_off_boiler) && (trnTime >Time))

      Qfluid = 0;
      Qboiler = 0.05 * Qfluid_max;
      mfuel = Qboiler/NCV;
      i=0;

        if mstoc_useful < mfuel*3600

            mfuel= storage
(mstoc_useful,mstoc_stand_by,Qfluid_max,NCV);

         end
      Qboiler = mfuel * NCV;
      mash = XASH/100 * mfuel;
      time = trnTime;
      Qloss = Qboiler;
      Yy = 0;
      T16 = T15;

end

mFileErrorCode = 190

%------------------------BIOMASS STORAGE-----------

if (trnInfo(7) == 0 )

    if (mstoc_useful >= mfuel_stand_by)

        mstoc_useful = mstoc_useful - mfuel*3600;

    else

        mstoc_stand_by = mstoc_stand_by - mfuel*3600;

    end

end

mFileErrorCode = 200

%--------------------OUTPUTS---------------------

trnOutputs(1) = mfuel;
trnOutputs(2) = T16;
```

```
trnOutputs(3) = m15;
trnOutputs(4) = i;
trnOutputs(5) = Qfluid;
trnOutputs(6) = Qboiler;
trnOutputs(7) = Qloss;
trnOutputs(8) = NCV;
trnOutputs(9) = Boiler_on;
trnOutputs(10) = mash;
trnOutputs(11) = Pload;
trnOutputs(12) = eta;
trnOutputs(13) = time2;
trnOutputs(14) = mstoc_useful;
trnOutputs(15) = mstoc_stand_by;
trnOutputs(16) = yy;


mFileErrorCode = 0;


return
```

Function of the partial load efficiency of the boiler

```
function [eta] = efficiency (Pload)


fouling = 0.05;
eta=(0.95*(Pload>=1) + 0.8*(Pload<=0.25) + (0.2986*(Pload)^3 -
0.855*(Pload)^2 + 0.8772*(Pload) + 0.6298)*(Pload>0.25 &&
Pload<1));
eta = eta - fouling


return
```

Function of the biomass storage

```
Function [mfuel] = storage (mstoc_useful
,mstoc_stand_by,Qfluid_max,NCV)

    mfuel = 0.05*Qfluid_max/NCV; %kg/s

    if (mstoc_useful + mstoc_stand_by < mfuel)

        mfuel = 0;

    end

return
```

MATLAB CODE OF THE BIOMASS BOILER AND HOT TANK RELATION

```
mFileErrorCode=300
```

```
%----------------------------- INPUTS-------------------------

% Inputs that vary over time:
% m9 = HTF flow rate required by the generator of the power block
in kg/h
% m_recirculation = The HTF flow rate that is heated by the hot
tank boiler in kg/h
% Vmin = Minimum hot storage volume in m3
% deltaT_MS = The difference between the outlet and the inlet HTF
temperature in the biomass boiler in °C
% Qnom_boiler = Nominal heat transfer rate of the biomass boiler
in MW

Tank_volume = trnInputs(1);
m9 = trnInputs(2)
yy= trnInputs(3);
m_recirculation = trnInputs(4);
Vmin = trnInputs(5);
Voff_boiler = trnInputs(6);
cp_MS = trnInputs (7);
deltaT_MS = trnInputs(8);
Qnom_boiler = trnInputs(9);

mFileErrorCode = 320

%------------------------- STORAGE TANK -------------------

% m7 = outlet flow rate of the hot tank
% Qboiler = heat transfer rate of the biomass boiler, in MW,
controlled by the hot tank volume
% m15_rr = HTF flow rate in the biomass boiler

if ((trnInfo(7) == 0 ) && (trnTime - trnStartTime <1e-6))

    yy=1;

end

if Tank_volume <= Vmin

    yy=1;

end

if yy ==1

V = Tank_volume/Voff_boiler;
Qboiler = (1*(Tank_volume <= 0.5 * Voff_boiler) + (1.8 - 1.6 *
V)*(Tank_volume > 0.5 * Voff_boiler))*(Pnom_boiler);
Pload = Qboiler/Qnom_boiler;
eta_boiler = efficiency (Pload);
```

```
m15_rr = Qboiler * eta_boiler/cp_MS/deltaT_MS * 3600;   %kg/h
m7 = m9 - m15_rr + m_recirculation ;

    if (m9-m15_rr < 1)

    m7 = m_recirculation;

    end

end

if Tank_volume >= Voff_boiler

    yy=0;

end

if yy==0

  m7= m9 + m_recirculation;

end

mFileErrorCode = 340


%--------------------------- OUTPUTS -----------------------

trnOutputs(1)=m7;
trnOutputs(2)=m9;
trnOutputs(3)=m15_rr;
trnOutputs(4)=m_recirculation;

mFileErrorCode = 0

return
```